TARGETED STIMULI-RESPONSIVE CARRIERS FOR EFFICIENT DELIVERY OF CHEMOTHERAPEUTIC DRUGS

A Dissertation
Submitted to the Graduate Faculty
of the
North Dakota State University
of Agriculture and Applied Science

By

Fataneh Karandish

In Partial Fulfillment of the Requirements
for the Degree of
DOCTOR OF PHILOSOPHY

Major Department:
Pharmaceutical Sciences

November 2017

Fargo, North Dakota

North Dakota State University
Graduate School

Title

TARGETED STIMULI-RESPONSIVE CARRIERS FOR EFFICIENT DELIVERY OF CHEMOTHERAPEUTIC DRUG

By

Fataneh Karandish

The Supervisory Committee certifies that this ***disquisition*** complies with North Dakota State University's regulations and meets the accepted standards for the degree of

DOCTOR OF PHILOSOPHY

SUPERVISORY COMMITTEE:

Dr. Sanku Mallik
Chair

Dr. Amanda Brooks

Dr. Kristine Steffen

Dr. D.K. Sirvastava

Approved:

01/26/2018
Date

Dr. Jagdish Singh
Department Chair

ABSTRACT

Chemotherapeutic agents for treating various cancers show considerable side effects and toxicity. Often cancer relapses after initial response to the chemotherapy. Tumor cells are heterogeneous and have the progenitor stem cells which can renew, causing the relapse of the disease. To overcome drug resistance, metastasis, and relapse in cancer, targeted therapy is a promising approach. Targeted delivery of chemotherapeutic agents decrease toxicity and improve efficacy for cancer treatment.

We have designed targeted, stimuli-responsive echogenic polymeric vesicles (polymersomes) to not only transport, and subsequently, release a chemotherapeutic drug in the nuclei or cytosol of cancer cells and image by diagnostic frequency ultrasound. Targeted polymersomes carry chemotherapeutic drugs through the body, recognize the cancer cells, internalize, and release the encapsulated chemotherapeutic drug in response to increased reducing agent concentration. We have employed different targeting moieties such as, neuropilin-1 peptide and prostate-specific membrane antigen agonist. We prepared redox-sensitive targeted polymersomes encapsulating the hydrophobic chemotherapeutic drug in the treatment of cancer cells, including cancer stem cells. Different formulation of targeted stimuli-responsive polymersomes was tested on monolayer as well as three-dimensional spheroids. Our results indicate that targeted polymersomes encapsulating both drugs are significantly reducing the cell viability in cancer cells. We also established the preliminary data on the penetration of iRGD peptide-decorated polymersomes in a xenograft mouse model of pancreatic cancer.

ACKNOWLEDGEMENTS

I would like to express my sincere gratitude towards my advisor Dr. Sanku Mallik for believing in me, for giving me an opportunity to work in his laboratory, and for providing me continuous support and guidance.

I would like to extend my genuine thanks to my graduate advisory committee members Dr. Amanda Brooks, Dr. Kristine Steffen, and Dr. D. K. Srivastava for their valuable suggestions on my preliminary proposal and continuous support.

I would like to thank our collaborators Dr. Kausik Sarkar (George Washington University), Dr. Kalpana Katti, Dr. Yongki Choi, Dr. Kara Gange, Dr. Bin Guo (University of Houston), Dr. John Wilkinson for their contribution and their commitment during projects. I would like to thank our department chair, Dr. Jagdish Singh and our dean of the college, Dr. Charles Peterson, for great leadership. I would like to thank all the faculty, staff and students of the Pharmaceutical Sciences department for their friendship and generous support.

I would like to thank Dr. Manas Haldar for practical contribution to my work and my lab mates Dr. Prajakta Kulkarni, Matthew Confeld, Dr. Michael D. Scott, Dr. Rahul Nahire, Dr. Li Feng and my great collaborators Lang Xia, MD Shahjaha Molla, and Jamie Froberg. Thanks to my former students, Desiree, Anessa, Rayat, and Grisha for making me a better mentor.

I would like to thank the Department of Pharmaceutical Sciences, the College of Health Professions, the NDSU Research and Technology Park, the Graduate School, and North Dakota State University for providing the great facility and support to make my studies possible.

Thanks to the National Institutes of Health, Grand Challenge project, the Office of President and Provost to support and fund my project during my studies.

I would like to thank my friends Denise Pinkney, Stephani Haugen, and Farnaz Fouladi for their encouragement and continuous support.

Finally, my mother and father, Khadijeh Edalati and Rahman Karandish, for supporting and encouraging me, and my supportive husband Ali and loving daughter Rosha for their faithful support and love.

DEDICATION

To my mother, father and my sister, Khadijeh, Rahman and Farideh

My supportive husband Ali and loving daughter Rosha

TABLE OF CONTENTS

LIST OF TABLES

LIST OF FIGURES

LIST OF SCHEMES

LIST OF ABBREVIATIONS

ACS ……	American Chemical Society
AFM ……..…….	Atomic Force Microscopy
AKT ……	Protein Kinase B
AML ……..…….	Acute Myeloid Leukemia
AR …….…….	Androgen Receptor
ATCC …….……	American Type Culture Collection
Avg ……	Average
C …….	Centigrade
CD …….…….	Circular Dichroism
CI ……	Combination Index
Cm …….	Centimeter
c-MYC ……..	myelocytomatosis Viral
CTCF …….	Corrected Total Cell Fluorescence
dB ……..	Decibel
DLS …….	Dynamic Light Scattering
DLE ……..	Drug loading efficacies
DMF …….	dimethylformamide
DSPE ……	1,2-distearoyl-sn-glycero-3-phosphoethanolamine
EDC ……	Ethyl-3-(3-dimethylaminopropyl) carbodiimide
ERK …….	Extracellular Signal Regulated Kinases
EPR …….	Enhanced Perm and retention effect
ELIPs ……..	echogenicity of echogenic liposomes

EMT …….	Epithelial to Mesenchymal Transition
FDA ……..	Federal Drug Administration
G ……	Grams
GSH …….....	Glutathione
H ……	Hours
HBSS ……	Hank's Blank salt solution
HER ……..	Human epidermal receptor
IL ……..	Interleukin
iRGD peptide ……	internalizing RGD
JAK ……..	Janus Kinase
KRAS ……...	Kirsten Rat Sarcoma Viral
KeV ……	Kiloelectronvolt
KHz ……	Kilohertz
LR ……..	1,2-dipalmitoyl-s*n*-glycero-3-phosphoethanolamine-N-(lissamine rhodamine B sulfonyl, ammonium salt)
M ……	Molar
MALDI-TOF……..	Matrix-assisted laser desorption/ionization- Time of Flight
mg …….	Milligrams
MHz …….	Mega Hertz
mL …….	Milliliters
Mmol ……	Millimolar
MAPK ……..	Mitogen Activated Protein Kinases
MMP ……	Matrix Metalloproteinase
m-PEG …….	Methoxy Polyethylene glycol
mTOR …….	Mammalian Target Of Rapamycin

MW ……..	Molecular Weight
n ……	Number
NF-kB ……..	Nuclear Factor Kappa-light-chain-enhancer of activated B cells
Nm ……	Nanometer
NMR …….	Nuclear Magnetic Resonance
PDAC ……	Pancreatic Ductal Adenoma Carcinoma
PSMA ……..…….	Prostate Specific Membrane Antigen
PBS ……..……..	Phosphate Buffered Saline
PDI ……	Polydispersity Index
PEG ……..……..	Polyethylene glycol
PI ……..	Propidium iodide
PI3K …….	phosphatidylinositol 3-kinase
PLA ……..……	Polylactic acid
PMDETA ……..……	N, N, N′,N′,N″-pentamethyldiethylenetriamine
ROS ……..	Reactive Oxygen Species
RPMI ……	Roswell Park Memorial Institute medium
SDS ……	Sodium Dodecyl Sulfate
STAT …….	signal transducer activator of transcription
SSEA …….....	Stage-specific Embryonic Antigens
TEM …….	Transmission Electron Microscopy
THF ……..	Tetrahydrofuran
µL …….	Microliter
µm …….	Micromoles
VGFR ……	Vascular Endothelial Growth Factor Receptor

UV …….	Ultraviolet
V ……..	Watts
W …….	Watts
Wnt ……..	W*ingless* and *I*NT-*1*
3D …….	Three dimensional

LIST OF APPENDIX FIGURES

GENERAL INTRODUCTION AND DISSERTATION ORGANIZATION

Cancer is the second leading cause of death in the United States.[1] By tradition, cancer has been exemplified by a collection of mutations in oncogenes and tumor suppressors.[2] Genetic and epigenetic alteration cause tumor heterogenicity during the development of the tumor that leads to genomic instability and epigenetic changes.[3] A subpopulation of cancer cells during the development may have the characteristic of initial stem cells that expand in different patterns.[2, 4] In both primary and metastasis, there are subpopulations of cells with the self-renewal and multi-lineage differentiation ability (known as the cancer stem cells).[3, 5, 6] Cancer stem cells with the tumor-initiating capability explain tumor heterogenicity.[4, 7, 8] Alteration of different genes, aberrant biochemical pathways, epithelial to mesenchymal transition (EMT), hypoxia, tumor microenvironment, and cancer stem cells lead to recurrence and drug resistance.[7] Solid tumors of prostate, colon, breast, and lung account for approximatly 80% of all cancers, and it is hypothesized that cancer stem cells might be the origin of the solid tumors.[9] Cancer stem cells express both embryonic stem cells markers (Nanog, Oct4, and Sox-2) and progenitor cell markers (CD33, CD44, and Nestin).[10, 11] Dysregulation of the notch, wnt/β-catenin, Janus kinase (JAK)/signal transducer activator of transcription (STAT), and hedgehog signaling (pathways that are highly conserved and control self-renewal ability) are observed in cancer stem cells.[12-14]

Cancer stem cells cause tumor initiation, recurrence, and metastasis after chemotherapy.[16] Cancer stem cells isolated from pancreatic tumors were defined by $CD133^+$cells[17] and $CD44^+$ $CD24^+$ $EPCAM^+$ cells.[18] Prostate cancer stem cells isolated from tumors overexpress the $CD44^+$, CD 133^+, SSEA3/4, Oct4 markers (www.celprogen.com).

Currently, surgical intervention, radiation, and conventional chemotherapy are the most common cancer treatments [19], with chemotherapy as the main option [20, 21]. However,

conventional chemotherapy distributes the drugs throughout the body, affecting the malignant as well as the normal cells. In addition, the lack of achievable therapeutic dose, acute toxicity, and the potential of drug resistance further limit the usefulness of conventional chemotherapy [22]. Most chemotherapy candidate drugs are water-insoluble.[23] Although, drug hydrophobicity is needed to pass through the cellular membranes, it causes poor absorption and low bioavailability. Intravenous administration of low water-soluble drugs cause aggregation and local toxicities.[23]

Nanocarriers

To increase the efficacy and overcome poor water solubility, a long-circulating drug delivery vehicle is needed, which recognizes the cancer cells, and releases its contents in the cytosol. In the design of a novel system for targeted delivery, one important factor is the selection of target moieties that can interact with the specific cells in a tumor microenvironment or cancer cells and eliminate the systemic toxicities. Targeted drug delivery systems increase the therapeutic index with a wide therapeutic window. The nanoparticles protect the chemotherapeutic drug from early degradation, increase absorption and biodistribution in solid tumors, and improve cellular internalization.[24]Various nanocarriers (e.g., polymeric micelles, liposomes, nanoparticle-aptamer, polymersomes, and nanoparticle delivering miRNA, siRNA, and cell penetrating peptide) have been developed for cancer treatment with varying degrees of success.[25-32] Therefore, there is a crucial need to develop delivery vehicles to carry and subsequently release anticancer drugs selectively to cancerous tissues.

Polymersomes

Polymersomes are self-assembled, bilayer vesicles prepared from amphiphilic block copolymers. These robust bilayer vesicles are prepared from synthetic, amphiphilic block copolymers. Usually, the hydrophilic part is polyethylene glycol (PEG) – a biocompatible polymer approved by the Food and Drug Administration (FDA). [33] The incorporation of polyethylene glycol (PEG) as the hydrophilic block renders the vesicles long circulating.[34] PEGylation facilitates steric stabilization, avoids protein adsorption, and decreases interactions with immune cells.[35] PEGylation also reduces the uptake by the mononuclear phagocyte system; consequently, more nanoparticles accumulate in the tumor with substantial reduction in clearance.[36] The bilayer of the polymersomes encapsulates hydrophobic drugs and the aqueous core incorporates the hydrophilic drugs.[34] Because of higher molecular weights, polymersomes have enhanced stability and mechanical robustness compared to liposomes, micelles, and polymer micelles.[37]

Tumor targeting strategies

Another major problem of chemotherapy is drug resistance that could be solved by targeted nanoparticles.[23] Fast proliferation of endothelial cells as well as a decreased number of pericytes in tumor areas cause leaky and big gap junction between the cells.[35] The resultant increased vascular permeability allows the circulating nanoparticles to reach the tumors. The nanocarriers usually escape through the leaky vasculature and accumulate in tumors due to the poor lymphatic drainage (termed the enhanced permeation and retention effect, EPR).[38] The targeting of the nanoparticle by the EPR effect is passive. Subsequent interactions with a specific receptor on the cell surface enables cellular internalization of the nanocarriers via endocytosis.[19]

The effectiveness of a drug delivery system depends on its ability to internalize in the tumor tissue, to kill the cancer cells with minimal effect on healthy cells, and to provide better pharmacokinetic and pharmacodynamics profiles with sustained release of a drug. As a result, having an effective drug delivery system that actively targets the cancer cells is essential. Targeted drug delivery means the accumulation of the drug in the specific area independent of method and route of administration.[39] Active targeting is the specific binding between drug/drug carrier and target cells through ligand-receptor interactions with subsequent cellular internalization. [40] Active targeting was classified to three categories: angiogenesis-associated targeting, uncontrolled cell proliferation targeting, and tumor cell targeting.[40] Targeting vascular endothelial growth factor receptor (VGFR), $\alpha_V\beta_3$ integrin, and matrix metalloproteinase are subclassifications of angiogenesis-associated targeting.[40]

Vascular endothelial growth factor receptor (VGFR)

Vascular endothelial growth factor receptor is a type III transmembrane tyrosine kinase receptor and induces angiogenesis through VGFR signaling cascade. Three different but structurally similar VGFRs are reported. VGFR-1 is critical in hematologic stem cells and is also known as a fms-like tyrosine kinase. The overexpression of VGFR-1 is observed in the oncogenes and hypoxia in tumor tissues. VGFR-2 (fetal liver kinase-1 receptor) is overexpressed in thyroid malignancy, melanoma, and ovarian cancer. VGFR-3 is a lymphatic endothelial cell development receptor expressed in human malignancies, such as lung, breast and colon cancers.[40, 41] Different approaches such as, targeting to inhibit and decrease ligand binding to VGFR-2 have been used.[42, 43]

$\alpha_V\beta_3$ integrin

The $\alpha_V\beta_3$ integrin receptor (also known as vitronectin receptor) belongs to the integrin superfamily of heterodimeric membrane adhesion glycoproteins.[44] Integrin participates in cell-cell interactions and signal transduction.[44] The $\alpha_V\beta_3$ integrin receptor is overexpressed in tumor vasculature, recognizes the conserved RGD(Arg-Gly-Asp) domain of plasma and matrix proteins, and facilitates extracellular matrix-cell adhesion.[44, 45] RGD-targeting has been employed in delivering imaging agents,[46] drugs,[47] nanoparticles,[48]and viruses[49] to the tumor vasculature. A short cyclic tumor-penetrating peptide known as iRGD (internalizing RGD) has been shown to interact with the integrin receptor.[45] The iRGD peptide has R/KXXR/K motif known as C-end Rule (CendR) that mediates cell and tissue penetration by interacting with the neuropilin-1 receptor.[45] Nanoparticles, antibodies, and drugs conjugated to the iRGD peptide were observed to accumulate in the tumors both in vitro and in animal studies.[50]

Matrix metalloproteinases (MMPs)

The matrix metalloproteinases (MMPs) are zinc-dependent endopeptidases and play a crucial role in remodeling extracellular matrix, tumor invasion, and metastasis.[40, 51] Overexpression of MMP-1 (collagenase), MMP-2 (gelatinases-A), MMP-7 (matrilysin), MMP-9 (gelatinase-B), MMP-10, MMP-11 (stromelysin), and MMP-13 (collagenase) is reported in pathological conditions and cancers.[52, 53] Several therapeutic agents and natural products have been delivered to cancer cells by targeting the MMP enzymes.[53-55]

Signal transducer and activator of transcription 3 (STAT3)

Signal transducer and activator of transcription 3 (STAT3) is overexpressed in many malignancies, such as breast, pancreatic, ovarian, and hematologic cancers.[16] STAT3 has a significant role in the regulation of cancer stemness.[7] Activation of STAT3 regulates expression

of many genes as well as cancer stemness proteins, e.g., nanog, c-MYC, and β-catenin.[56] It has been shown that inhibition of cancer stem cell needs direct inhibition of STAT3, not the upstream pathway (JAK).[16] Targeting cancer stem cell with the STAT3 inhibitor napabucasin (BBI608) is a promising approach to block the self-renewal and exhaust the cancer stem cell population in the tumor without causing significant toxicity to the healthy cells.[16] Currently, napabucasin is in several clinical trials.[57-64]

Human epidermal receptor(HER)

Several receptors are overexpressed on the surface of cancer cells due to the uncontrolled proliferation in cancer. Hence, many studies demonstrate the effectiveness of targeting these receptors to deliver drugs selectively to the cancer cells. Active targeting of the human epidermal receptor, folate receptor, and transferrin receptor is well established.[40] The human epidermal receptor (HER) belongs to the tyrosine kinase receptor family. HER-2 is overexpressed in breast, ovarian, gastric, and oral cancers.[65, 66] Recombinant anti-HER 2 monoclonal antibody, trastuzumab was developed by Genentech, Inc for the treatment fo HER-2 positive breast cancer.[65, 67]

Transferrin receptor (TFR-1)

Transferrin receptor (TFR-1) mediates endocytosis and helps the cellular uptake of iron.[68] Transferrin receptor-1 is expressed in all nucleated cells, such as red blood cells, monocytes, erythrocytes, intestinal cells, and the endothelial cells of the blood-brain barrier.[68] Transferrin receptor is overexpressed in cancer cells and has been targeted for imaging and cancer diagnosis, delivering anticancer drugs, and for inhibiting iron uptake in the cancer cells.[69,70]

Folate receptor

The folate receptor is a cell surface glucosyl phosphatidylinositol-anchored glycoprotein, widely investigated for targeting cancer cells.[40] Healthy cells do not transport any folate conjugates; only the reduced form of folate diffuses through the cell membrane.[40] Folic acid is inexpensive, safe, stable in organic solvents, easy to conjugate, and does not cause any immunogenic response.[71] Cellular internalization of anti-folate antibodies and folic acid conjugates occur by receptor-mediated endocytosis.[72] In Europe, folate-targeted vintafolide (Vynfinit®) is approved for treating ovarian cancer in women who are resistant to platinum drugs.[73]

Prostate-specific membrane antigen (PSMA)

Prostate-specific membrane antigen (PSMA) is over expressed in prostate cancer cells, and is an excellent target to deliver drugs.[74] Aptamer-conjugated nanoparticles have been developed to target the PSMA receptor.[26] Androgen receptor (AR), PI3K/AKT/mTOR, and MAPK signaling pathways are altered in prostate cancer cells.[75] Taking advantage of these aberrant signaling pathways has excellent potential to develop a therapeutic treatment.

Kirsten rat sarcoma viral (KRAS)

Kirsten rat sarcoma viral (KRAS) mutation occurs in 75% of PDAC.[53] KRAS mutations and activation of downstream signaling pathways, such as MEK, AKT, and ERK are exacerbated treatment of pancreas cancer.[76] Currently, Kamerkar at el developed the iExosome targeting KRAS that deliver the short interfering RNA which significantly increased the survival rate in KPC mouse model of pancreatic cancer.[76]

Opportunities for drug delivery in tumor microenvironment

The Tumor microenvironment has a crucial role in tumor growth, progression and, tumor evolution.[77, 78] Cancer pathogenesis depends on the interaction with the microenvironmental components.[77]This microenvironment consists of proliferating cells, the tumor stroma, blood vessels, and infiltrating inflammatory cells. [79] Immune cells that exist in the tumor microenvironment are T lymphocytes, dendritic cells, sporadic B cells, macrophages, polymorphonuclear leukocytes, and rare natural killer cells.[79] Macrophages that exist in the tumor microenvironment inhibit lymphocyte functions with the release of inhibitory cytokines, such as IL-10, prostaglandins, and reactive oxygen species (ROS).[79] The NF-kB signaling pathway may have the role in cancer and inflammatory interactions.[79] It is also reported that the tumor microenvironment factors, such as hypoxia and oncogenes, synergistically cause expression of vascular epithelial growth factor and lead to angiogenesis.[80]

Stimuli-responsive nanocarriers

Stimuli-responsive drug carriers have the potential to enhance therapeutic efficacy and reduce toxicity by selectively delivering cytotoxic chemotherapeutic drugs to cancerous tissues.[81] Stimuli-responsive nanocarriers are constructed to be stable in normal tissues but they release the encapsulated drugs in response to physical or chemical stimulus. They reduce therapy induced side effects and enhance the benefit of the chemotherapeutic drug.[81] These nanoparticle carriers are classified as either external or internal stimuli-responsive based on the method that triggers the release the encapsulated contents. External stimuli-responsive nanocarriers release their content in response to the chemical or physical stimuli, such as heat, light, ultrasound. [82-84] Internal stimuli-responsive nanocarriers release their encapsulated drug in response to biochemical alterations in the tumor tissues, such as decreased pH, hypoxia, elevated enzymes

(MMPs), elevated reducing agents (glutathione), and overexpressed receptors (folate, transferrin, etc.).[52, 70, 85-87]

pH-responsive nanocarriers

Both normal and tumor tissues display different pH values. In tumors, pH is usually acidic.[88] pH-responsive nanocarriers utilize low extracellular and lysosomal pH.[89] In the extracellular matrix, the pH is slightly lower (6.5-7.2) than the normal tissues (7.4). After cellular uptake, the pH-responsive nanoparticles reach the lysosomes (pH 4.5-5), where proteolytic enzymes release the drug.[88]

Hypoxia-responsive nanocarriers

Hypoxic regions are usually at the core of tumors and are approximately180 μm away from blood vessels. [85] These regions have low levels of oxygen quantify compared to normal tissues and enhance angiogenesis, vasculogenesis, invasiveness, and metastasis. [90] Hypoxic cells show anaerobic metabolism which is different from the normal tissues. [85] Furthermore, hypoxia induces resistance to chemotherapy through repair before progression to S or M phase, mutagenesis, and expression of ABC transporters, etc. [90] Since the hypoxic regions are far from blood supplies and efflux transporters are overexpressed, transport of drug carriers to these regions poses significant challenges.[91] Tumor hypoxia and genetic aberration cause HIF-1α expression (hypoxia marker), which leads to upregulation of vascular endothelial growth factor and platelet- derived growth factor or tumor necrosis factor α, causing cell survival, angiogenesis, and invasion.[92]

Enzymes-responsive nanocarriers

High levels of proteolytic enzymes, such as matrix metalloproteinases (MMPs) can be exploited in stimuli responsive-nanoparticles. The elevated levels of matrix metalloproteinases is

associated with cell transformation, morphology, and cancer.[52] In response to overexpression of proteolytic enzyme (e.g. MMP-9), the nanoparticle can release the encapsulated drug, decreased cell viability, and shrunk the tumor in a the mouse model of pancreatic cancer.[55]

Reduction-sensitive carriers

Reduction-sensitive carriers (utilizing the disulfide bond) also exploit the elevated levels of reducing agents in the intracellular matrix of cancer cells. [93] Gemtuzumab ozogamicin (Mylotarg®) is an FDA approved disulfide-linked antibody-drug conjugate used in the treatment of CD33-positive acute myeloid leukemia (AML).[94]

Echogenic polymersomes

Ultrasound responsive nanoparticles have gained attention in diagnostics and therapeutics since they carry drug, have the ability to be tracked, and release their contents in response to external ultrasound.[95] The echogenic characteristic of the nanoparticles enables real-time imaging of the vesicles employing a high-frequency ultrasound scanner.[95] Echogenic polymersomes contain small amounts of air, although the exact location and size of the entrapped air bubbles in the nanoparticle is not established. [37] Coupling with gas pockets renders the polymersomes responsive to high-frequency ultrasound. [37] Ultrasound has been exploited to deliver genes (DNA) in the different cells *in vitro* and in an *in vivo* animal model.[96]

Organization of the thesis

The essential goal of target-specific delivery is to increase the efficacy of chemotherapeutic drugs, reducing the systemic toxicities and improving the quality of life in cancer patients. I have developed and characterized three targeted, reduction-responsive drug delivery systems (polymersomes) that release their encapsulated chemotherapeutic drugs in response to the high amount of reducing agent present in cancer cells. To show the goal of the

approach and applicability, I have used both prostate and pancreatic cancer as model systems to demonstrate the effectiveness of the polymersomes. Prostate cancer is the most common cancer in men after skin malignancy in the United States. One out of seven men will be diagnosed with the prostate cancer in their lifetime.[74] Pancreatic ductal adenocarcinoma (PDAC) is the fourth leading cause of death in the United States with the approximate five-year survival rate of only 1%–7%.[97] Pancreatic cancer treatment is complicated because of invasiveness, rapid metastasis, and the complex nature of the disease. Considering that some cancers show early invasion and metastasis, there is an urgent need for developing new treatment options.

The following disquisition report three independent studies. The first chapter is published in the American Chemical Society journal ACS Omega. We are revising the manuscript describing the results discussed in Chapter 2 for the ACS journal Biomacromolecules. The manuscript for Chapter 3 is published in the Elsevier journal Colloids and Surfaces B: Biointerfaces.

In chapter 1, prostate-specific membrane antigen targeted polymersomes for delivering mocetinostat and docetaxel to prostate cancer cell spheroids, we prepared prostate-specific membrane antigen targeted polymersomes for delivering mocetinostat and docetaxel to prostate cancer cell spheroids. We studied the synergistic effect of the two drugs in prostate cancer cell lines.

In chapter 2, nucleus-targeted, echogenic polymersomes for delivering a cancer stemness inhibitor to pancreatic cancer cells, we prepared nucleus-targeted, echogenic polymersomes to deliver a cancer stemness inhibitor to pancreatic cancer cells. These polymersomes are echogenic, and we imaged them employing a high-frequency ultrasound instrument.

In chapter 3, peptide-targeted, stimuli-responsive polymersomes for delivering a cancer stemness inhibitor to cancer stem cell microtumors, we demonstrated the expression of nuropilin-1 receptor on prostate and pancreatic cancer stem cells. We also prepared peptide-targeted, stimuli-responsive polymersomes for delivering a cancer stemness inhibitor to cancer stem cell microtumors.

1. PROSTATE-SPECIFIC MEMBRANE ANTIGEN TARGETED POLYMERSOMES FOR DELIVERING MOCETINOSTAT AND DOCETAXEL TO PROSTATE CANCER CELL SPHEROIDS[1]

1.1. Abstract

Prostate cancer cells overexpress prostate-specific membrane antigen (PSMA) receptors on the surface. Targeting the PSMA receptor creates a unique opportunity for drug delivery. Docetaxel is an FDA approved drug for treating metastatic and androgen-independent prostate cancer, and mocetinostat is a potent inhibitor of the class I histone deacetylase. In this study, we prepared reduction-sensitive polymersomes presenting folic acid on the surface and encapsulating either docetaxel or mocetinostat. The presence of the folic acid allowed efficient targeting of the PSMA receptor and subsequent internalization of the polymeric vesicles in cultured LNCaP prostate cancer cell spheroids. The intracellular reducing agents efficiently released docetaxel and moctinostat from the polymersomes. The combination of the two drug-encapsulated polymersome formulation significantly ($p < 0.05$) decreased the viability of the LNCaP cells (compared to free drugs or control) in three-dimensional spheroid cultures. The calculated combination index (CI) value indicated a synergistic effect for the combination of moctinostat and docetaxel. Thus, a combination of our PSMA targeted drug-encapsulated polymersomes have the potential to lead to a new direction in prostate cancer therapy that decreases the toxicity and increases the efficacy of the drug delivery systems.

[1] The material in this chapter was co-authored by Fataneh Karandish, Manas Haldar, Seungyong You, and Sanku Mallik. Fataneh Karandish had primary responsibility to conduct all experiment listed in the section and analyze the data. Fataneh Karandish also drafted and revised all versions of this chapter. Manas Haldar had synthesized polymer. Seungyong You imaged polymersomes by AFM. Sanku Mallik served as proofreader and checked the math in the statistical analysis conducted by Fataneh Karandish.

1.2. Introduction

In the United States, prostate cancer is the most common carcinoma in men after skin malignancy.[98] Approximately one in seven men will be diagnosed with prostate cancer during their lifetime.[99] Surgery, radiation, and conventional chemotherapy are the common treatment options. However, in conventional chemotherapy, the anticancer drugs distribute throughout the body and destroy the normal cells as well as cancer cells, causing cytotoxicity and side effects.[19, 22] To increase the efficacy, a long-circulating drug delivery vehicle is needed which recognizes the cancer cells, and releases the contents in the cytosol. Various nanocarriers (e.g., polymeric micelles, liposomes, nanoparticle-aptamer, polymersomes, and nanoparticle delivering miRNA, siRNA, and cell penetrating peptide) have been developed for cancer treatment with varying degree of success.[25-32] Polymersomes are robust bilayer vesicles prepared from synthetic, amphiphilic block copolymers. The incorporation of polyethylene glycol (PEG) as the hydrophilic block renders the vesicles long circulating.[34] The bilayer of the polymersomes encapsulates hydrophobic drugs and the aqueous core incorporates the hydrophilic drugs.[34] The nanocarriers usually escape through the leaky vasculature and accumulate in the tumor due to the poor lymphatic drainage (termed as the enhanced permeation and retention effect, EPR).[38] After passive targeting by the EPR effect, interactions with a specific receptor on the cell surface enables cellular internalization of the nanocarriers via endocytosis.[19]

Prostate-specific membrane antigen (PSMA) is an extracellular transmembrane glycoprotein overexpressed in the malignant prostate tissue,[100] and responsible for the uptake of folic acid. [101]

The androgen-dependent LNCaP prostate cancer cell line expresses the PSMA receptor. However, the PC3 cells lose the expression of PSMA as the cancer progresses from the

androgen-dependent to the androgen-independent stage. [102, 103] Capromab pendetide (PSMA antibody) is the only prostate cancer imaging agent approved by the US FDA.[104] Mocetinostat (MGCD0103) is an aminophenyl benzamide histone deacetylase (class I enzymes) inhibitor. Mocetinostat induces hyperacetylation of histones and leads to apoptosis and cell cycle arrest in cancer cell lines and human tumor xenograft mouse model.[105] Currently, mocetinostat is used in the clinical trials as a monotherapy or as an adjuvant in many malignancies, although the mechanism is poorly understood.[106] Docetaxel belongs to the taxoid family and is extracted from the European yew tree.[107] It inhibits microtubule depolymerization, causes mitotic spindle poisoning, and block mitoses.[108] US FDA approved docetaxel in 2004 for the treatment of metastatic, androgen-independent prostate cancer.[109] Recently, we have reported that mocetinostat augments the activity of docetaxel to induce apoptosis. Mocetinostat upregulates the miR-31, decreases the anti-apoptotic protein E2F6, and induces apoptosis in prostate cancer cells and prostate cancer stem cells.[110]

Herein, we report a polymersome-based, PSMA-targeted, delivery system for prostate cancer, encapsulating either docetaxel or mocetinostat. We employed two FDA approved polymers to prepare the polymersomes: polyethylene glycol (PEG) as the hydrophilic block and the polylactic acid (PLA) as the hydrophobic block. We connected the two polymer blocks employing the reduction-sensitive disulfide linker. We observed that the targeted polymersomes are recognized by the PSMA receptor and internalized in the prostate cancer cells LNCaP. Subsequently, the intracellular environment reductively cleaves the disulfide bond, disturbs the polymersome bilayer structure, and efficiently releases the encapsulated drugs. We observed that the combination of the two drug-encapsulated, PSMA-targeted polymersome formulations

significantly *($p < 0.05$)* decreased the viability of the LNCaP cells (compared to free drugs or control) in three-dimensional spheroid cultures.

1.3. Experimental Section

The PEG-S-S-PLA was synthesized by ring opening polymerization as previously reported from our laboratory.[111] Briefly, PEG (MW:2000) was reacted with succinic anhydride then conjugated to cystamine dihydrochloride in the presence of EDC. The PLA polymer was subsequently synthesized from D, L-lactide and a catalytic quantity of octyl tin (II).

1.3.1. Preparation and characterization of polymersomes

The polymersomes were prepared by the solvent-exchange method[34] using the synthesized PEG_{2000}-SS-PLA_{6200} and the commercially available fluorescent lissamine rhodamine lipid [LR; 1,2-dipalmitoyl-*sn*-glycero-3-phosphoethanolamine-N-(lissamine rhodamine B sulfonyl) (ammonium salt)] in molar proportions of 95:5, respectively. The LR lipid was dissolved in chloroform (0.01 mg/mL). The polymer (0.9% w/v) was dissolved in tetrahydrofuran (THF). The chloroform was removed using a rotary evaporator to prepare a thin film. The polymer solution was added slowly to the thin film, and then the mixture was added dropwise to a stirred 10 mM HEPES buffer (pH 7.4). Polymersome solutions were stirred for 45 minutes at room temperature, and then air was passed for 45 minutes through the mixture to remove the organic solvent. The formed polymersomes were sonicated at 25 °C for 70 minutes (Symphony 117 V, 60 Hz). Subsequently, the polymersomes were passed through a Sephadex™ G100 (GE Healthcare) size exclusion column to collect dye encapsulated polymersomes. These polymersomes were used for the cell viability assays.

1.3.2. Preparation polymersomes encapsulating moctinostat or docetaxel (with and without PSMA targeting)

The nanovesicles were prepared by using PEG_{1900}-SS-PLA_{6000} polymer, DSPE-PEG_{2000}-Folate lipid, and the LR lipid in the molar proportions of 95:5:5, respectively. Mocetinostat and docetaxel were encapsulated into the polymersomes by the solvent exchanged method.[112] The non-targeted polymersomes encapsulating moctinostat or docetaxel were prepared the same way without using the DSPE-PEG_{2000}-Folate lipid. Briefly, the polymer and the lipid were dissolved in chloroform. Mocetinostat and docetaxel (0.125% w/v) were dissolved in THF. The two drugs were added to the polymer solutions in two different vials and slowly added to the solution of folate-conjugated lipid in two different vials. For the ease of visualization, the LR lipid was incorporated in the polymersomes encapsulating mocetinostat and carboxyfluoresein (100 µM) was encapsulated along with docetaxel in the other formulation. The resultant solutions were added dropwise to stirred HEPES buffer (10 mM, pH 7.4). Polymersomes were stirred for 45 minutes then air was passed through drug-loaded nanovesicles for another 45 minutes. The nanovesicles were sonicated at 25°C for 70 minutes (Symphony 117 V, 60 Hz). The polymersomes (1 mg/mL) were passed through the Sephadex™ G100 size exclusion column to remove the unencapsulated drug.

Drug loading efficacies (DLE) of the polymersomes were determined using UV−vis spectroscopy. After passing through the size-exclusion column, the absorption of the polymersomes was recorded at 230 nm. The calibration curves were generated for each drug separately. The DLE for Mocetinostat and Docetaxel were determined according to the following equation

$$DLE\ \% = \frac{mass\ of\ drug\ loaded\ into\ Polymersomes}{Total\ drug\ added} * 100$$

1.3.3. Size-distribution analysis

The size distributions of the polymersomes were conducted by dynamic light scattering method (DLS) employing the NanoZS 90 Zetasizer (Malvern Instruments). The measurements were conducted in disposable polystyrene cuvette at the scattering angle 90° (polymersomes concentration: 1mg/mL). The samples were equilibrated for two minutes; five repeats were recorded with 10 measurements for each sample.

1.3.4. Transmission electron microscopy

Copper TEM grids (300-mesh, formvar-carbon coated, Electron Microscopy Sciences, Hatfield, Pennsylvania, USA) were prepared by applying a drop of 0.01% poly-L-lysine, allowing it to stand for 30 seconds, wicking off the liquid with torn filter paper, and allowing the grids to air dry. A drop of the polymersomes was placed on the prepared grid for 30 seconds and wicked off; grids were allowed to air dry again. Phosphotungstic acid 0.1%, pH adjusted to 7-8, was dropped onto the grid containing the sample, allowed to stand for 2 min, and wicked off. After the grids were dry, images were obtained using a JEOL JEM-2100 LaB6 transmission electron microscope (JEOL USA, Peabody, Massachusetts) running at 200 keV.

1.3.5. Atomic force microscopy

Polymersomes (0.5 mg/mL) were diluted (10X) in 10 mM HEPES buffer (pH 7.4), dropped on silica substrates, and incubated for a minute and subjected to an air blow gun. The AFM measurements were conducted in non-contact mode at a resonance frequency of 145 kHz and scanning rate of 1.3 Hz and using an NT-MDT INTEGRA (NT-MDT America). The scanning areas were $5 \times 5\ \mu m^2$ at the resolution of 512 points per line, respectively.

1.3.6. Redox-triggered release study

The release of Mocetinostat from the PSMA-targeted polymersomes was monitored in the presence of glutathione (GSH). Polymersomes loaded with the drug (500 µL of 1 mg/mL solution) were dispensed into a dialysis tube (Spectra/Por Float-A-LyzerG2 Dialysis Tubes, MWCO: 500-1000 Da, diameter: 10 mm, volume: 1 mL). GSH was added after five minutes, and the concentration of GSH was increased every thirty minutes. The GSH concentrations were 2 µM (circulation levels of glutathione)[113], 50 µM (extracellular matrix level)[111], 1 mM, and 5 mM (cytosolic concentration of glutathione)[111] after the successive addition steps. The absorbance of the aqueous solution (at 230 nm) from the outside tube was measured every 5 minutes with a UV spectrophotometer (Spectramax M5, Molecular Devices). Subsequently, the percent release was calculated from the calibration curve.

1.3.7. Culture of human prostate carcinoma cells

The prostate cancer cell lines LNCaP and PC3 were purchased from ATCC. The cells were maintained in RPMI 1640 medium (without phenol red) supplemented with 1% v/v antibiotics (penicillin and streptomycin), 10% v/v fetal bovine serum, and 2.05 mM L-glutamate. The cell culture flasks were incubated at 37 °C in a 5% CO_2 atmosphere.

1.3.8. Cellular uptake of PSMA-targeted polymersomes

The cultured LNCaP cells (3×10^3) were seeded in an uncoated 8 well glass bottom plate for 24 hours before the experiment. When 90% confluent, the PSMA-targeted (20 µL) and the control polymersomes (20 µL) encapsulating carboxyfluorescein were incubated with the cells for 30 min. Subsequently, the media was removed, and the cells washed three times with Hanks' balanced salt solution (HBSS) to remove the non-internalized polymersomes. Subsequently, the cell nuclei were stained with HOESCHT 33342 dye (Enzo Life Sciences, 1 /1000 dilution) and

imaged employing a fluorescence microscope. The same experiment was repeated with 1 h incubation time with the polymersomes.

1.3.9. Cytotoxicity studies in monolayer cell cultures

The Alamar Blue assay was conducted to evaluate the viability of the human prostate carcinoma cells. The LNCaP and PC3 cells were seeded at a density of 1×10^3/200 µL in a 96-well tissue culture plate before the experiment, and were allowed to grow until 80-95% confluent. The plate was divided into six groups: control, free drugs, non-targeted polymersomes, non-targeted polymersomes encapsulating drugs, PSMA-targeted polymersomes, PSMA-targeted polymersomes encapsulating the drugs. Separately, similar experiments were conducted for mocetinostat and docetaxel. The control group did not receive any treatment. Cells treated with mocetinostat formulations received 5 µM, 10 µM, 20 µM of free and an equivalent amount of encapsulated drug. The docetaxel treatment group consisted at 1 nM, 5 nM, 10 nM of free drug, and the docetaxel-encapsulated polymersomes containing the same amounts of the drug. The cells were treated with the free or encapsulated drugs for 48 hours at 37° C, in a 5% CO_2 atmosphere. Subsequently, the cells were washed three times with sterile HBSS and replaced with 200 µL fresh media. The cell viability was determined using Alamar Blue assay following the manufacturer's protocol. Subsequently, we evaluated the effects of the combination of both drug formulations on the treated the cells using the same protocol. The data presented are normalized to the control.

1.3.10. Cytotoxicity studies in a three-dimensional spheroid cell culture

The LNCaP and PC3 cell spheroids were prepared by using 96-well 3D Petri Dishes (Microtissues). Briefly, 2% w/v agarose solution in water was prepared and autoclaved. The cell suspension (1×10^4 cell/60 µL media) was added to each 3D scaffold. The cells were allowed to

grow for 10 days to form the spheroids. The scaffold was then divided into six groups: control, non-targeted polymersomes, non-targeted polymersomes encapsulating drugs, targeted polymersomes, targeted polymersomes encapsulating mocetinostat or docetaxel. The spheroids were treated for 48 hours with the same concentration of drugs as used for the monolayers studies. Subsequently, the excess media was removed, and the spheroids were incubated with TryPLE (recombinant trypsin, Life Technologies, 100 µL) for 10 minutes. The dislodged spheroids were removed and subjected to the Alamar Blue assay. The data presented are normalized to the control.

1.3.11. Live-dead cellular assay

The LNCaP spheroids were prepared as described in the previous paragraph. The live-dead cellular assays were performed on the spheroids treated with a combination of Mocetinostat-encapsulated and Docetaxel-encapsulated PSMA-targeted polymersomes, PSMA-targeted polymersomes, polymersomes, free drugs, and control. After the treatment and washing, 160 µm thick slices of the spheroids were prepared using microtome HM 355 S. A commercially available live-dead assay kit (Calcein-AM/Ethidium homodimer-1, Biotium) for mammalian cells was used to image the live and the dead cells in each of the slices. We analyzed the images employing the Image J software. We selected three random regions and calculated the corrected total cell fluorescence (CTCF) using the formula:

CTCF = Integrated Density – (Area of selected cell × Mean fluorescence of background readings).

1.4. Results and discussion

1.4.1. Synthesis of the block copolymer and formation of polymersomes

To form the polymersomes, we synthesized amphiphilic block copolymers with the hydrophilic fraction (f) of 25%. We have previously demonstrated that 25% is the optimal amount of the hydrophilic polymer for forming the bilayer vesicles.[111] The reduction-sensitive polymer PEG_{2000}-SS-PLA_{2000} (Figure 1.1) was synthesized as reported previously.[111] We estimated the molecular weight of the synthesized polymer employing ^1H NMR spectroscopy. We expected the disulfide bond to cleave in the reducing microenvironment of the cell cytosol.

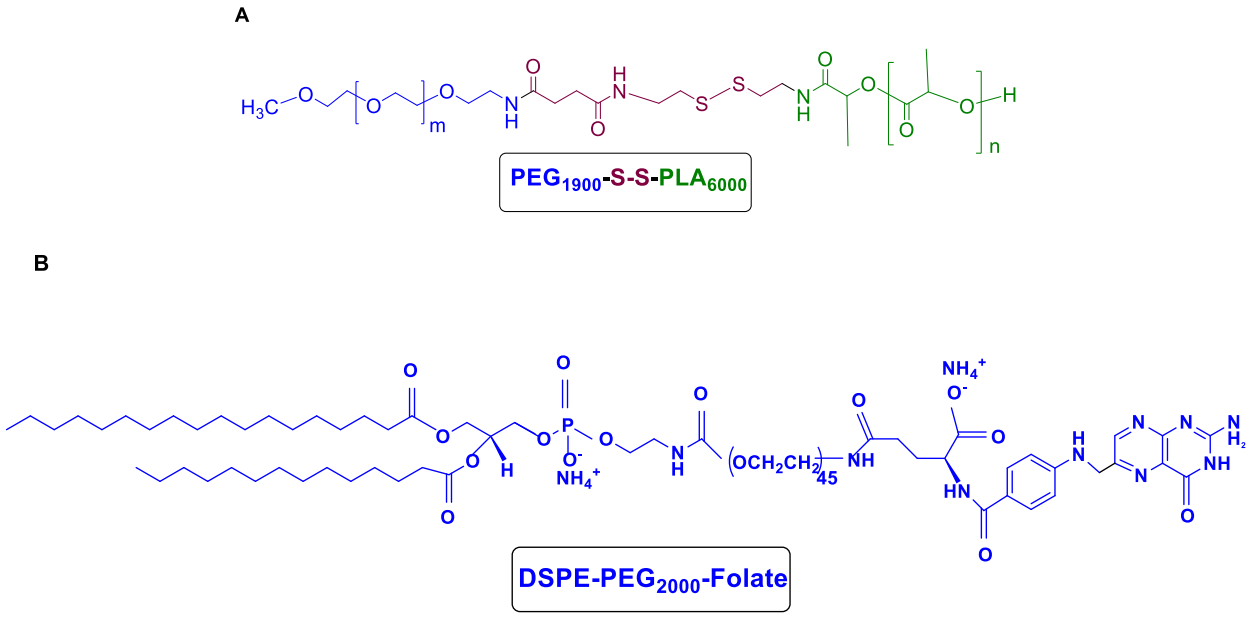

Figure 1.1. Structures of the synthesized amphiphilic polymer (**A**) and the commercially available DSPE-PEG-folate lipid (**B**).

Polymersomes were prepared by the solvent exchange method.[112] We incorporated 5 mol% of the DSPE-PEG_{2000}-Folate lipid in the polymersomes to target them to the prostate-specific membrane antigen (PSMA). PSMA is highly expressed in prostate cancer cells and hydrolyze folate.[100, 104] The size distribution and polydispersity index of prepared polymersomes were evaluated by dynamic light scattering (Table 1.1 and Figure 1.2). The morphology of

polymersomes was characterized by transmission electronic microscopy (TEM) and atomic force microscopy (AFM) (Figures 1.3, 1.4). We observed that the polymersomes incorporating the folate lipid were slightly larger in size (238 $\pm$ 2 nm) compared to the vesicles without the lipid (216 $\pm$ 4 nm, Table 1.1). Encapsulation of mocetinostat and docetaxel in the PSMA-targeted polymersomes increased the size of the nanovesicles, likely due to the accumulation of the drugs in the bilayer. The encapsulation efficiency for mocetinostat and docetaxel were 80% and 44% respectively. For ease of visualization, we incorporated 1 mol% of the fluorescent LR lipid in the bilayer of the polymersomes encapsulating mocetinostat. We encapsulated a small amount of the dye carboxyfluoresein in the docetaxel-encapsulated vesicles.

Table 1.1. Size and polydispersity index (PDI) of the polymersomes.

Formulations	**Particle Size Z-Average (nm)**	**Zeta Potential**	**PDI**
Polymeromes	216 ± 4	-5.92 ± 0.52	0.1 ± 0.03
PSMA-targeted polymersomes	238 ± 2	-4.87 ± 0.36	0.16 ± 0.02
Polymeromes encapsulating mocetinostat	220 ± 3	-5.02 ± 0.42	0.22 ± 0.02
PSMA-targeted polymersomes encapsulating moctinostat	271 ± 3	-8.06 ± 1.89	0.2 ± 0.01
Polymeromes encapsulating carboxyfluorescein	226 ± 7	-12.88 ± 2.4	0.3 ± 0.05
Polymersomes encapsulating docetaxel	218 ± 2	-5.36 ± 0.22	0.28 ± 0.01
PSMA-targeted polymersomes encapsulating carboxyfluorescein	220 ± 4	-6.77 ± 1.89	0.3 ± 0.03
PSMA-targeted polymersomes encapsulating docetaxel and carboxyfluorescein	251 ± 4	-4.75 ±1.02	0.24 ± 0.03

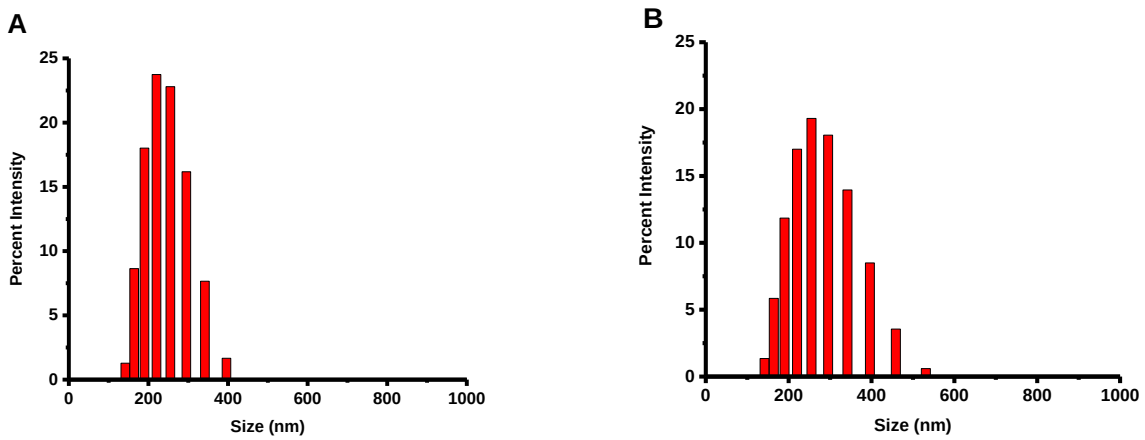

Figure 1.2. Size distribution of the polymersomes determined by dynamic light scattering. **(A)** PSMA-targeted polymersomes encapsulating docetaxel; **(B)** PSMA-targeted polymersomes encapsulating mocetinostat.

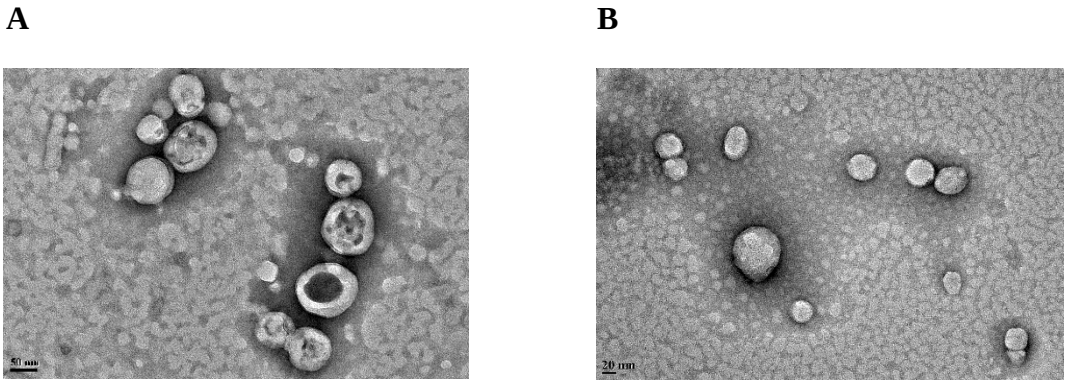

Figure 1.3. Transmission electron microscopic (TEM) images. **(A)** polymersomes encapsulating docetaxel (scale bar is 50 nm). **(B)** polymersomes encapsulating mocetinostat (scale bar is 20 nm).

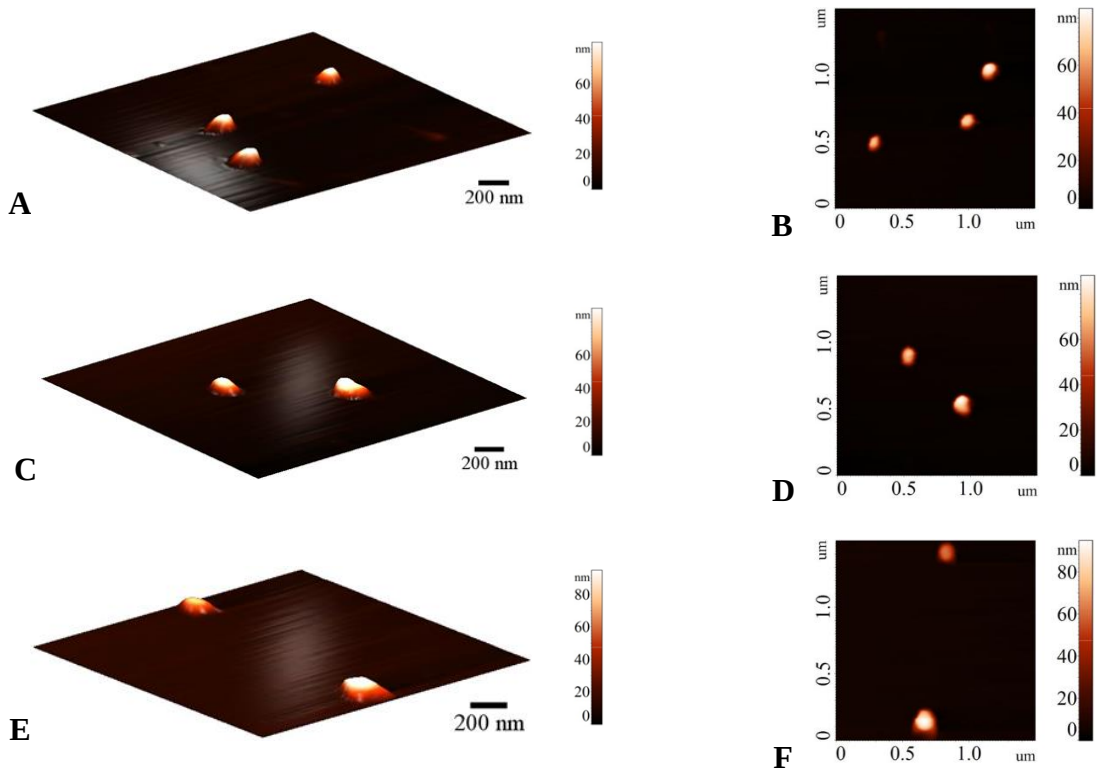

Figure 1.4. Atomic force microscopy (AFM) images of the polymersomes. (**A**, **B**) Polymersomes, (**C**, **D**) PSMA-targeted polymersomes encapsulating mocetinostat, and (**E**, **F**) PSMA-targeted polymersomes encapsulating docetaxel.

1.4.2. Demonstration of triggered contents release from the polymersomes

We encapsulated mocetinostat in the polymersomes and monitored the reduction-triggered release of the drug as a function of time with different concentrations of added glutathione (GSH). GSH is a tripeptide consisting of glutamic acid, cysteine, and glycine. The majority of GSH (90%) is available in the cytosol, and its increased level is correlated with progression, and proliferation of cancerous cells.[114] Treatment with circulation levels of glutathione (2 μM) released less than 1% of the drug in 30 minutes (Figure 1.5, black squares). We increased the concentration of GSH to match the extracellular matrix level (50 μM) and observed 10% release of encapsulated mocetinostat (Figure 1.5, red circles). The cytosolic concentration of glutathione (1-5 mM) led to substantial release (30 – 85%) of the encapsulated

drug from the polymersomes (Figure 1.5, blue triangles and magenta stars). Due to the very low amount of docetaxel encapsulated in the polymersomes (nanomolar concentration), we did not study the release profile from these vesicles in the presence of varying concentration of added reducing agents.

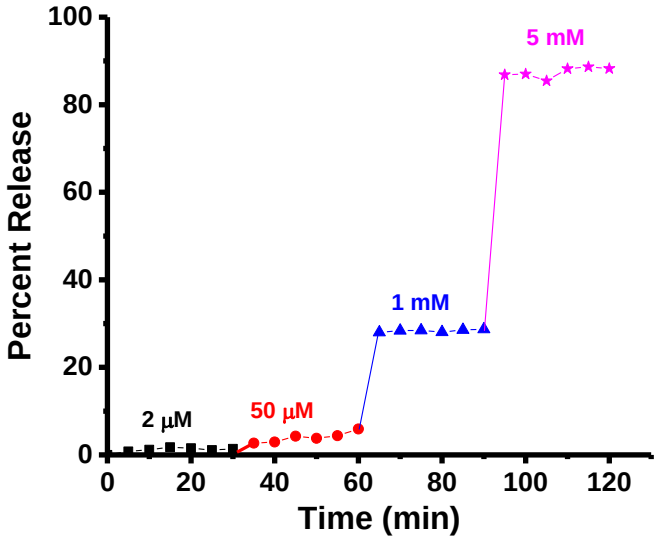

Figure 1.5. The reduction-mediated release profile of encapsulated mocetinostat from the polymersomes.
The drug encapsulated vesicles were treated with 2 μM (black squares), 50 μM (red circles), 1 mM (blue triangles), and 5 mM (pink stars) of GSH. The lines connecting the data points are also shown.

1.4.3. Uptake of the polymersomes in monolayer culture of prostate cancer cells

To demonstrate cytosolic localization in the prostate cancer cells, we prepared polymersomes incorporating 5% DSPE-PEG_{2000}-Folate in the bilayer. The LNCaP prostate cancer cells overexpress the PSMA receptor on the surface.[115] We incubated the cultured LNCaP cells with PSMA-targeted and non-targeted polymersomes (encapsulating carboxyfluorescein) for different times, washed the cells, and imaged them employing a fluorescence microscope (Figure 1.6). We observed higher localization of the targeted polymersomes after 1 hour of incubation with the LNCaP cells. We analyzed the images employing the Image J software. The

corrected total cell fluorescence (CTCF) intensity clearly indicated that the targeted polymersomes internalized more in the LNCap cells compared to the non-targeted vesicles (Figure 1.7).

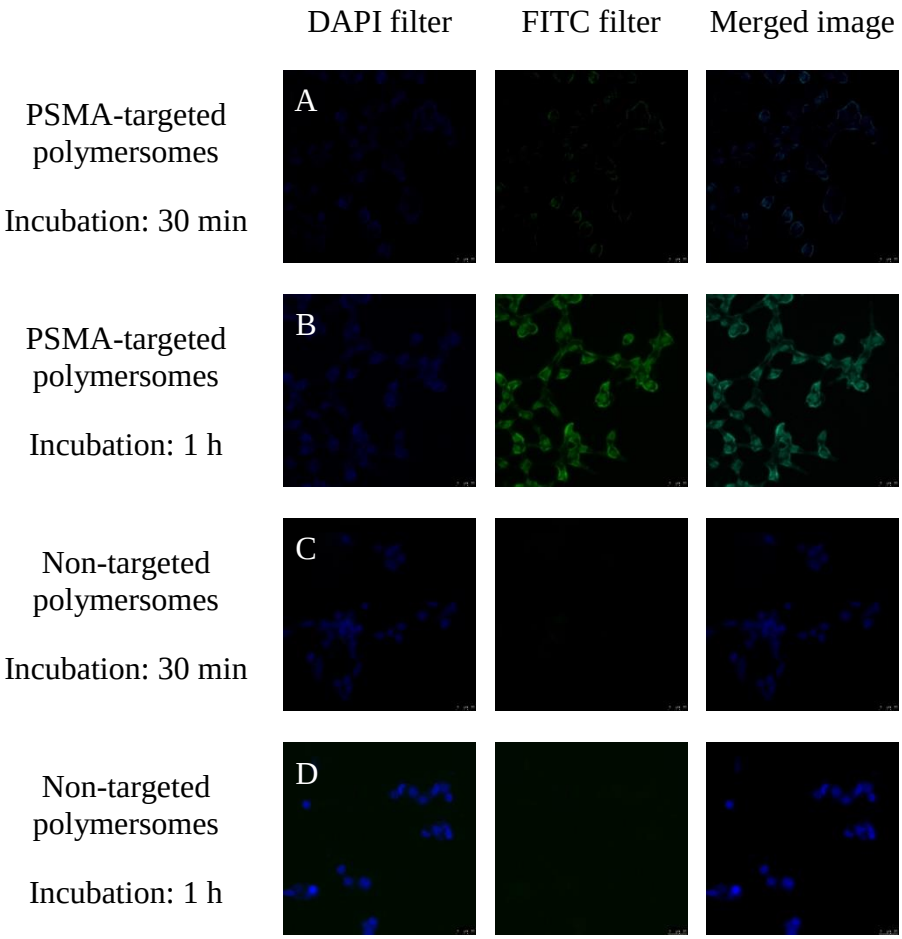

Figure 1.6. Fluorescence microscopic images of LNCaP cell incubated with the polymersomes. (Magnification: 20 X) The nuclei of the cells were stained with the Hoechst dye (blue image, DAPI filter). The polymersome images are green due to the encapsulated carboxyfluorescein (FITC filter). The merged images are shown in the third panel. (**A**) PSMA-targeted polymersomes after 30-minute incubation, (**B**) PSMA-targeted polymersomes after 1-hour incubation, (**C**) non-targeted polymersomes after 30-minute incubation, and (**D**) non-targeted polymersomes polymersomes after 1-hour incubation.

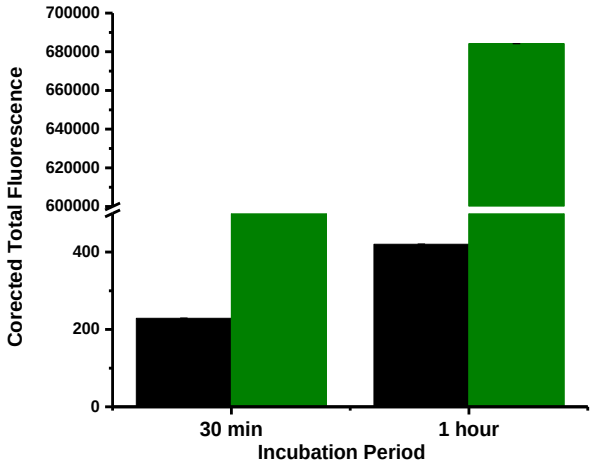

Figure 1.7. The corrected total cell fluorescence (CTCF).
Analysis of the images of LNCaP cells incubated with the PSMA-targeted polymersomes (green bars), and the non-targeted polymersomes (black bars).

After demonstrating efficient cellular internalization, we proceeded to determine the effectiveness of the PSMA-targeted drug-encapsulated polymersomes. We investigated the effect of targeted polymersomes on both PSMA-positive (LNCaP) and PSMA-negative (PC3) prostate cancer cell lines. The cultured LNCaP and PC3 cells were treated with the polymersomes formulations encapsulating mocetinostat or docetaxel and the free drugs for 48 hours. Subsequently, the cell viability was examined by the Alamar Blue assay since the reagents used for this assay do not interact with nanoparticles.[116] We observed that the PSMA-targeted polymersomes encapsulating mocetinostat (or docetaxel) significantly reduced ($p \leq 0.001$) the cell viability compared to the control (medium only) for the LNCaP cells. We also observed dose-dependent cellular toxicity for the drug-encapsulated polymersomes (Figure 1.8). As the concentration is increased, the PSMA-targeted, drug-encapsulated polymersomes showed higher toxicity to the LNCaP cells. For example, with 10 nM encapsulated docetaxel, the viability of the LNCaP cells decreased to 54% (Figure1. 8B). Interestingly, we also observed much less cellular toxicity in the PC3 cells, suggesting that the PSMA-targeted polymersomes encapsulating

moctinostat/docetaxel can internalize through the PSMA receptor on the LNCaP cells (Figure1. 9). Literature reports indicate that the PC3 cells express a small amount of the PSMA receptors on the surface, and the expression level is upregulated by basic fibroblast growth factor. [102]

After demonstrating the effects of the PSMA-targeted drug-encapsulated polymersomes, we proceeded to determine the synergistic effect of the two formulations encapsulating mocetinostat and docetaxel. The cells were treated with the combination of docetaxel and mocetinostat encapsulated vesicles as well as the appropriate controls. The results revealed significant ($p \leq 0.0001$) cytotoxicity for the combination formulation (5 nM docetaxel + 10 μM mocetinostat) compared to the controls for the LNCaP cells (Figure 1. 8C). However, we observed that the cell viability of the combination formulation was similar to that of the mixture of the two free drugs (Figure 1.8C). We note that the drug encapsulated polymersomes will be advantageous due to the passive targeting of the vesicles by the EPR effect, and the resultant reduced systemic toxicity. To determine any synergistic effects in the LNCaP cells, we calculated the combination index (CI) for combining the targeted polymersomes encapsulating mocetinostat and the targeted polymersomes encapsulating docetaxel employing the CalcuSyn software (www.biosoft.com). The CI values indicated that the combination formulation is synergistically reducing the viability of the LNCaP cells (Table 1.2). The drug-encapsulated polymersomes were significantly less toxic to the PC3 cells compared to the LNCaP cells. We did not observe enhanced cellular toxicity of the combination of the two drug-encapsulated polymersomes in the PC3 cells (Figure 1.9). Co-administration of PSMA-targeted polymersomes encapsulating mocetinostat and docetaxel significantly decreased the viability of the LNCaP cells ($p < 0.05$) compared to the PC3 cells in monolayer cultures.

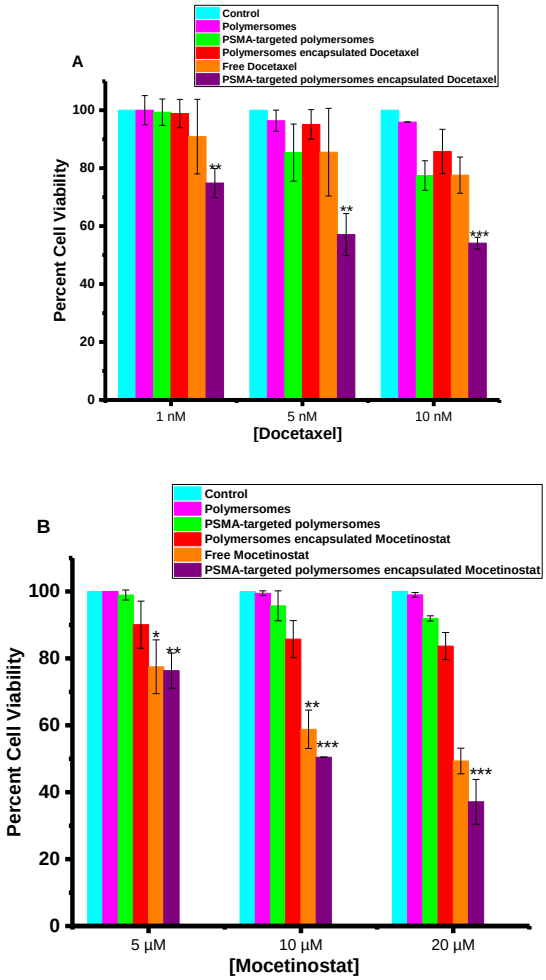

Figure 1.8. The viability of the LNCaP cells in the monolayer cultures.
(**A**) Cell viability with media only (control, cyan bar), non-targeted polymersomes (pink bar), on-targeted polymersomes encapsulating docetaxel (red bar), targeted polymersomes (green bar), free Docetaxel (orange bar), and targeted polymersomes encapsulating docetaxel (purple bar). (**B**) Cell viability with media only (control, cyan bar), non-targeted polymersomes (pink bar), non-targeted polymersomes encapsulating mocetinostat (red bar), targeted polymersomes (green bar), free mocetinostat (orange bar), and targeted polymersomes encapsulating mocetinostat (purple bar). (**C**) Cell viability with media only (control, cyan bar), non-targeted polymersomes (pink bar), non-targeted polymersomes encapsulating docetaxel/mocetinostat (red bar), targeted polymersomes (green bar), free docetaxel and mocetinostat (orange bar), and the combination of targeted polymersomes encapsulating docetaxel/mocetinostat (purple bar). The data presented are representative of three individual experiments. Error bars denote the mean ± SEM. Statistical analysis: Student's t-test where *$p < 0.05$, **$p < 0.001$, and ***$p < 0.0001$.

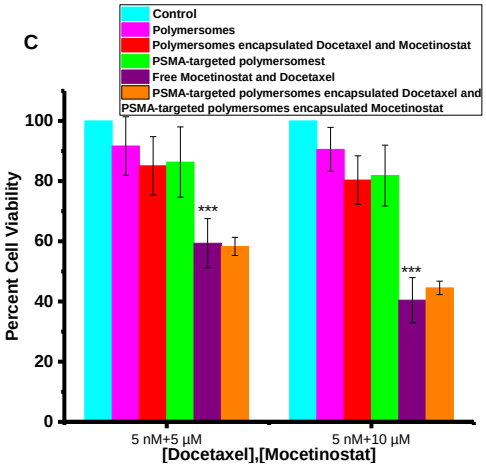

Figure 1.8. The viability of the LNCaP cells in the monolayer cultures. (continued) (**A**) Cell viability with media only (control, cyan bar), non-targeted polymersomes (pink bar), on-targeted polymersomes encapsulating docetaxel (red bar), targeted polymersomes (green bar), free Docetaxel (orange bar), and targeted polymersomes encapsulating docetaxel (purple bar). (**B**) Cell viability with media only (control, cyan bar), non-targeted polymersomes (pink bar), non-targeted polymersomes encapsulating mocetinostat (red bar), targeted polymersomes (green bar), free mocetinostat (orange bar), and targeted polymersomes encapsulating mocetinostat (purple bar). (**C**) Cell viability with media only (control, cyan bar), non-targeted polymersomes (pink bar), non-targeted polymersomes encapsulating docetaxel/mocetinostat (red bar), targeted polymersomes (green bar), free docetaxel and mocetinostat (orange bar), and the combination of targeted polymersomes encapsulating docetaxel/mocetinostat (purple bar). The data presented are representative of three individual experiments. Error bars denote the mean ± SEM. Statistical analysis: Student's t-test where *$p < 0.05$, **$p < 0.001$, and ***$p < 0.0001$.

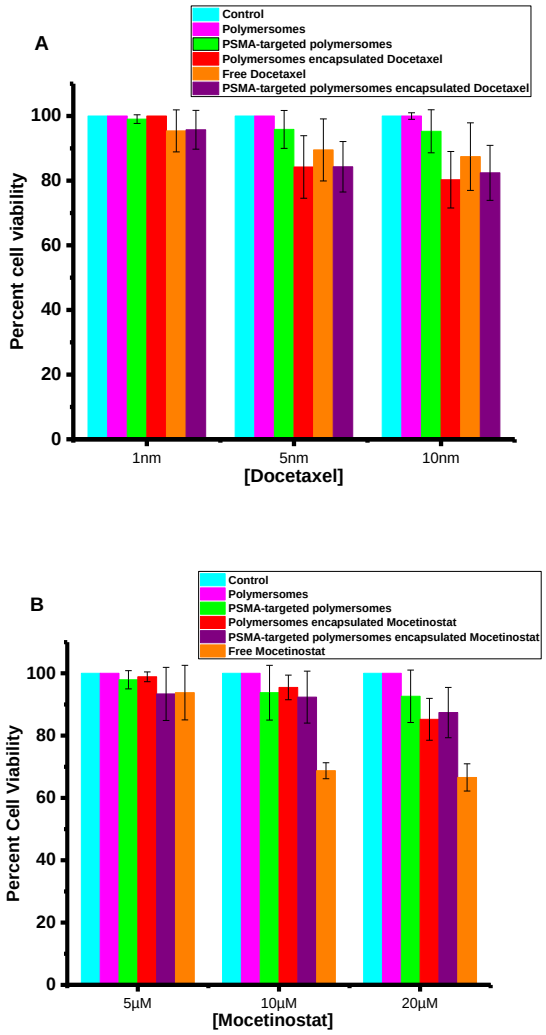

Figure 1.9. The viability of the PC3 cells in the monolayer cultures.
(**A**) Cell viability with media only (control, cyan bar), non-targeted polymersomes (pink bar), targeted polymersomes (green bar), non-targeted polymersomes encapsulating docetaxel (red bar), free docetaxel (orange bar), and targeted polymersomes encapsulating docetaxel (purple bar). (**B**) Cell viability with media only (control, cyan bar), non-targeted polymersomes (pink bar), targeted polymersomes (green bar), non-targeted polymersomes encapsulating mocetinostat (red bar), free mocetinostat (orange bar), and targeted polymersomes encapsulating mocetinostat (purple bar). (**C**) Cell viability with media only (control, cyan bar), non-targeted polymersomes (pink bar), targeted polymersomes (green bar), non-targeted polymersomes encapsulating docetaxel/mocetinostat (red bar), free docetaxel and mocetinostat (orange bar), and the combination of targeted polymersomes encapsulating docetaxel/mocetinostat (purple bar). Error bars denote the mean ± SEM.

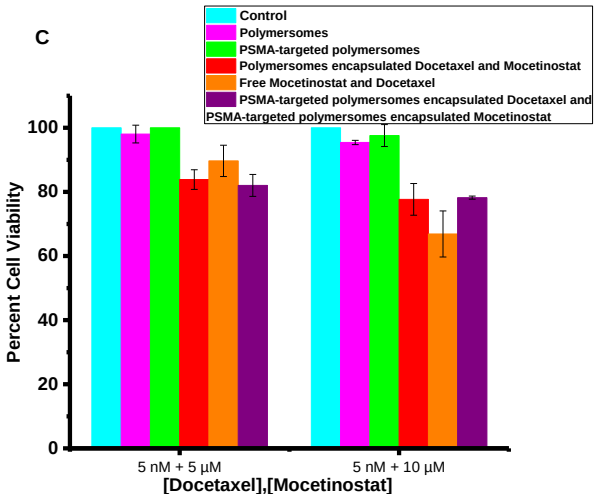

Figure 1.9. The viability of the PC3 cells in the monolayer cultures. (continued) (**A**) Cell viability with media only (control, cyan bar), non-targeted polymersomes (pink bar), targeted polymersomes (green bar), non-targeted polymersomes encapsulating docetaxel (red bar), free docetaxel (orange bar), and targeted polymersomes encapsulating docetaxel (purple bar). (**B**) Cell viability with media only (control, cyan bar), non-targeted polymersomes (pink bar), targeted polymersomes (green bar), non-targeted polymersomes encapsulating mocetinostat (red bar), free mocetinostat (orange bar), and targeted polymersomes encapsulating mocetinostat (purple bar). (**C**) Cell viability with media only (control, cyan bar), non-targeted polymersomes (pink bar), targeted polymersomes (green bar), non-targeted polymersomes encapsulating docetaxel/mocetinostat (red bar), free docetaxel and mocetinostat (orange bar), and the combination of targeted polymersomes encapsulating docetaxel/mocetinostat (purple bar). Error bars denote the mean ± SEM.

Table 1.2. The calculated combination index for the combination targeted polymersomes encapsulating Mocetinostat and the targeted polymersomes encapsulating Docetaxel in the LNCaP cells.

[Mocetinostat]	[Docetaxel]	Combination Index
5 µM	2 nM	0.45
10 µM	4 nM	0.29
20 µM	8 nM	0.19

1.4.4. Cytotoxicity in the three-dimensional spheroid cultures

Monolayer cell cultures do not adequately model prostate cancer due to the lack of cell-cell and cell-matrix interactions.[117] In contrast to the monolayer cultures, three-dimensional (3D) spheroids have intercellular interactions, necrotic cores, and heterogeneity that mimics the *in vivo* tumors.[118] To demonstrate the usefulness of our approach, we have tested the polymersomes on cultured, uniform-sized 3D spheroids of the LNCaP and PC3 cells. We prepared the spheroids using an agar mold, and after growing for 10 days incubated them with the polymersomes and the free drugs. Based on the results from the monolayer cultures of the LNCaP cells, we used 5 nM docetaxel and 10 mM mocetinostat (either free or polymersome-encapsulated) in the spheroids of LNCaP and PC3 cells. We observed enhanced cytotoxicity (by the Alamar Blue assay) of the polymersome-encapsulated mocetinostat (or docetaxel) compared to the control or the unencapsulated drugs (Figures 1.10A and 1.10B). We also observed that the combination of the two drugs encapsulated polymersomes was more potent compared to either mocetinostat or docetaxel (free or encapsulated in the vesicles, Figure 1.10C). The combination decreased the cell viability to 39% in the LNCaP spheroids (Figure 1.10 C, purple bar). The

effect of the drug encapsulated polymersomes were significantly less in the spheroids of the PC3 cells (Figure 1.11) compared to the LNCaP cells ($P < 0.001$).

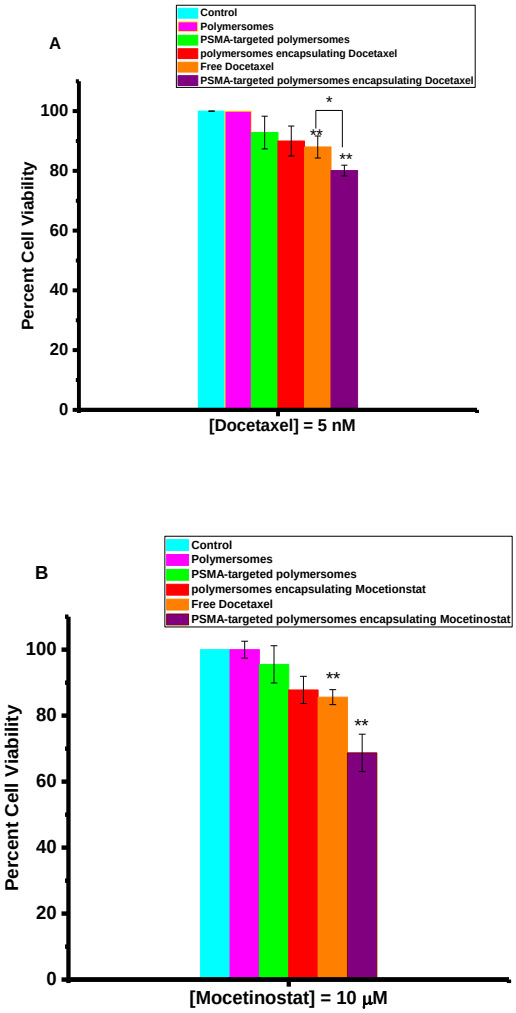

Figure 1.10. The viability of LNCaP cells in 3D spheroid cultures.
(**A**) The Docetaxel encapsulated, targeted polymersomes (purple bar) was more potent compared to the free drug (orange bar), the targeted vesicles without any drug (green bar), non-targeted polymersomes without any drug (pink bar), and the media (cyan bar). (**B**) The mocetinostat encapsulated, targeted polymersomes (purple bar) was more potent compared to the free drug (orange bar), the targeted vesicles without any drug (green bar), non-targeted polymersomes without any drug (pink bar), and the media (cyan bar). (**C**) The combination of docetaxel/mocetinostat encapsulated, targeted polymersomes (purple bar) was more potent compared to the free drug (orange bar), the targeted vesicles without any drug (green bar), non-targeted polymersomes without any drug (pink bar), and the media (cyan bar). The data presented are representative of three individual experiments. Error bars denote the mean ± SEM. Statistical analysis: Student's t-test where *$p < 0.05$, **$p < 0.001$, and ***$p < 0.0001$.

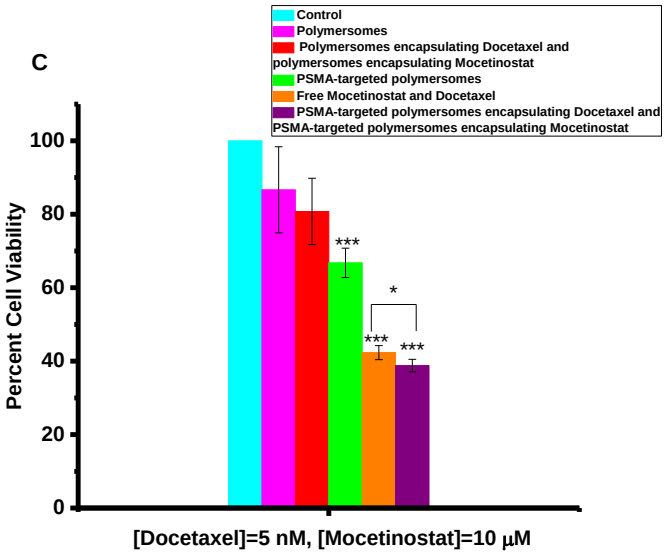

Figure 1.10. The viability of LNCaP cells in 3D spheroid cultures. (continued) (**A**) The Docetaxel encapsulated, targeted polymersomes (purple bar) was more potent compared to the free drug (orange bar), the targeted vesicles without any drug (green bar), non-targeted polymersomes without any drug (pink bar), and the media (cyan bar). (**B**) The mocetinostat encapsulated, targeted polymersomes (purple bar) was more potent compared to the free drug (orange bar), the targeted vesicles without any drug (green bar), non-targeted polymersomes without any drug (pink bar), and the media (cyan bar). (**C**) The combination of docetaxel/mocetinostat encapsulated, targeted polymersomes (purple bar) was more potent compared to the free drug (orange bar), the targeted vesicles without any drug (green bar), non-targeted polymersomes without any drug (pink bar), and the media (cyan bar). The data presented are representative of three individual experiments. Error bars denote the mean ± SEM. Statistical analysis: Student's t-test where *$p < 0.05$, **$p < 0.001$, and ***$p < 0.0001$.

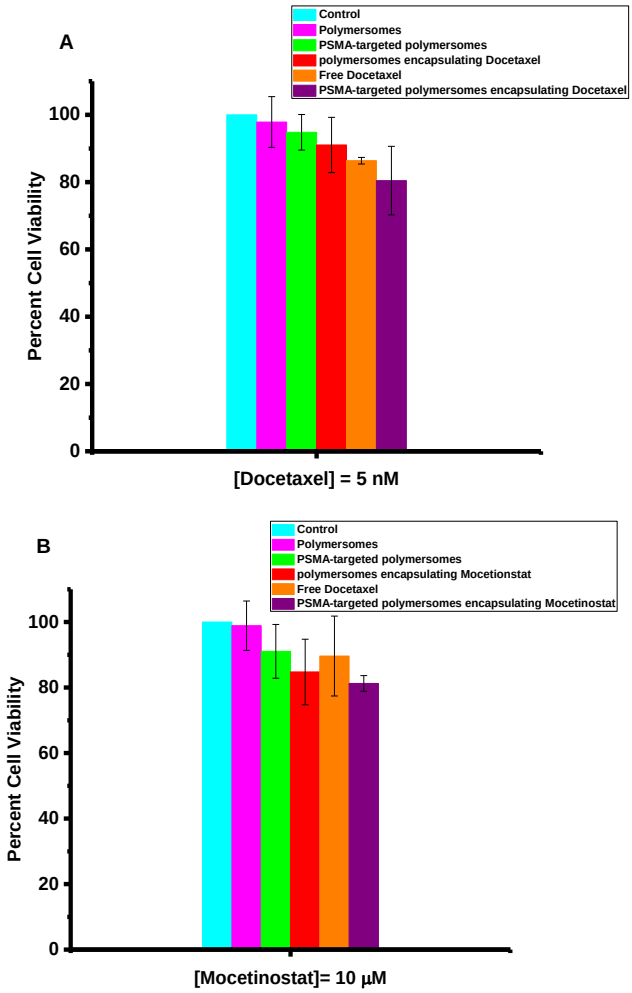

Figure 1.11. The viability of PC3 cells in 3D spheroid cultures.
(A) The docetaxel encapsulated, targeted polymersomes (purple bar) was more potent compared to the free drug (orange bar), the targeted vesicles without any drug (green bar), non-targeted polymersomes encapsulated docetaxel (red bar), non-targeted polymersomes without any drug (pink bar), and the media (cyan bar). (B) The mocetinostat encapsulated, targeted polymersomes (purple bar) was more potent compared to the free drug (orange bar), the targeted vesicles without any drug (green bar), non-targeted polymersomes encapsulated mocetinostat (red bar), non-targeted polymersomes without any drug (pink bar), and the media (cyan bar). (C) The combination of docetaxel/mocetinostat encapsulated, targeted polymersomes (purple bar) was as potent as compared to the free drug (orange bar), and non-targeted polymersomes encapsulated docetaxel /moctinostat (red bar) Targeted vesicles without any drug (green bar), non-targeted polymersomes without any drug (pink bar), and the media (cyan bar). The data presented are representative of three individual experiments. Error bars denote the mean ± SEM. The data presented are representative of three individual experiments. Error bars denote the mean ± SEM. Statistical analysis: Student's t-test where *$p < 0.05$, **$p < 0.001$, and ***$p < 0.0001$.

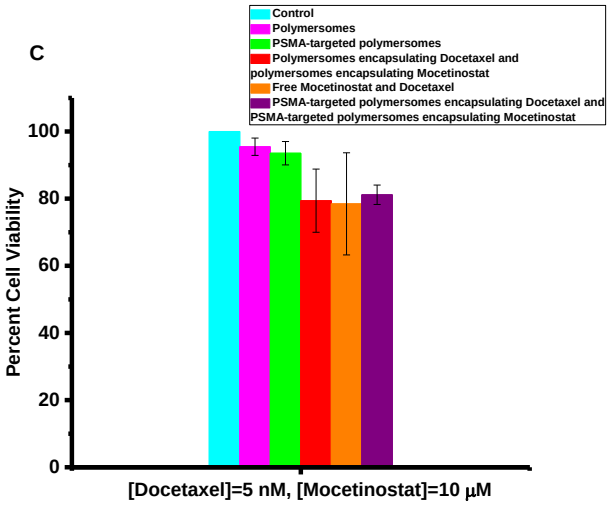

Figure 1.11. The viability of PC3 cells in 3D spheroid cultures. (continued) (**A**) The docetaxel encapsulated, targeted polymersomes (purple bar) was more potent compared to the free drug (orange bar), the targeted vesicles without any drug (green bar), non-targeted polymersomes encapsulated docetaxel (red bar), non-targeted polymersomes without any drug (pink bar), and the media (cyan bar). (**B**) The mocetinostat encapsulated, targeted polymersomes (purple bar) was more potent compared to the free drug (orange bar), the targeted vesicles without any drug (green bar), non-targeted polymersomes encapsulated mocetinostat (red bar), non-targeted polymersomes without any drug (pink bar), and the media (cyan bar). (**C**) The combination of docetaxel/mocetinostat encapsulated, targeted polymersomes (purple bar) was as potent as compared to the free drug (orange bar), and non-targeted polymersomes encapsulated docetaxel /moctinostat (red bar) Targeted vesicles without any drug (green bar), non-targeted polymersomes without any drug (pink bar), and the media (cyan bar). The data presented are representative of three individual experiments. Error bars denote the mean ± SEM. The data presented are representative of three individual experiments. Error bars denote the mean ± SEM. Statistical analysis: Student's t-test where *$p < 0.05$, **$p < 0.001$, and ***$p < 0.0001$.

To determine the penetration depth and the effect of the drug encapsulated polymersomes, we sliced (160 μm thick) the treated, LNCaP cell spheroids using a microtome (Figure 1.12). We imaged the spheroid slices using a commercially-available live-dead cell imaging kit. The live cells hydrolyze the calcein-AM dye to calcein (green fluorescence).[119] Ethidium homodimer-1 passes through the membranes of damaged cells, bind to the DNA, and emit a red fluorescence.[119] We observed that co-treatment of the spheroids with mocetinostat- and docetaxel-encapsulated, targeted polymersomes lead to primarily dead cells (Figure1.13, Panels A and B). The cells in the control spheroids (without any treatment) were alive,

producing the green fluorescence (Figure 1.13, Panels C and D). The corrected total cell fluorescence (CTCF) was calculated using software ImageJ (Figure 1.14). The analysis indicated that the control spheroid slices contain primarily live cells, while the treated slices have mainly the dead cells.

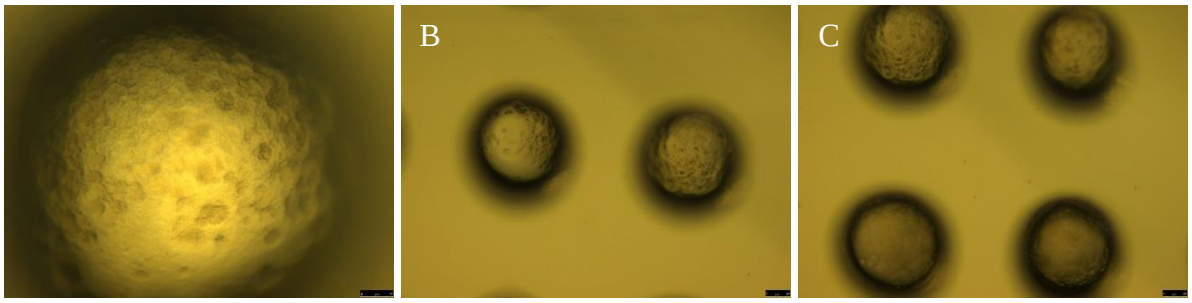

Figure 1.12. Optical images of the slices from the 3D spheroids of LNCaP cells. (scale bars: 25 μm) Bright field images of the LNCaP cell spheroids in 20X (**A**), 10X (**B**), and 4X (**C**) magnifications. The 3D spheroids were treated with the combination of PSMA-targeted polymersomes encapsulating docetaxel (5 nM)/moctinostat (10 μM).

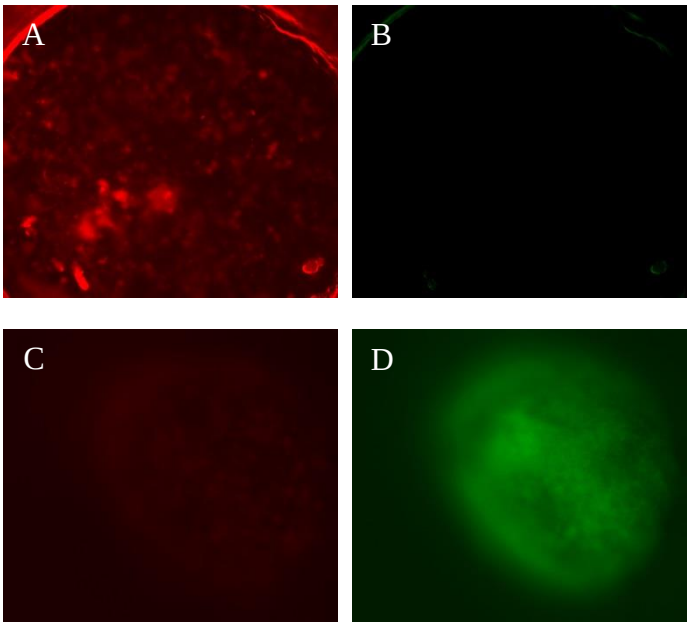

Figure 1.13. Live-dead cell assays for slices of LNCaP cell spheroids. Treatment of the LNCaP spheroids with m ocetinostat (10 μM) and docetaxel (5 nM) encapsulated, targeted polymersomes, produces primarily dead cells (**A**) with very few live cells (**B**). The Control sample showed a few dead cells (**C**) and mainly live cells (**D**).

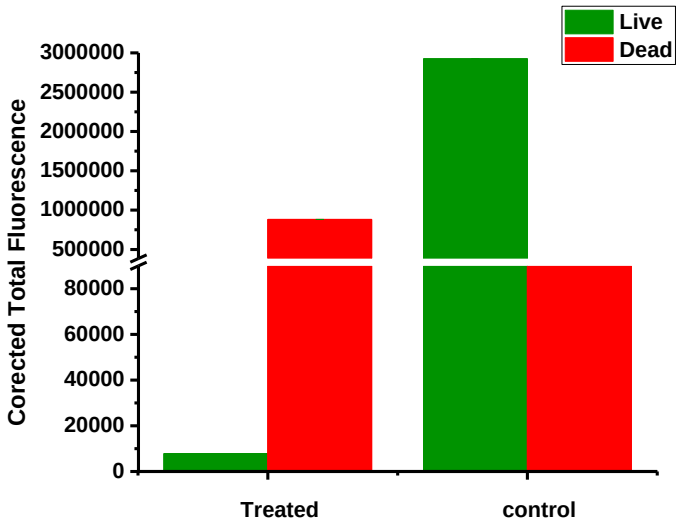

Figure 1.14. The corrected total cell fluorescence (CTCF) analysis of the spheroid slices after live-dead assay. The LNCaP spheroids were treated with mocetinostat (10 µM) and docetaxel (5 nM) encapsulated PSMA-targeted polymersomes. The green bars indicate the intensity of images for the live cells and red bars indicate the intensity of the images for the dead cells.

1.5. Conclusions

We have prepared polymersomes from the synthesized, amphiphilic polymers containing PEG as the hydrophilic block. We have successfully demonstrated that the prostate-specific membrane antigen can be used to target the polymersomes actively to prostate cancer cells. After internalization, the high amount of reducing agent in the cytosol triggers the release of encapsulated hydrophobic drugs from the polymersomes. A combination of PSMA-targeted vesicles encapsulating mocetinostat and docetaxel reduced the viability of LNCaP prostate cancer cells (expressing the PSMA receptor) in three-dimensional spheroid cultures. The combination index value (CI < 1) indicated that combination of mocetinostat and mocetaxel-encapsulated polymersomes had a synergistic effect in reducing the viability of the prostate cancer cells. Our imaging analysis confirmed that the combination of the two drug-encapsulated polymersomes primarily kills the cancer cells. We expect our results will motivate further research into stimuli-responsive, targeted polymersomes and the use of 3D cellular models for testing the cytotoxicity of drug formulations.

2. NUCLEUS-TARGETED, ECHOGENIC POLYMERSOMES FOR DELIVERING A CANCER STEMNESS INHIBITOR TO PANCREATIC CANCER CELLS[2]

2.1. Abstract

Chemotherapeutic agents for treating cancers show considerable side effects, toxicity, and drug resistance. To mitigate the problems, we designed nucleus-targeted, echogenic, stimuli-responsive polymeric vesicles (polymersomes) to transport and subsequently release the encapsulated anti-cancer drugs within the nuclei of pancreatic cancer cells. We synthesized an alkyne-dexamethasone derivative and conjugated it to N_3–polyethylene glycol (PEG)–polylactic acid (PLA) copolymer employing the Cu^{2+} catalyzed "Click" reaction. We prepared polymersomes from the dexamethasone-PEG-PLA conjugate along with a synthesized stimuli-responsive polymer PEG–S–S–PLA. The dexamethasone group dilates the nuclear pore complexes and transports the vesicles to the nuclei. We designed the polymersomes to release the encapsulated drugs in the presence of a high concentration of reducing agents in the nuclei of pancreatic cancer cells. We observed that the nucleus-targeted, stimuli-responsive polymersomes released 70% of encapsulated contents in the nucleus-mimicking environment in 80 minutes. We encapsulated the stemness inhibitor BBI608 in the vesicles and observed that the BBI608 encapsulated polymersomes reduced the viability of the BxPC3 cells to 43% in three-dimensional spheroid cultures. The polymersomes were prepared following a special protocol so that they scatter ultrasound, allowing imaging by a medical ultrasound scanner. Therefore, these

[2] The material in this chapter was co-authored by Fataneh Karandish, Lang Xia, Kausik Sarkar, and Sanku Mallik. Fataneh Karandish had primary responsibility to conduct all experiment listed in the section and analyze the data. Fataneh Karandish also drafted and revised all versions of this chapter. Characterization of echogenic polymersomes was performed by Lang Xia. Sanku Mallik and Kausik Sarkar served as proofreader and checked the math in the statistical analysis conducted by Fataneh Karandish and Lang Xia.

echogenic, targeted, stimuli responsive, drug-encapsulated polymersomes have the potential as a trackable, targeted carrier of chemotherapeutic drugs to cancer cell nuclei.

2.2. Introduction

Pancreatic ductal adenocarcinoma (PDAC) is the fourth leading cause of death in the United States with an approximate five-year survival rate of only 1%–3%.[97] Pancreatic cancer treatment is complicated because of its invasiveness, rapid metastasis, and the complex nature of the disease. Alteration of different genes, aberrant biochemical pathways, epithelial to mesenchymal transition (EMT), a hypoxic tumor microenvironment, and the subpopulation of cancer stem cells lead to recurrence and drug resistance.[7] Considering that pancreatic cancer shows early invasion and metastasis, there is an urgent need for developing new treatments for this devastating disease. In the solid tumor tissue, EMT leads to a subpopulation of cancer stem cells, which can initiate a tumor, self-renew, and increase resistance to chemotherapeutic drugs.[120] The small molecule napabucasin (BBI608) inhibits gene transcription of STAT3, reduces the expression of cancer stemness markers, and inhibits cell proliferation and apoptosis in both cancer stem cells and non-stem cells.[7, 120] BBI608 is currently in Phase III clinical trials as an adjuvant therapy for a variety of solid tumors, including pancreatic cancer (www.clinicaltrials.gov).

Targeted, stimuli-responsive drug carriers have the potential to enhance therapeutic efficacy and reduce off target toxicity by selectively delivering the cytotoxic chemotherapeutic drugs to cancerous tissues.[81] Polymersomes are vesicles prepared from synthetic, amphiphilic block copolymers. Because of higher molecular weights, polymersomes have enhanced stability and mechanical robustness compared to liposomes, micelles, and polymer micelles. The bilayer of the polymersomes encapsulate hydrophobic drugs, and the aqueous core incorporates the

hydrophilic molecules. Polymersomes responsive to pH [121], heat [83], hypoxia [122], and light [82] have been used to deliver chemotherapeutic drugs to the cancerous cells. The polymeric nanoparticles accumulate in the tumor tissues by the enhanced permeation and retention effect [123]; however, for efficient cellular internalization, specific ligands are necessary on the vesicle surface.

Nuclear pore complex is a large multi-protein assembly, which spans the nuclear envelope. Approximately 2000 nuclear pore complexes exist in the nuclear envelope. Dexamethasone is a synthetic steroid that dilates the nuclear pore complex from 38 nm to 300 nm. [123, 124] Glutathione (GSH), the abundant cellular reducing agent, is a tripeptide consisting of glutamic acid, cysteine, and glycine. GSH is involved in several important processed in the cell nuclei, such as transcription, DNA replication, nuclear protein import and export, and chromatin stability. [125, 126] High levels of GSH are related to increased cell proliferation. [126]

Herein, we report nucleus-targeted, echogenic, redox-sensitive polymersomes to deliver the cancer stemness inhibitor BBI608 to pancreatic cancer cells. We have used dexamethasone as a targeting group to dilate the nuclear pore complexes [123] and deliver the polymersomes inside the nucleus. In the synthesized copolymer, we used polyethylene glycol (PEG) as the hydrophilic block and polylactic acid (PLA) as the hydrophobic block. The two polymer blocks were linked by a reduction sensitive disulfide linker. We observed that the vesicles, presenting dexamethasone on the surface, internalize in the nuclei of pancreatic cancer cells. The high reducing agent concentration in the nuclei [127] cleaves the disulfide bonds of the polymers, compromises the polymersome structure, and rapidly releases the encapsulated drug. We observed that nucleus-targeted polymersomes encapsulating BBI608 significantly ($p < 0.05$) decreased the viability in the BxPC3 cells compared to control and the non-targeted vesicles. The polymersomes were shown to be responsive to ultrasound offering the possibility of

concurrent ultrasound imaging of the cancerous tumor. We have used a preparation protocol incorporating lyophilization in the presence of mannitol that has proved previously effective in rendering liposomes [128-133] and polymersomes [37] echogenic.

2.3. Materials and methods

All chemicals and solvents were purchased either from VWR International or TCI America and used as received.

2.3.1. Synthesis of alkyne-dexamethasone

Dexamethasone (100 mg, 0.26 mmol) was dissolved in anhydrous pyridine (2 mL) in a round bottom flask and stirred on ice (0 °C) with methane sulfonyl chloride (250 µL, 3.2 mmol) under nitrogen for four hours. Then, an additional amount of methane sulfonyl chloride (18 µL, 0.23 mmol) was added, and the reaction continued for an additional hour. After five hours of stirring under nitrogen, 40 mL of ice water was added to precipitate the product. The precipitate was filtered and washed with 40 mL of additional ice water. The crude product was purified by recrystallization from tetrahydrofuran (THF) twice to afford the pure product. The product (0.026g, 0.06 mmol) and propargyl amine (0.10 mL, 1.561 mmol), was stirred in 800 µL dimethylformamide (DMF) at 65 °C under nitrogen gas for two hours. After cooling to room temperature, the product was purified by automated flash chromatography using dichloromethane and methanol in silica gel (Rf = 0.3). The pure product (16 mg, 62%) was characterized by 1H NMR spectroscopy. 1H NMR (400 MHz, CHLOROFORM-d) δ = 7.37 - 7.28 (m, 1H), 6.46 - 6.37 (m, 3H), 6.23 - 6.17 (m, 3H), 4.63 (d, J = 19.8 Hz, 2H), 4.43 - 4.30 (m, 5H), 4.27 (s, 2H), 3.99 (s, 4H), 3.52 (s, 4H), 3.41 (d, J = 1.5 Hz, 2H), 3.10 (td, J = 3.6, 7.3 Hz, 4H), 2.73 - 2.53 (m, 5H), 2.51 - 2.33 (m, 9H), 2.27 (s, 1H), 2.24 - 2.15 (m, 3H), 2.11 (s, 1H),

1.99 - 1.72 (m, 8H), 1.65 - 1.56 (m, 6H), 1.54 - 1.35 (m, 4H), 1.34 - 1.20 (m, 6H), 1.13 - 1.02 (m, 8H), 1.02 - 0.87 (m, 8H).

HRMS calcd. for C25 H32FNO4: 429.2315. Observed: 429.2406

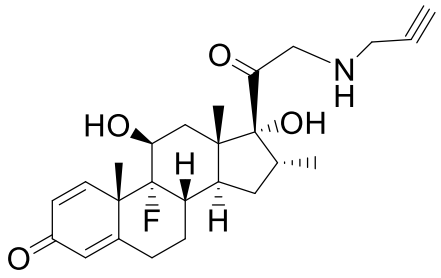

Figure 2.1. Structure of the synthesized alkyne conjugated dexamethasone

2.3.2. Synthesis of dexamethasone–PEG_{1900}–PLA_{6000} polymer conjugate

We synthesized N_3–PEG_{1900}–PLA_{6000} polymer (supporting information A). The alkyne-dexamethasone was reacted with the N_3–PEG_{1900}–PLA_{6000} polymer using the [2+3]-cycloaddition reaction.[134] Briefly, we prepared the copper (II) complex by mixing the $CuSO_4$ (71.3 mg in 3 mL water, 0.53 mmol) and pentamethyl diethylenetriamine (440 μL in 3 mL water, 2 mmol). The N_3–PEG_{1900}–PLA_{6000} polymer (20 mg) and alkyne-dexamethasone (2 mg) were dissolved in 6 mL tetrahydrofuran (THF), 400 μL of the 53 mM copper complex and 400 μL of 53 mM aqueous sodium ascorbate solution were added, and the reaction mixture was stirred at room temperature for 24 hours. The clear blue solution was dialyzed against THF in a dialysis cassette (molecular weight cut off: 1000) for 48 hours, and freeze-dried. The product was characterized by ^{1}H NMR (Supporting Information). ^{1}H NMR (400 MHz, CHLOROFORM-d) δ = 8.01 - 8.01 (m, 1H), 6.34 (br s, 1H), 6.15 (br s, 1H), 5.43 - 5.04 (m, 22H), 4.47 - 4.25 (m, 1H), 3.66 (s, 38H), 2.61 - 2.44 (m, 1H), 2.28 (td, *J* = 7.5, 15.3 Hz, 1H), 1.33 - 1.16 (m, 5H), 0.85 (br s, 5H).

The PEG_{1900}–S–S–PLA_{6000} polymer was synthesized by protocols developed in our laboratory.[74]

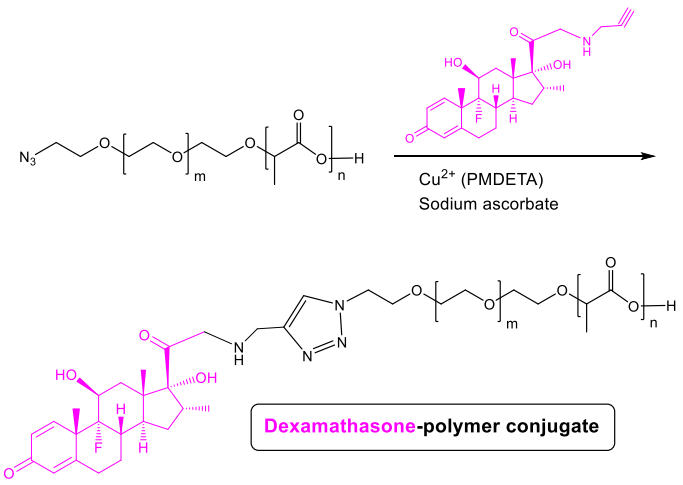

Scheme 2.1. [2+3]-cycloaddition reaction of N3-PEG$_{1900}$-PLA$_{6000}$ polymer and alkyne-dexamethasone

2.3.3. Preparation of nucleus targeted polymersomes encapsulating BBI608

Polymersomes were prepared by the solvent exchange method [135] with PEG$_{1900}$–S–S–PLA$_{6000}$, dexamethasone–PEG$_{1900}$–PLA$_{6000}$ polymer, and 1,2-dipalmitoyl-*sn*-glycero-3-phosphoethanolamine-N-lissamine rhodamine B sulfonyl ammonium salt (fluorescent dye, LR, Avanti Polar Lipids) with a molar ratio of 35:60:5, respectively (Figure 2.1). The polymers were dissolved in THF (9 mg/mL), BBI608 in THF (3 mg/mL), and LR in chloroform (0.01 mg/mL). First, a rotary evaporator was used to evaporate the chloroform from LR lipid to form a thin layer film. The THF solutions of the polymers and BBI608 were added to the thin film. The resultant fluorescent THF solution was added dropwise to an aqueous HEPES buffer (10 mM, pH 7.4) and stirred for 45 minutes. To remove the THF, a gentle stream of air was passed through the mixture for 45 minutes. The polymersomes formed were bath sonicated for 60 minutes (Symphony 117 V, 60 Hz, Power level 9). The polymersomes (1 mg/mL) were passed through a Sephadex^{TM} G-100 size exclusion column to remove the unencapsulated drug. Drug loading efficacies (DLE) of the polymersomes were determined using UV−Vis spectroscopy. After passing through the size-exclusion column, the absorption of the polymersomes was recorded at 235 nm.

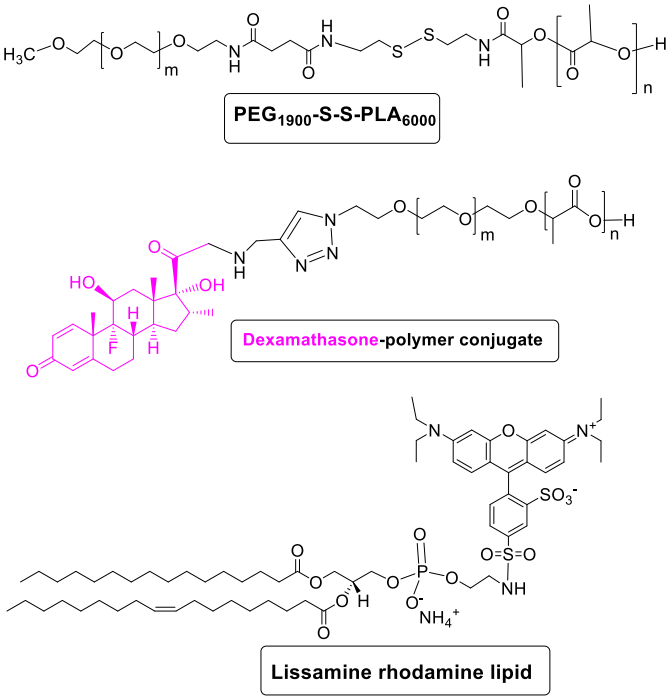

Figure 2.2. The structure of synthesized polymers.
PEG_{1900}–S–S–PLA_{6000}, dexamethasone–PEG_{1900}–PLA_{6000} polymer conjugate, and the commercially available fluorescent lipid 1,2-dipalmitoyl-*sn*-glycero-3-phosphoethanolamine-N-lissamine rhodamine B sulfonyl ammonium salt.

2.3.4. Preparation of control polymersomes

The control polymersomes were prepared following the same method as the nucleus-targeted vesicles. PEG_{1900}–S–S–PLA_{6000}, N_3–PEG_{1900}–PLA_{6000}, and lissamine rhodamine (LR) were used in the molar ratio of 35:60:5, respectively. The PEG_{1900}–S–S–PLA_{6000} and N_3–PEG_{1900}–PLA_{6000} polymers were dissolved in THF. The polymer solution was added slowly to the thin film of the LR dye, and then the mixture was added dropwise to a stirred 10 mM HEPES buffer (pH 7.4). The polymersome solutions were stirred for 45 minutes at room temperature, and then air was passed for 45 minutes through the mixture. The polymersomes were sonicated for 60 minutes (Symphony 117 V, 60 Hz). Subsequently, the polymersomes were passed through a Sephadex G100 (GE Healthcare) size exclusion column to collect lissamine rhodamine

dye incorporated polymersomes. These polymersomes were used as a control for the cell viability assays.

2.3.5. Polymersomes size analysis

The nucleus-targeted polymersomes encapsulating BBI608 and control polymersomes were characterized by dynamic light scattering at 90 using a Zeta Sizer Nano ZS 90 (Malvern Instrument). Polymersomes were equilibrated for 120 seconds, and five measurements were recorded with 10 repeats each.

2.3.6. Transmission electron microscopy (TEM)

Samples were prepared on 300 mesh copper grids with a formvar-carbon support film. Grids were pretreated with 1% poly-L-lysine and air-dried; 5 μL of the polymersome suspension was added and allowed to stand 1 min, then wicked off with a filter paper. Negative staining was performed using 0.1% phosphotungstic acid for 2 minutes, then wicking off and air-dried before observation and imaging in a JEOL JEM-2100 LaB6 transmission electron microscope.

2.3.7. Atomic force microscopic (AFM) Imaging

The size and morphology of polymersomes were characterized using atomic force microscopy. Polymersomes (1 mg/mL) were diluted (20X) in HEPES buffer (pH 7.4, 10 mM). Polymersomes were dropped on silica substrates, incubated for a minute and the extra liquid was evaporated by an air blowgun. The AFM measurements were performed in non-contact mode (resonance frequency of 145 kHz and a scanning rate of 1.3 Hz) using an NT-MDT INTEGRA instrument (NT-MDT America). The scanning areas were $5 \times 5\ \mu m^2$ at the resolution of 512 points per line, respectively.

2.3.8. Redox triggered release studies

Polymersomes encapsulating 20 μM calcein dye were prepared to perform the release study. Release was assessed using cobalt chloride as the quencher[136] and glutathione as the reducing agent. The cobalt (II) chloride (10 mM) was used to quench the fluorescence from the unencapsulated calcein outside the vesicles. We used 20 μL of calcein-encapsulated polymersomes (total polymer concentration: 1 mg/mL) in 10 mM HEPES buffer (180 μL, pH =7.4) in a 96-well plate. The release from the polymersomes were monitored in the presence of 10 mM glutathione for 40 minutes; subsequently, the concentration was increased to 50 mM, and the release was monitored for an additional 40 minutes using (excitation: 495 nm, emission: 515 nm) fluorescence microplate reader (Spectramax M5, Molecular Devices). The amount of calcein release form polymersomes was calculated according to the equation:

Percent Release = [(Emission Intensity after 80 min – Initial Intensity before treatment)/Initial Intensity before treatment] ×100

2.3.9. Preparation and characterization of echogenic polymersomes

Polymersomes were prepared by dissolving the PEG_{1900}–S–S–PLA_{6000} and N_3–PEG_{1900}–PLA_{6000} polymers with the molar ratio of 40:60 (total 5 mg in 1 mL of THF), respectively. Then, the polymer mixture was added dropwise to 0.32 M mannitol (weak cryoprotectant) prepared in HEPES buffer (10 mM, pH 7.4). Subsequently, THF was evaporated for 45 min by passing air through the solution, and the polymersomes were sonicated for 60 minutes (Symphony 117 V, 60 Hz). To make the polymersomes echogenic, they were subjected to three freeze (-80 ^{o}C, 24 h) and thaw (60 °C) cycles. Finally, the polymersomes were lyophilized (Labconco freeze dryer) and reconstituted in HEPES buffer (10 mM, pH 7.4) for further experiments.

2.3.10. Ultrasound experimental setup to measure scattering in echogenic polymersomes

Two spherically focused transducers (each having a central frequency of 2.25 MHz/5 MHz/10 MHz, Figure 2.3) with the same specifications (V310-SU, Olympus NDT) were employed for scattering measurements. The transmitting and receiving transducers were placed perpendicularly by two separate linear stages (433 series, 360-90, Newport) and immersed in a bigger water tank filled with DI water. A 20-mL syringe served as a sample chamber, in which polymersome suspension was injected. A function generator (Model AFG 3251; Tektronix) was utilized to generate a 32-cycle sinusoidal pulse of 5 MHz frequency at a PRF of 100 Hz. These signals were then amplified using a 55dB power amplifier (Model A-300, ENI) and sent to the transmitting transducer. The input signals were scattered by the polymersomes inside the focal volume of the transducer. The scattered signals were received by the receiving transducer connected to a pulser/receiver (DPR300, 475v, JSR) in the through mode with a 27dB gain. The output signals were then transmitted to an oscilloscope (TDS2012, Tektronix) for real time visualization. The output voltage-time RF signals were obtained by the oscilloscope by averaging over every 64 sequences. Finally, the data from the oscilloscope wastransmitted and saved onto a desktop computer using the software Signal Express Tektronix Edition (version 2.5.1, Labview NI). In time dependent scattering experiments, all the setups and procedures were the same except that the data were recorded over a 20-minute period (corresponding to about 344 acquisitions). As for the degassed experiment, all the setups and procedures were still the same, the only difference being that the PBS solution had been degassed using a vacuum pump.

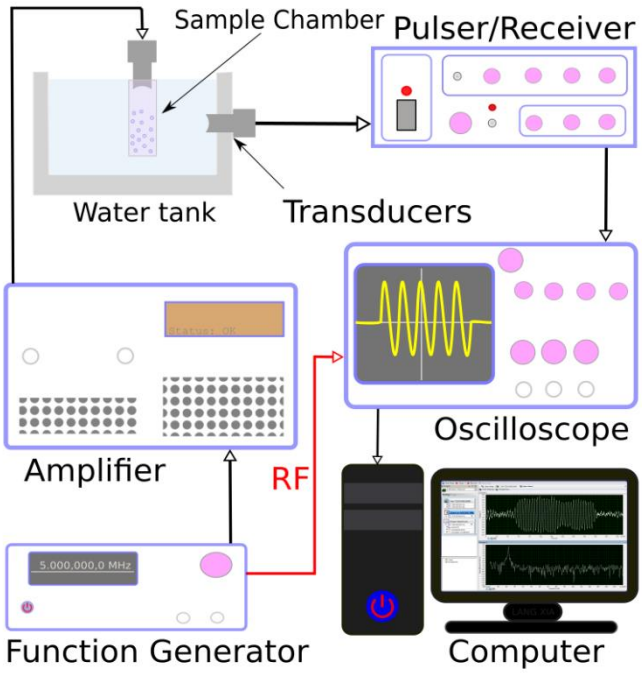

Figure 2.3. Experimental setups for the ultrasound scattering measurements from the echogenic polymersomes.

2.3.11. Echogenic polymersomes' experimental procedure and data reduction

For the scattering experiment, the suspension was made by reconstituting the dry powder in phosphate buffered saline (PBS) solution to obtain a concentration of 10 μg polymer/mL. We injected 20 mL of the resulting suspension into the sample chamber. The measurement was repeated five times to assess the reliability of the experimental data. The measurement of the control signal, i.e., without polymersomes and the responses due to the polymersomes were acquired by the procedures above. The Fourier transform of the signal was performed using a Matlab program to get the average scattered power spectra in the frequency domain (50 voltage time acquisitions were used for averaging). The scattered response was converted into a dB scale by taking a unit reference. Fundamental, second- and sub-harmonic scattered responses were extracted from the power spectrum. The final data is reported as an enhancement over the control. The scattered response was also checked in the presence of 50 mM of glutathione.

2.3.12. Ultrasound imaging

Dried polymersomes were reconstituted in 10 mM HEPES buffer, pH 7.4 with the concentration of 10 µg/mL. In a 96-well plate, 0.2 mL of polymersomes were dispensed into each well; then the plate was covered with parafilm. Subsequently, an ultrasound gel (Aquasonic 100, Parker Laboratories) was applied, and a 15 MHz linear ultrasound transducer was used for the imaging experiments employing a Terason t3200 instrument (MediCorp LLC).

2.3.13. Cell culture

The pancreatic cancer cell line BxPC3 was purchased from American Tissue Culture Consortium (ATCC). The cells were maintained in RPMI 1640 medium (without phenol red) supplemented with 1% v/v antibiotics (penicillin and streptomycin) and 10% v/v fetal bovine serum. The cell culture flasks were maintained in an incubator at 37 °C in a 5% CO_2 atmosphere.

2.3.14. Nuclear uptake studies

The BxPC3 cells (3×10^3) were seeded in a 12-well tissue culture plate for 24 hours before the experiment. Once the culture is 80-90% confluent, the nucleus-targeted (20 µL) and non-targeted (20 µL) polymersomes were incubated with the cells for 3 hours. Subsequently, the cell culture media and polymersomes were removed, and the cells were washed twice with Hanks' balanced salt solution (HBSS) to remove the non-internalized vesicles. The cell nuclei were stained with HOESCHT 33342 dye (Enzo Life Sciences, 1:1000 dilution) and imaged using the 20X objective of a Leica fluorescence microscope.

2.3.15. Cell viability in monolayer cultures

To evaluate the efficacy of the nucleus-targeted polymersomes on the human pancreatic cancer cells (BxPC3), the Alamar Blue assay was performed. The BxPC3 cells were seeded at a

density of 10^3/well in a 96-well tissue culture plate and were allowed to grow until 80−95% confluent. The plate was divided into four groups: control, free drug (BBI608), non-targeted polymersomes, and nucleus-targeted polymersomes encapsulating BBI608. The control group did not receive any treatment. Cells treated with BBI608 received 1, 4, and 8 μM of free and an equivalent amount of encapsulated drug in nucleus-targeted polymersomes. The cells were treated for 48 hours at 37 °C, in a 5% CO_2 atmosphere. Subsequently, the cells were washed with sterile HBSS and replaced with 200 μL fresh media. Then 20 μL Alamar Blue was added to all the wells and fluorescence were measured after 4 hours. The data presented are normalized to the control.

2.3.16. Cell viability in three-dimensional (3D) spheroid cultures

The 24-well 3D petri dishes (Microtissues) were used to prepare BxPC3 spheroids. Briefly, 2% w/v agarose solution was prepared and autoclaved. The BxPC3 cell suspension (10^4 cells in 60 μL media) was then added to each 3D scaffold. The spheroids were allowed to grow for 7 days. Then scaffolds were divided into four groups: control, non-targeted polymersomes, nucleus-targeted polymersomes encapsulating BBI608, and free drug. Spheroids were treated for 48 hours with the same concentration of drug as used for the monolayer studies. Subsequently, the spheroids were washed with sterile HBSS and then incubated with 100 μL TryPLE (recombinant trypsin, Life Technologies) for 10 minutes. The spheroids were removed and subjected to the Alamar Blue assay. The data presented are normalized to the control.

2.4. Results and discussion

2.4.1. Polymer synthesis and polymersome preparation

To prepare nucleus targeted polymersomes, we synthesized alkyne-dexamethasone conjugate (Figure 2.1) and N_3-–EG_{1900}–PLA_{6000} (Figure 2.2). The redox-sensitive polymer PEG_{1900}–S–S–PLA_{6000} (Figure 2.2) were synthesized as previously reported by our group. [74, 122] The dexamethasone–PEG_{1900}–PLA_{6000} polymer conjugate was synthesized using the Click chemistry [2+3 cycloaddition]. The polymersomes were prepared by the solvent exchange method [135] and characterized by dynamic light scattering (Figure 2.4), transmission electron microscopy (Figure 2.5), and atomic force microscopy (Figure 2.6). We encapsulated the stemness gene transcription inhibitor BBI608 (napabucasin) [120] in the polymersomes with an efficiency of 68 $\pm$ 5%. We observed that the nucleus-targeted polymersomes had a hydrodynamic diameter of 200 ± 2 nm, with a polydispersity index (PDI) of 0.2 ± 0.02. The average hydrodynamic diameter for the non-targeted polymersomes was 140 ± 3 nm with a PDI of 0.2 ± 0.03. The nucleus-targeted polymersomes were slightly larger than nontargeted polymersomes. We hypothesize that the encapsulation of hydrophobic BBI608 in the polymer bilayer of the vesicles increases the size of vesicles.

The dexamethasone–PEG_{1900}–PLA_{6000} polymer was incorporated into polymersome composition to target the nanoparticles to the cell nucleus. We expected that the dexamethasone on the polymersomes would open the nuclear pore complex [123] and transport the vesicles into the nucleus. The disulfide bond in the redox-sensitive polymer will subsequently be reduced in the nucleus, releasing the encapsulated BBI608.

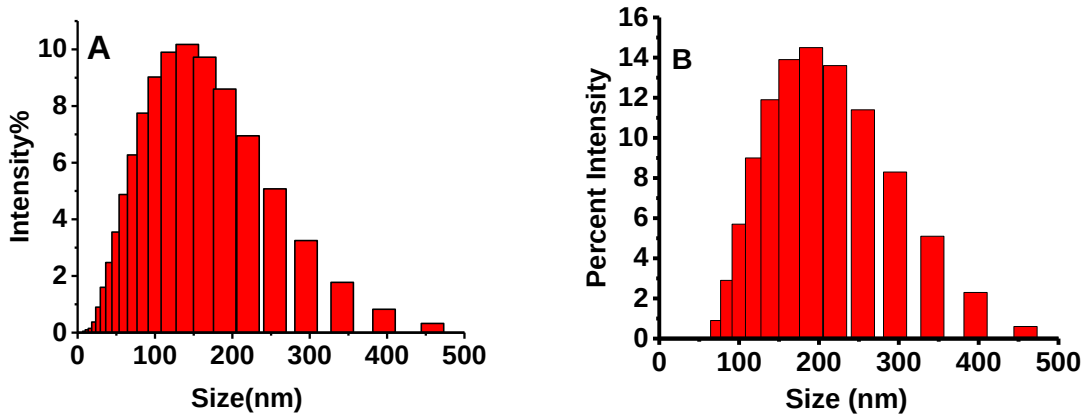

Figure 2.4. The hydrodynamic diameters of the polymersomes.
(**A**) non-targeted and (**B**) nucleus-targeted polymersomes encapsulating the stemness inhibitor BBI608, as determined by dynamic light scattering.

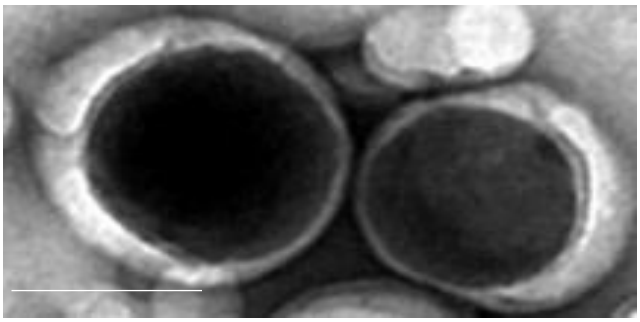

Figure 2.5. Transmission electron microscopy.
Images of the non-targeted polymersomes **(**scale bar: 50 nm).

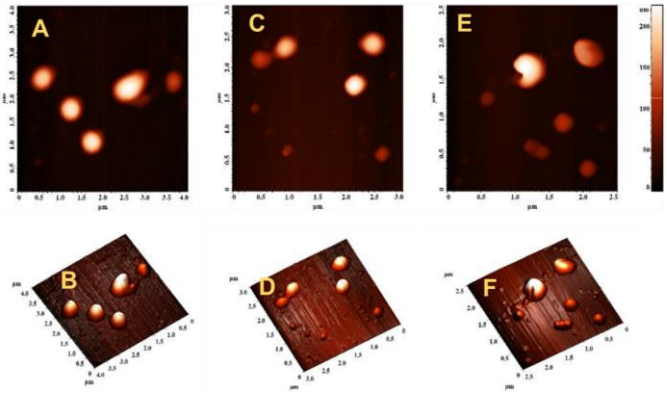

Figure 2.6. Atomic force microscopy (AFM) images of the non-targeted polymersomes.
(**A**, **B**) Polymersomes, (**C**, **D**) Polymersomes treated with 10 mM glutathione for 5 minutes, and (**E**, **F**) polymersomes treated with 50 mM GSH for 5 minutes.

2.4.2. Demonstration of reduction-triggered contents release from the polymersomes and structural characterization

We studied the reduction-triggered release of the dye calcein from the polymersomes as a function of time in the presence of different concentrations of added glutathione (GSH). GSH is an important intracellular reducing agent, comprising of glutamic acid, cysteine, and glycine.[127] It's increased level is correlated with progression and proliferation of various cancers, such as breast [120], colon [137], lung [137], pancreas [127]; it has also been associated with resistance to chemotherapy.[127] We observed that the polymersomes released 45% of the encapsulated dye in the presence of 10 mM (mimicking the cytosol) GSH. However, the release increased to 70% with 50 mM GSH (mimicking the nucleus, Figure 2.7). We also observed that both of the releases were rapid. Our atomic force microscopic studies indicated that 10 mM GSH slightly changed the morphology of the polymersomes (Figure 2.8A); however, 50 mM GSH completely disrupted the vesicle structure (Figure 2.8B).

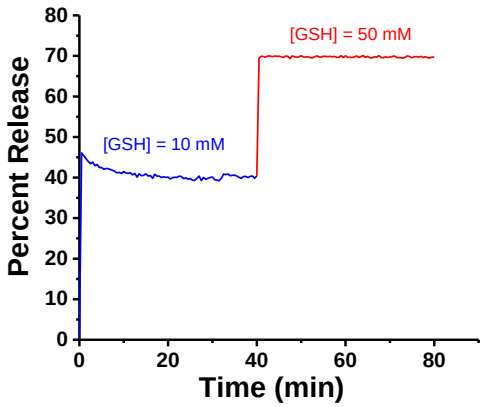

Figure 2.7. The glutathione-triggered release of the encapsulated calcein from the polymersomes.

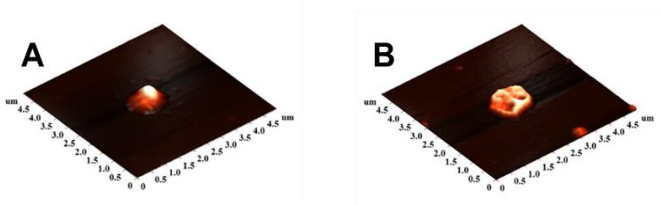

Figure 2.8. Structural characterization of the polymersomes after release study employing atomic force microscopy.
(**A**) Polymersomes treated with 10 mM GSH. (**B**) Polymersomes treated with 50 mM GSH.

2.4.3. Demonstration of polymersomes' echogenicity

Polymersomes' echogenicity was confirmed by a Terason medical ultrasonic imaging system (t3200) using a 15 MHz transducer. We observed that the echogenic polymersomes reflected ultrasound even after a week in the aqueous solution. The ultrasound reflection suggests the presence of air pockets in polymersomes (Figure 2.9B and 2.9C) while control (buffer without any polymersomes) did not show any contrast (Figure 2.9A).

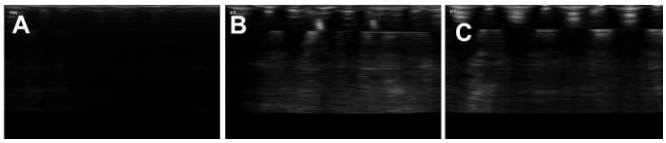

Figure 2.9. Ultrasound contrast images of the polymersomes.
(A) Control, (**B**) freshly reconstituted echogenic polymersomes, and (**C**) echogenic polymersomes after one week in aqueous solution at 15 MHz.

The scattered power spectra of the polymersomes at three excitation frequencies, 2.25, 5, and 10 MHz, are displayed in Figure 10. Power spectra show the responses of the polymersomes as a function of frequencies. Contributions at frequencies other than the excitation frequency indicate nonlinear responses of the polymersomes, which in turn offers the possibility of a nonlinear imaging modality with a potentially better signal to noise ratio [138, 139]. Polymersomes are echogenic in aqueous phosphate buffered saline (PBS, pH = 7.4), but not in the degassed solution (Figure 2.10D). Although the exact mechanism of the echogenicity of echogenic liposomes (ELIPs) or polymersomes is still unknown, we concluded that the dissolved gas in the solution plays a key role in generating echogenic signal. There is a significant nonlinear response, specifically subharmonic, only at 2.25 MHz (Figure 2.10A).

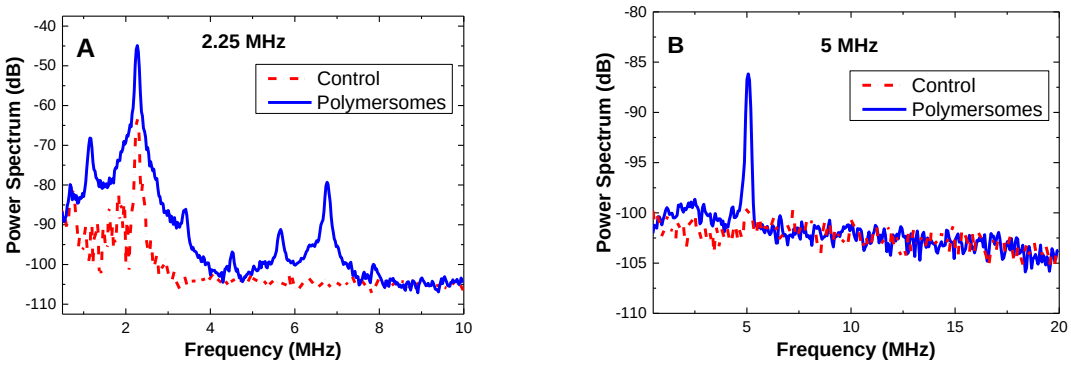

Figure 2.10. Scattered responses of echogenic polymersomes.
In PBS at 500 kPa excitation pressure and excitation frequencies of **(A)** 2.25 MHz, **(B)** 5 MHz, and **(C)** 10 MHz. Control is without polymersomes. **(D)** Scattered response in degassed solution at 500 kPa and 5 MHz.

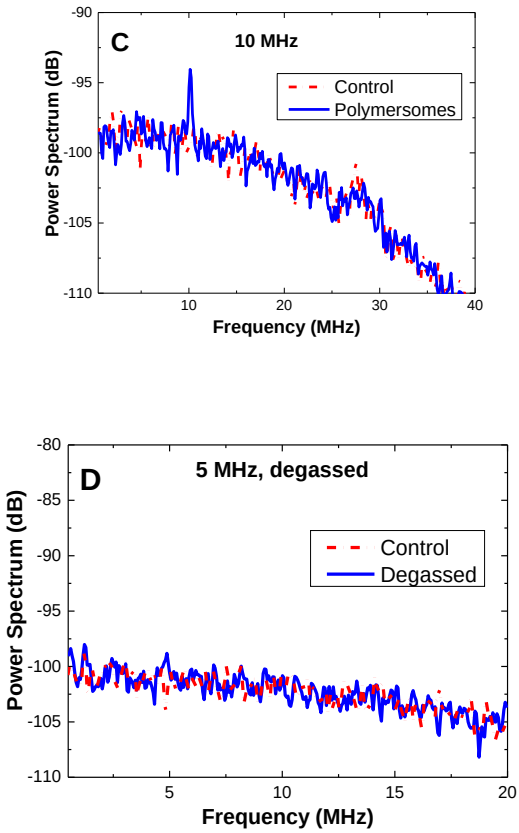

Figure 2.10. Scattered responses of echogenic polymersomes. (continued)
In PBS at 500 kPa excitation pressure and excitation frequencies of **(A)** 2.25 MHz, **(B)** 5 MHz, and **(C)** 10 MHz. Control is without polymersomes. **(D)** Scattered response in degassed solution at 500 kPa and 5 MHz.

Figure 2.11A shows the enhancement at different excitation frequencies. The enhancement in fundamental response is strongest at 5 MHz excitation, whereas the highest subharmonic enhancement appears at 2.25 MHz. The latter indicates the possibility of polymersome aided subharmonic imaging. [130, 140] We also examined the scattered responses over a 20-minute period in Figure 2.11B to investigate the long-term stability of their echogenicity crucial for clinical applications. During the 20-minute sonication, the polymersomes produced an almost constant signal indicating their suitability for use in contrast enhanced imaging. Polymersomes in degassed solution expectedly did not generate any scattered response.

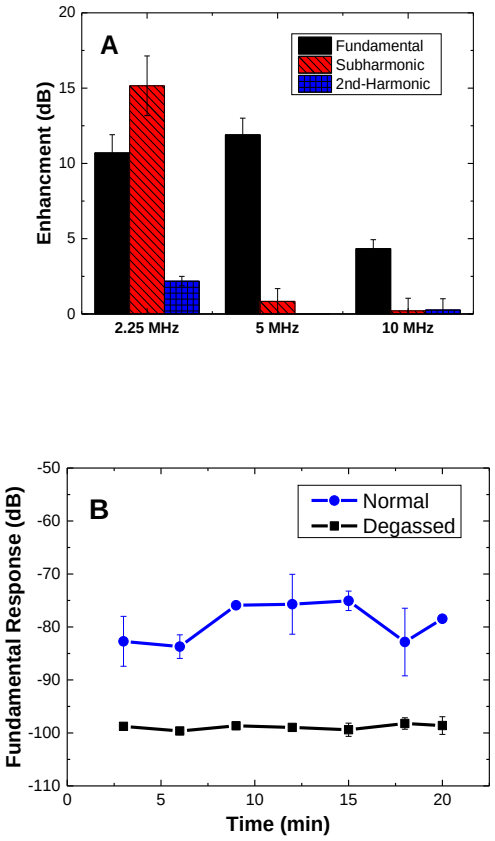

Figure 2.11. Enhancements in fundamental, sub– and second harmonic scattered. **(A)** Enhancements in fundamental, sub– and second harmonic scattered responses polymersomes at 500 kPa and 2.25, 5, and 10 MHz.**(B)** Time-dependent fundamental responses of the echogenic polymersomes in normal (blue trace) and degassed PBS (black trace) at 5 MHz and 500 kPa (N = 5).

Glutathione cleaves the disulfide bond destabilizing the bilayer of the polymersomes. We repeated the scattering experiments in the presence of 50 mM GSH. As expected, we observed that the fundamental enhancement decreased by 10 dB, and the subharmonic enhancement decreased by 4 dB (Figure 2.12) due to the loss of structural integrity of the polymersomes.

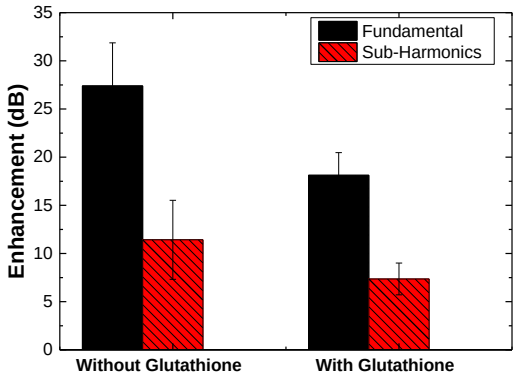

Figure 2.12. Fundamental and sub-harmonic enhancements of echogenic polymersomes in response to glutathione.
Fundamental (black bars) and sub-harmonic (red bars) enhancements of echogenic polymersomes at 5 MHz and 500 kPa with and without glutathione.

2.4.4. Nuclear uptake studies

To determine the localization within the pancreatic cancer cells, we prepared the polymersomes incorporating 5% of the DSPE– lissamine rhodamine lipid (structure shown in Figure 2) into the bilayer. We anticipated that the dexamethasone would open the nuclear pore complexes and transport the polymersomes inside the nucleus.[141] We incubated the BxPC3 pancreatic cancer cells with nucleus-targeted and nontargeted polymersomes for 3 hours. Subsequently, the cell nuclei were stained with the HOESCHT 33342 dye and imaged employing a fluorescence microscope (Figure 2.13). We observed localization of the targeted polymersomes in the nuclei of the BxPC3 cells while the non-targeted polymersomes did not internalize in the nucleus.

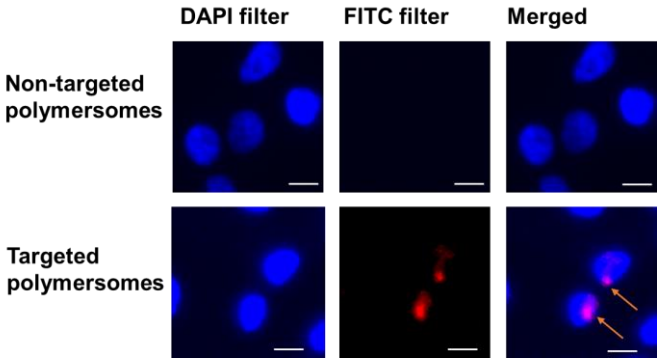

Figure 2.13. Cellular uptake studies with the BxPC3 cells.
The non-targeted polymersomes (top panel) did not enter the cell nucleus. The targeted polymersomes (bottom panel) were present in the cell nuclei after 3 hours of incubation (indicated by arrows; scale bar: 10 μm).

2.4.5. Viability studies in monolayer cultures of pancreatic cancer cells

After validating efficient nuclear localization, we proceeded to determine the effectiveness of the nucleus-targeted, drug-encapsulated polymersomes in the BxPC3 pancreatic cancer cells. The monolayer culture of the BxPC3 cells was treated with the nucleus-targeted polymersomes encapsulating BBI608, the non-targeted vesicles, and the free drug for 48 hours. The cell viability was determined by the Alamar Blue assay (Figure 2.14). We observed that the control polymersomes devoid of the dexamethasone group did not change the cell viability likely due to their inability to enter the cytosol (corroborated by the imaging studies, see Figure 2.13, top panel). However, the nucleus-targeted polymersomes encapsulating BBI608 significantly reduced the cell viability (30%, $p < 0.05$) compared to the control in a dose dependent manner (Figure 2.14).

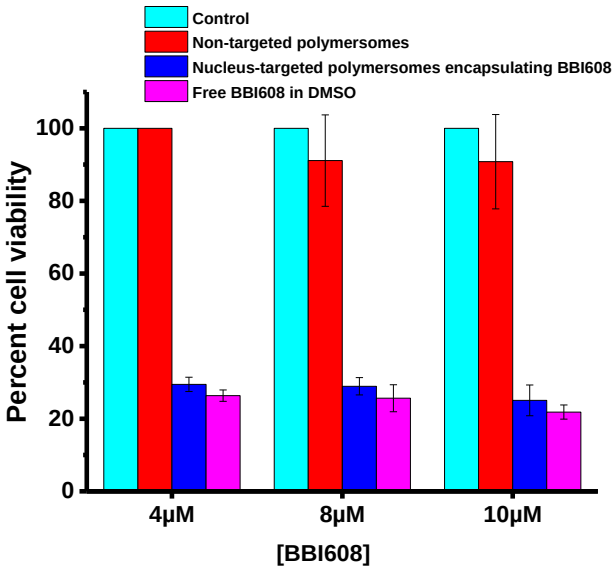

Figure 2.14. The viability of the BxPC3 cells in monolayer cultures at three different concentrations of encapsulated BBI608.
(**A**) Cell viability with media only (control, media treated, cyan bar), non-targeted polymersomes (red bar), nucleus-targeted polymersomes encapsulating BBI608 (blue bar), and free BBI608 (magenta bar, N = 4).

2.4.6. Viability studies in three-dimensional spheroid cultures of pancreatic cancer cells

Compared to the monolayer cultures, the spheroids demonstrate cellular heterogeneity, cell-cell interactions, and better mimic real tumors.[74, 118] To evaluate the effectiveness of the polymersome formulations, BxPC3 spheroids were prepared using the 24-well 3D petri dishes (Microtissues). We treated the 7-day old BxPC3 cells spheroids (Figure 2.15A) with nucleus-targeted polymersomes encapsulating BBI608, non-targeted polymersomes encapsulating BBI608, and free drug for 48 hours. The cell viability was determined by the Alamar Blue assay. We observed that the nucleus-targeted polymersomes encapsulating BBI608 decreased ($p \leq 0.05$) the cell viability to 43% in compared to non-targeted polymersomes (84%) and the control (Figure 2.15B). We speculate that dexamethasone in the composition of polymersomes opens the nucleus pores, the vesicles enter the nuclei and release the cancer stemness inhibitor, leading to the enhanced toxicity in the BxPC3 cells.

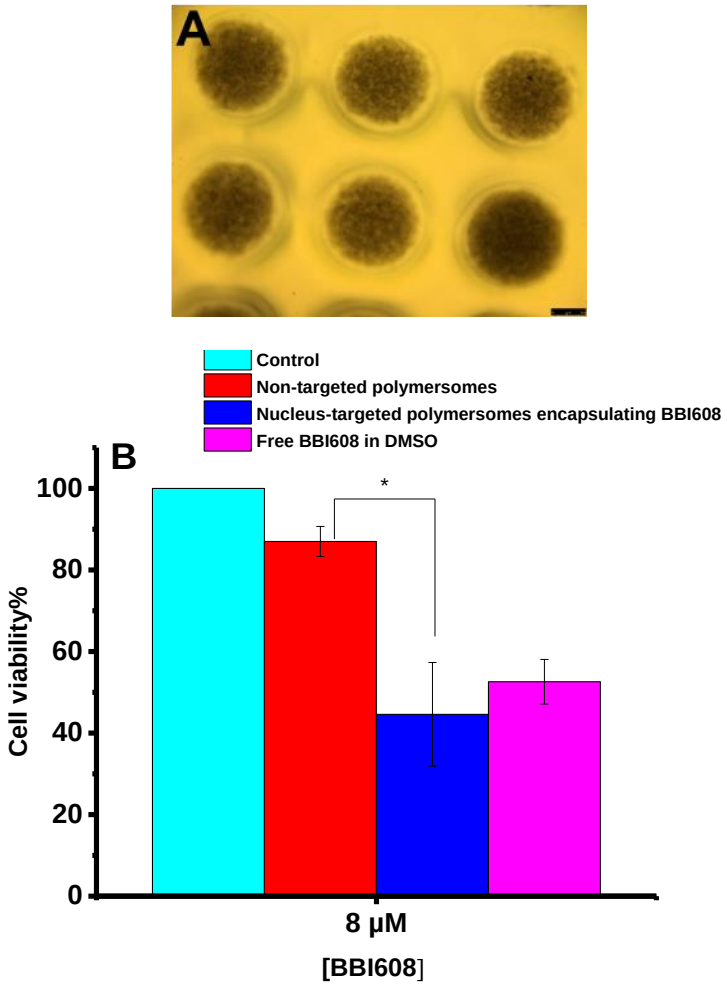

Figure 2.15. (**A**) Optical microscopic image of the 7- day old three-dimensional spheroids of the BxPC3 cells. (**B**) The viability of the BxPC3 cells in spheroid cultures.
Cell viability with media only (control, media treated, cyan bar), non-targeted polymersomes (red bar), nucleus-targeted polymersomes encapsulating BBI608 (blue bar), and the free BBI608 (magenta bar, N = 4). (scale bar: 25 µm).

2.5. Conclusions

We successfully synthesized alkyne dexamethasone and conjugated it to the N_3 – PEG_{1900}–PLA_{6000} polymer. The nucleus-targeted polymer was combined with a redox-sensitive polymer to form stable polymeric vesicles, which encapsulate air bubbles and a stemness inhibitor. Our echogenic nucleus-targeted polymersomes respond to ultrasound and release the encapsulated BBI608 to the nucleus of pancreatic cancer cells. The nucleus-targeted drug-encapsulated polymersomes reduced the viability of pancreatic cancer cells in monolayer and spheroidal cultures to 30% and 43% respectively. The polymersomes scattered ultrasound and responded to the medical ultrasound imager, confirming the echogenicity. They have the potential to image and deliver chemotherapeutic drugs to the tumor cells simultaneously. This is a non-invasive strategy to monitor targeted drug delivery to improve the therapeutic outcome of chemotherapy. The results of this research will pave the way for other ultrasound reflective nanoparticles for targeted drug delivery and simultaneous imaging.

3. PEPTIDE-TARGETED, STIMULI-RESPONSIVE POLYMERSOMES FOR DELIVERING A CANCER STEMNESS INHIBITOR TO CANCER STEM CELL MICROTUMORS[3]

3.1. Abstract

Often cancer relapses after an initial response to the chemotherapy because of the tumor's heterogeneity and the presence of progenitor stem cells, which can renew. To overcome drug resistance, metastasis, and relapse in cancer, a promising approach is the inhibition of cancer stemness. In this study, the expression of the neuropilin-1 receptor in both pancreatic and prostate cancer stem cells was identified and targeted with a stimuli-responsive, polymeric nanocarrier to deliver a stemness inhibitor (napabucasin) to cancer stem cells. Reduction-sensitive amphiphilic block copolymers PEG_{1900}-S-S-PLA_{6000} and the N_3-PEG_{1900}-PLA_{6000} were synthesized. The tumor penetrating iRGD peptide-hexynoic acid conjugate was linked to the N_3-PEG_{1900}-PLA_{6000} polymer via a Cu^{2+} catalyzed "Click" reaction. Subsequently, this peptide-polymer conjugate was incorporated into the polymersomes for tumor targeting and tissue penetration. Polymersomes containing 85% PEG_{1900}-S-S-PLA_{6000}, 10% iRGD-polymer conjugate, and 5% DPPE-lissamine rhodamine dye were prepared. The iRGD targeted polymersomes encapsulating the cancer stemness inhibitor napabucasin were internalized in both prostate and pancreatic cancer stem cells. The napabucasin encapsulated polymersomes significantly ($p < 0.05$) reduced the viability of both prostate and pancreatic cancer stem cells and decreased the stemness protein expression compared to the control and vesicles without any

[3] The material in this chapter was co-authored by Fataneh Karandish, James Froberg, Pawel Borowicz, and Sanku Mallik. Fataneh Karandish had primary responsibility to conduct all experiment listed in the section and analyze the data. Fataneh Karandish also drafted and revised all versions of this chapter. James Froberg imaged polymersomes by AFM and Pawel Borowicz imaged microtumors by fluorescence microscope . Sanku Mallik served as proofreader and checked the math in the statistical analysis conducted by Fataneh Karandish.

drug. The napabucasin encapsulated polymersome formulations have the potential to lead to a new direction in prostate and pancreatic cancer therapy by penetrating deeply into the tumors, releasing the encapsulated stemness inhibitor, and killing cancer stem cells.

3.2. Introduction

Cancer stem cells which contribute to tumor heterogenicity are a subpopulations of cells with tumor-initiating capability.[7] These cells have the stem-like properties of normal stem cells, such as self-renewal [5] and multi-lineage differentiation.[6] It is hypothesized that cancer stem cells might be the origin of solid tumors of prostate, colon, breast, and lung.[9] Cancer stem cells express both embryonic stem cells markers (Nanog, Oct4, and Sox-2) and progenitor cell markers (CD33, CD44, and Nestin).[10] Pancreatic cancer stem cells isolated from pancreatic tumors were defined by the $CD133^{+}$[17] and the $CD44^{+}$ $CD24^{+}$ $EPCAM^{+}$ cells.[18] Prostate cancer stem cells isolated from prostate tumors displayed CD44, CD 133, SSEA3/4, and Oct4 markers (http://www.celprogen.com).Cancer stem cells are mostly responsible for metastasis, recurrence, and drug resistance in cancer.[142]

Napabucasin (BBI608) is a cancer stemness inhibitor that interferes with gene transcription through the STAT3-dependent pathway. In vitro and in vivo studies demonstrated the ability of napabucasin to inhibit cell proliferation and induce cell death.[7, 120] Napabucasin is currently in Phase III clinical trials for the treatment of gastric, colon, and pancreatic cancers (www.clinicaltrials.gov).

Stimuli-responsive nanoparticles respond to an altered physical or chemical microenvironment in the tumor and release their encapsulated contents only when the abnormalities are encountered.[74] In this study, we have used reduction sensitive polymersomes to deliver napabucasin to prostate and pancreatic cancer stem cells. Polymersomes are bilayer

vesicles prepared from amphiphilic block copolymers. These block copolymers spontaneously form a vesicular structure in an aqueous solution, with an aqueous core, enabling the encapsulation of hydrophobic drugs in the bilayer and hydrophilic drugs in the core.[74]

To target and penetrate the tumor, we have used the reported cell penetrating cyclic iRGD peptide. This peptide interacts with the integrin and neuropilin receptors on the cancer cell surface.[143] The C-terminal of the peptide that stimulates the neuropilin-1 receptor and vascular permeability is known as the C-end rule (CendR).[143] The neuropilin-1 receptor is expressed in cancer and vascular endothelial cells and contributes to tumor progression and angiogenesis.[144] Nanoparticles, antibodies, and drugs conjugated to the iRGD peptide were observed to accumulate in the tumors both in vitro and in animal studies.[50]

Our goal is to develop a unique, polymeric drug delivery system to target cancer stem cells. In this study, the expression of neuropilin-1 receptor on the surface of both pancreatic and prostate cancer stem cells was identified; thus, the cyclic iRGD peptide was synthesized and conjugated with a polymer. We prepared the iRGD targeted, reduction sensitive polymersomes encapsulating the cancer stemness inhibitor napabucasin were prepared. We hypothesized that iRGD peptide decorated polymersomes would penetrate a solid tumor and internalize in cancer stem cells. Subsequently, the high reducing agent concentration in the cytosol will reduce the disulfide linker of the amphiphilic polymer, disturb the bilayer structure of the vesicles, and release the encapsulated napabucasin.[74] We observed that iRGD-targeted polymersomes encapsulating napabucasin significantly ($p < 0.05$) decreased the viability of prostate and pancreatic cancer stem cell microtumors compared to the controls. The cancer stemness marker proteins also decreased after treatment with iRGD-targeted polymersomes encapsulating napabucasin.

3.3. Materials and methods.

3.3.1. Synthesis and characterization of Hex-iRGD peptide

The iRGD peptide was synthesized by using a microwave assisted, solid phase peptide synthesizer (Liberty Blue, CEM Corporation). We used the commercially available CLEAR-amide resin (Peptides International) and synthesized the peptide in 0.2 mM scale. The peptide sequence was hexynoic acid-Cyclo (Arg-Gly-Asp-Lys-Gly-Pro-Asp-Asp-Cys). After the solid phase synthesis, the resin was washed with 15 mL acetone, centrifuged for 10 minutes at 2000 RPM and kept in a desiccator overnight. Subsequently, the resin was stirred with thallium trifluoroacetate (0.1 mmol) in dimethylformamide at room temperature for 3 hours to cyclize the peptide on the resin. The resin was filtered and washed with a mixture of DMF and dichloromethane (3X), and the residue was collected. Next, the peptide was cleaved from the resin with trifluoroacetic acid (19 mL), triisopropylsilane (0.5 mL), and distilled water (0.5 mL) at room temperature for 2 hours. The resin was filtered, ice-cold diethyl ether was added to the filtrate, the precipitate was filtered, and dried in a vacuum desiccator. The peptide was characterized using mass and circular dichroism spectroscopy.

3.3.2. Synthesis of iRGD-hex-N_3-PEG_{1900}-PLA_{6000} polymer conjugate

We synthesized N_3-PEG_{1900}-PLA_{6000} polymers following a reported protocol from our laboratory. To conjugate the iRGD-hexynoic acid to N_3-PEG_{1900}-PLA_{6000} polymer, we used the Click chemistry ([2+3]-cycloaddition).[134] Briefly, the N_3-PEG_{1900}-PLA_{6000} polymer (20 mg) and iRGD-hexynoic acid (2 mg) were dissolved in 5 mL of deionized water. The reaction was catalyzed by 400 µL copper (II) sulfate complex (0.053 M) and 400 µL of sodium ascorbate (27 mg/mL). The copper (II) complex was papered by mixing the copper (II) sulfate (0.53 mmol) and pentamethyl diethylenetriamine (2 mmol). The solution was stirred at room temperature for

3 hours, and 4 mL of water was added to produce the final concentration of 0.053M. The reaction was stirred at room temperature for 24 hours. The compound was dialyzed against water (molecular weight cutoff: 1,000) for 48 hours. The product was characterized by FT-IR and circular dichroism spectroscopy (Supporting Information).

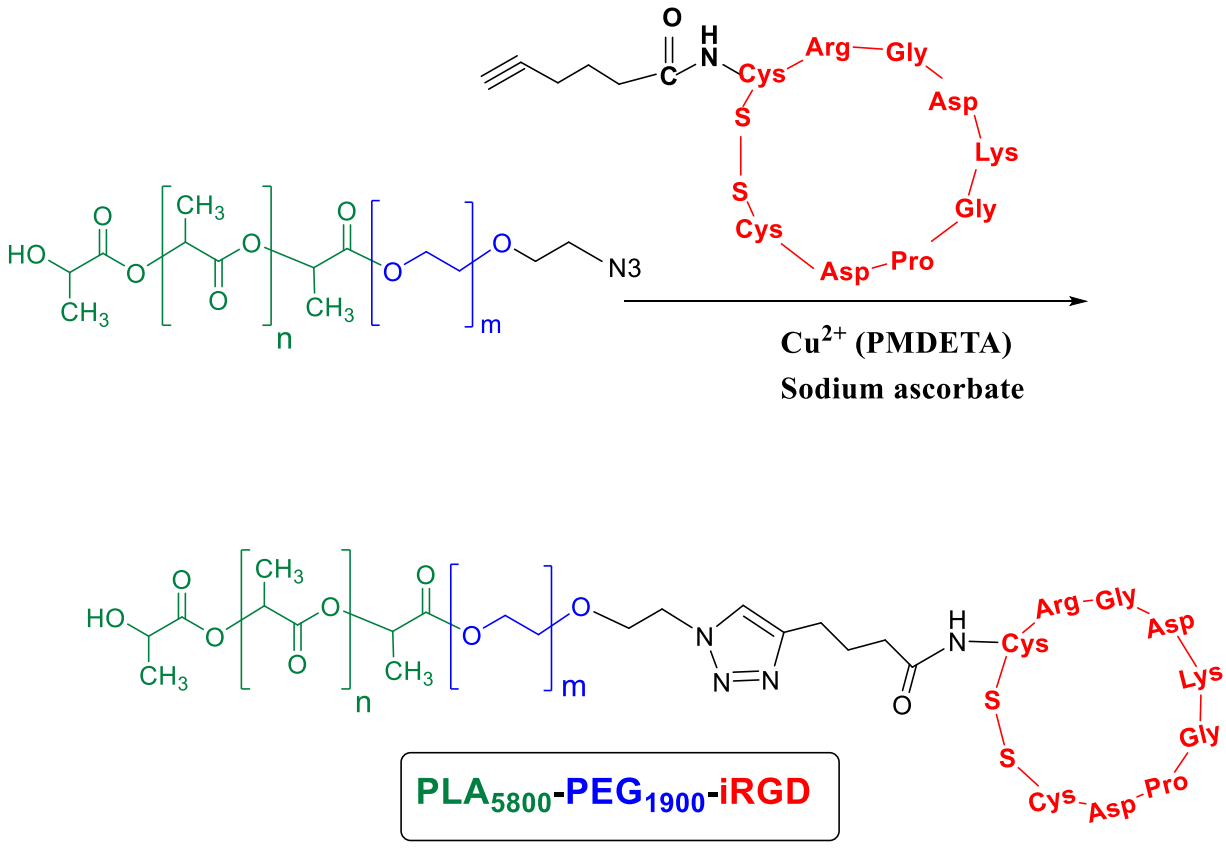

Scheme 3.1. [2+3]-Cycloaddition reaction of N3-PEG$_{1900}$-PLA$_{6000}$ polymer and iRGD-hexynoic acid peptide.

3.3.3. Preparation of iRGD-targeted and non-targeted polymersomes encapsulating napabucasin

The iRGD- targeted polymersomes encapsulating napabucasin were prepared from PEG$_{1900}$-S-S-PLA$_{6000}$ (85%), iRGD-PEG$_{1900}$-PLA$_{6000}$ (10%), and 1,2-dipalmitoyl-*sn*-glycero-3-phosphoethanolamine-N-lissamine rhodamine B sulfonyl ammonium salt (LR, 5%). The non-targeted vesicles encapsulating napabucasin contained PEG$_{1900}$-S-S-PLA$_{6000}$ (95%) and LR (5%).

The polymers were dissolved in THF (9 mg/mL for the disulfide polymer, 2 mg/mL for the iRGD-PEG_{1900}-PLA_{6000}, 3 mg/mL for napabucasin and 0.01 mg/mL LR in chloroform). The chloroform solution (1.1 mL) of LR lipid was evaporated to form a thin film. The polymers and napabucasin (200 µL, 2.5 mg/mL) were added to the thin layer film. The final mixture was added dropwise to an aqueous solution (10 mM HEPES buffer, pH 7.4) and stirred for 1 hour. To remove the organic solvents, air was passed through the mixture for 45 minutes. Subsequently, the polymersomes were sonicated in a bath for 60 minutes (Symphony 117 V, 60 Hz, Power 9). Then polymersomes (1 mg/mL) were filtrated through a Sephadex^{TM} G-100 size exclusion column to remove the unencapsulated drug. Polymersomes drug loading efficacies (DLE) were determined by UV−Vis spectroscopy. After passing through the size-exclusion column, the absorption of the polymersomes was recorded at 235 nm.

3.3.4. Preparation of control polymersomes

Control polymersomes were prepared by using PEG_{1900}-S-S-PLA_{6000} (95%) and LR (5%). The thin film of LR was prepared by evaporating chloroform solution of the dye. Then, a solution of the PEG_{1900}-S-S-PLA_{6000} polymer in THF (9 mg/mL, 160 µL) was added slowly to the thin film, and the mixture was added dropwise to a stirred aqueous buffer solution (10 mM HEPES buffer, pH 7.4). The resultant polymersomes were stirred for 45 minutes at room temperature, and air was passed for 45 minutes through the mixture to remove the organic solvent. The polymersomes were sonicated for 60 minutes (Symphony 117 V, 60 Hz) and passed through a Sephadex G100 (GE Healthcare) size exclusion column to collect lissamine rhodamine B dye incorporated vesicles. These control polymersomes were used for the cell viability assays.

3.3.5. Polymersomes' size analysis

The iRGD-targeted and the non-targeted polymersomes encapsulating napabucasin, and the control polymersomes were characterized by dynamic light scattering at 90^{o} using a Zeta Sizer Nano ZS 90 (Malvern Instrument). The polymersomes were equilibrated for 2 minutes; five measurements were recorded with 10 repeats each.

3.3.6. Atomic force microscopic (AFM) imaging

The samples were prepared by incubating 10 μL (1 mg/mL) of each polymersome solution on silicon substrates for 10 minutes in a closed container to prevent evaporation at room temperature. Then, the samples were rinsed with de-ionized water (Millipore) and dried under purified air flow. A commercial atomic force microscope (NT-MDT NTEGRA AFM) was used to perform the imaging measurements under ambient conditions in semi-contact mode with a resonant frequency of 190 kHz AFM probes (Budget sensors).

3.3.7. Release studies

Napabucasin release from polymersomes was monitored in the presence of different concentrations of glutathione (GSH) as a function of time. The polymersomes encapsulating napabucasin (500 μL of 1 mg/mL solution) was placed in Spectra/Por Float-A-Lyzer G2 Dialysis Tubes, MWCO 500−1000 Da. Subsequently, glutathione was added to make the final concentration of 2 μM, 50 μM, 1 mM, and 5 mM. The absorbance of fluid outside of dialysis tubes was measured at 235 nm using a UV-VIS spectrophotometer (Spectramax M5, Molecular Devices) every 5 minutes. The percent release was calculated from the calibration curve. After the release study, the polymersomes were imaged using atomic force microscopy.

3.3.8. Cell culture

Human prostate and pancreatic cancer stem cells were purchased from Celprogen. Prostate cancer stem cells were maintained in human prostate cancer stem cell complete growth media with serum and antibiotics, and pancreatic cancer stem cells were maintained in human pancreatic cancer stem cell complete growth media with serum and antibiotics from Celprogen. Human prostate and pancreatic cancer stem cell extracellular matrix-coated plates and flasks (Celprogen) were used in all experiments. The cell culture flasks were maintained in an incubator at 37 °C in a 5% CO_2 atmosphere. Cell passages between 3-6 were used in all the experiments.

3.3.9. Uptake studies employing monolayer and three-dimensional spheroids

Prostate and pancreatic cancer stem cells (5×10^3) were seeded in 12-well cancer stem cell extracellular matrix-coated plates for prostate and pancreatic cancers 24 hours before the experiments. Once the culture was 80-90% confluent, the iRGD-targeted (20 µL) and the control polymersomes (20 µL) were incubated with either prostate or pancreatic cancer stem cells for 3 hours. Then, the cell culture media and treatment were removed, and the cells were washed three times with PBS to remove the non-internalized vesicles. The cell nuclei were stained with HOESCHT 33342 dye (1:1000 dilution) and imaged using the 20X objective of a Lucia fluorescence microscope.

For the uptake experiments in the three-dimensional (3D) spheroids, the 35-well 3D petri dishes (Microtissues) were used to prepare prostate and pancreatic cancer stem cells spheroids. Agarose solution (2% w/v) was prepared and autoclaved. Prostate and pancreatic cancer stem cells suspensions (1×10^4 cells in 70 µL media) were then added to each 3D scaffold. Prostate and pancreatic cancer stem cell spheroids were allowed to grow for 2-3 days. Then iRGD-targeted (20

μL) and control polymersomes (20 μL) were incubated with either prostate or pancreatic cancer stem cell spheroids for 7 hours. After incubation, culture media and polymersomes were removed, and the cells were washed three times with PBS to remove the non-internalized vesicles. Cell nuclei were stained with HOESCHT 33342 dye (1:1000 dilution). Subsequently, the spheroids were cut into 15 μm section and placed on slides. Images of spheroids were acquired with a Zeiss AxioObserver Z1 microscope equipped with LSM700 laser scanning module (Zeiss, Thornwood, NY), at 40X magnification with 40x/1.3 Plan-Apochromat lens using a 590 nm solid-state laser for Lissamine rhodamine B and a 405 nm lasers for DAPI excitation. Following the acquisition of 3D microscopy images were imported to Imaris 8.3 (Bitplane) software where 50 microns thick computer-generated representation of the spheroids were created.

3.3.10. Viability of prostate and pancreatic cancer stem cells in monolayer cultures

Prostate and pancreatic cancer stem cells were seeded at a density of 10^3/well in a 96-well human prostate and pancreatic cancer stem cell extracellular matrix-coated plates. Once they reached 90% confluency, the plate was divided into five groups: control, control polymersomes, polymersomes encapsulating napabucasin, iRGD-targeted polymersomes encapsulating napabucasin, and free drug (napabucasin). In the control group, we added only the media. Cells treated with napabucasin received 1 μM and 4 μM of free and an equivalent amount of encapsulated drug in iRGD-targeted and non-targeted polymersomes. The cells were treated for 48 hours at 37 °C, in a 5% CO_2 atmosphere. Subsequently, the cells were washed with sterile PBS twice and replaced with 200 μL fresh media. Then 20 μL Alamar Blue was added to all the wells and fluorescence was recorded at excitation 565 nm and emission at 590 nm after 4 hours. The data presented are normalized to the control.

3.3.11. Viability of prostate and pancreatic cancer stem cells in spheroids

Prostate and pancreatic cancer stem cell spheroids were prepared by using 35-well 3D petri dishes (Microtissues). Once the microtumors formed (after 3-5 days), the plates were divided into five groups: control, control polymersomes, non-targeted polymersomes encapsulating napabucasin, iRGD-targeted polymersomes encapsulating napabucasin, and free drug (napabucasin). We treated the spheroids for 48 hours at 37 °C, in a 5% CO_2 atmosphere. After 48 hours, the solutions were removed, and the microtumors were washed twice with PBS. The spheroids were incubated with 100 μL of recombinant trypsin (TryPLE, Life Technologies) for 10 minutes. Then spheroids were removed and subjected to the Alamar Blue assay. The data presented are normalized to the control.

3.3.12. Western blotting

The prostate cancer stem cells were treated with different formulations of polymersomes (buffer encapsulated, napabucasin encapsulated, iRGD targeted with napabucasin encapsulation, and free napabucasin) for 5 hours. Subsequently, the cells were collected and lysed in RIPA buffer with complete protease inhibitor cocktail (Roche), and 0.1% sulfate (SDS). Protein concentration in each sample was verified by Bio-Rad DC protein assay. Protein samples were separated by SDS-PAGE and transferred to a nitrocellulose membrane. The membrane was blocked in 5% non-fat milk in TRIS buffer containing 1% Tween 20 (1X) for 30 minutes and then incubated with the primary antibody (1:1000 dilution in 5% non-fat milk) overnight and subsequently with appropriate secondary antibody (1:2000). ECL reagents (Pierce, Rockford, IL, USA) were used to developed signals and exposed to X-ray films. The anti-notch-1, Nanog, and GAPDH polyclonal antibody were purchased from Cell Signaling Technology and Neuropilin-1 monoclonal antibody from Santa Cruz Biotechnology.

3.3.13. Cell apoptosis assay by flow cytometry

After treatment of both prostate and pancreatic cancer stem cells with different formulations of polymersomes for 48 hours, the cells were collected and washed with PBS and diluted in annexin-binding buffer to 1×10^6 cells in 0.5 mL. Then cells were stained with Annexin V-FITC and PI (5 µL) for 10 minutes in the dark at room temperature. After incubation, samples were analyzed by flow cytometry using an Accuri C6 flow cytometer. Apoptosis was determined by data analysis using FlowJo software (FlowJo, LLC).

3.3.14. Statistical analysis

Graph pad Prism 7 software was used to perform statistical analysis. All the results presented are representative of at least four independent experiments. Error bars denote the mean ± SEM. Statistical analysis: Student's t-test was used to find the significance between two groups, where significance $*p < 0.05$.

3.4. Results and discussion

3.4.1. iRGD peptide characterization

To prepare iRGD targeted polymersomes encapsulating napabucasin, cyclic iRGD peptide was synthesized and conjugated to hexynoic acid (Figure 3.1A) using a solid phase microwave assisted peptide synthesizer. The synthesized hexynoic acid conjugated cyclic iRGD was characterized by mass spectrometry (Supporting Information).

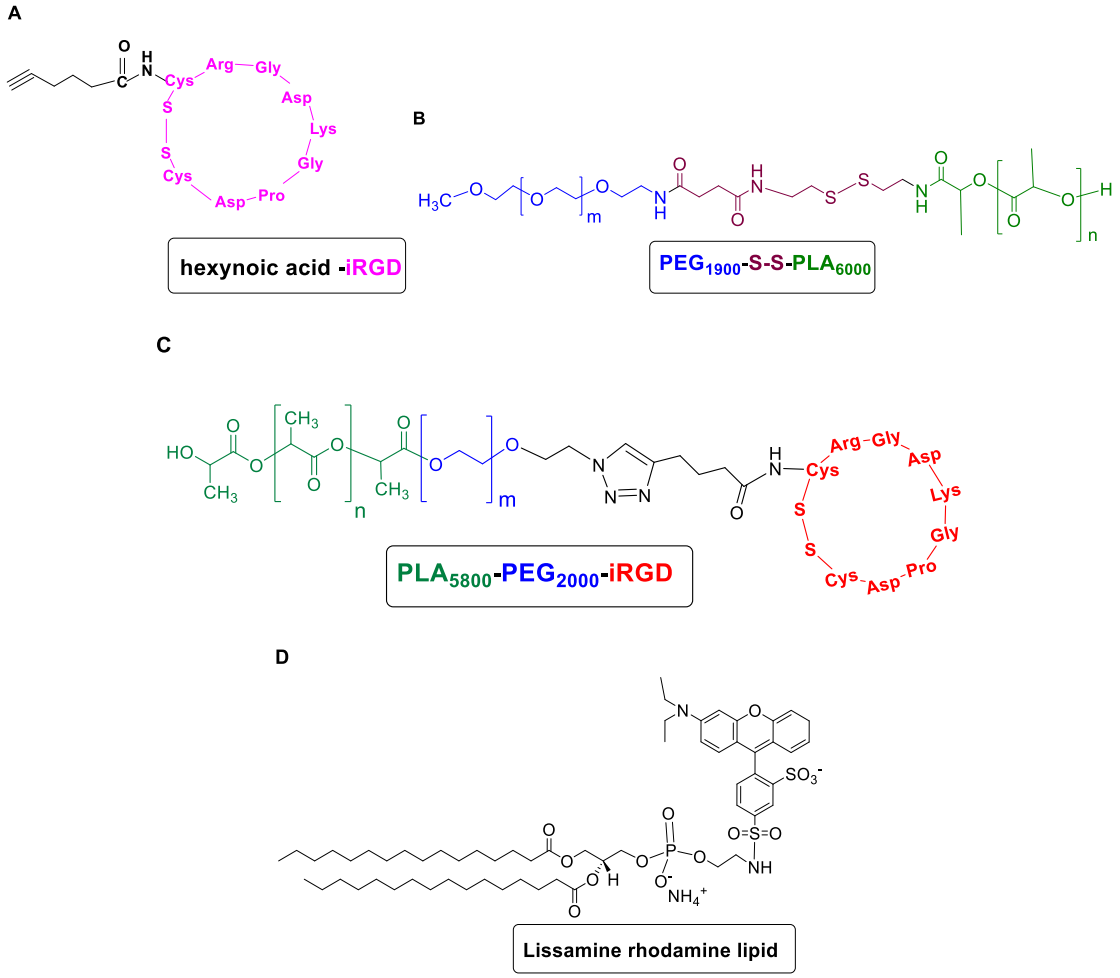

Figure 3.1. Structure of synthesized polymers, peptide and, the fluorescent lipid. **(A)** Structure of the synthesized cyclic iRGD peptide conjugated to hexynoic acid, **(B)** PEG_{1900}-S-S-PLA_{6000}, **(C)** PLA_{6000}- PEG_{1900}-iRGD polymer, and **(D)** 1,2-dipalmitoyl-*sn*-glycero-3-phosphoethanolamine-N-lissamine rhodamine B sulfonyl ammonium salt (commercially available).

3.4.2. Polymer synthesis and polymersome formation

The redox-sensitive polymer PEG_{1900}-S-S-PLA_{6000} (Figure 3.1B) was synthesized as previously reported.[74] The Click reaction [2+3 cycloaddition] to conjugate the cyclic iRGD peptide to the N_3-PEG_{1900}-PLA_{6000} polymer. The resultant iRGD-PEG_{1900}-PLA_{6000} (Figure 3.1C) was characterized by FT-IR and circular dichroism spectroscopy (Supporting Information). Targeted polymersomes were prepared from the redox-sensitive polymer PEG_{1900}-S-S-PLA_{6000} (85%), iRGD-PEG_{1900}-PLA_{6000} (10%), and DPPE–lissamine rhodamine lipid (5%) using the solvent exchange method.[74] The polymersomes were characterized by dynamic light scattering (Figure 3.2A – C) and atomic force microscopy (Figure 3.2D – I). The stemness gene transcription inhibitor, napabucasin, [120] was incapsulated in the polymersomes with an efficiency of (67 $\pm$ 6%). The iRGD-targeted and the non-targeted polymersomes encapsulating napabucasin had hydrodynamic diameters of 220 $\pm$ 10 nm (polydispersity index, PDI 0.2 ± 0.02) and 220 $\pm$ 5 nm (PDI 0.2 ± 0.01) respectively. The average hydrodynamic diameter for the control polymersomes was 137 $\pm$ 10 nm with a PDI of 0.2 ± 0.02. We observed the targeted and non-targeted polymersomes encapsulating napabucasin were larger than the control polymersomes. It is hypothesized that the incorporation napabucasin in the hydrophobic bilayer of the vesicles increases the size. The cyclic iRGD–PEG_{1900}–PLA_{6000} polymer in polymersomes composition targets the neuropilin-1 receptor. The Cend R motif on iRGD peptide is hypothesized to enable penetration into the microtumors (through the neuropilin-1 receptor) and internalizeation in the cells. The disulfide bond in the redox-sensitive polymer will subsequently be reduced in the cytosol, releasing the encapsulated cancer stemness inhibitor napabucasin.

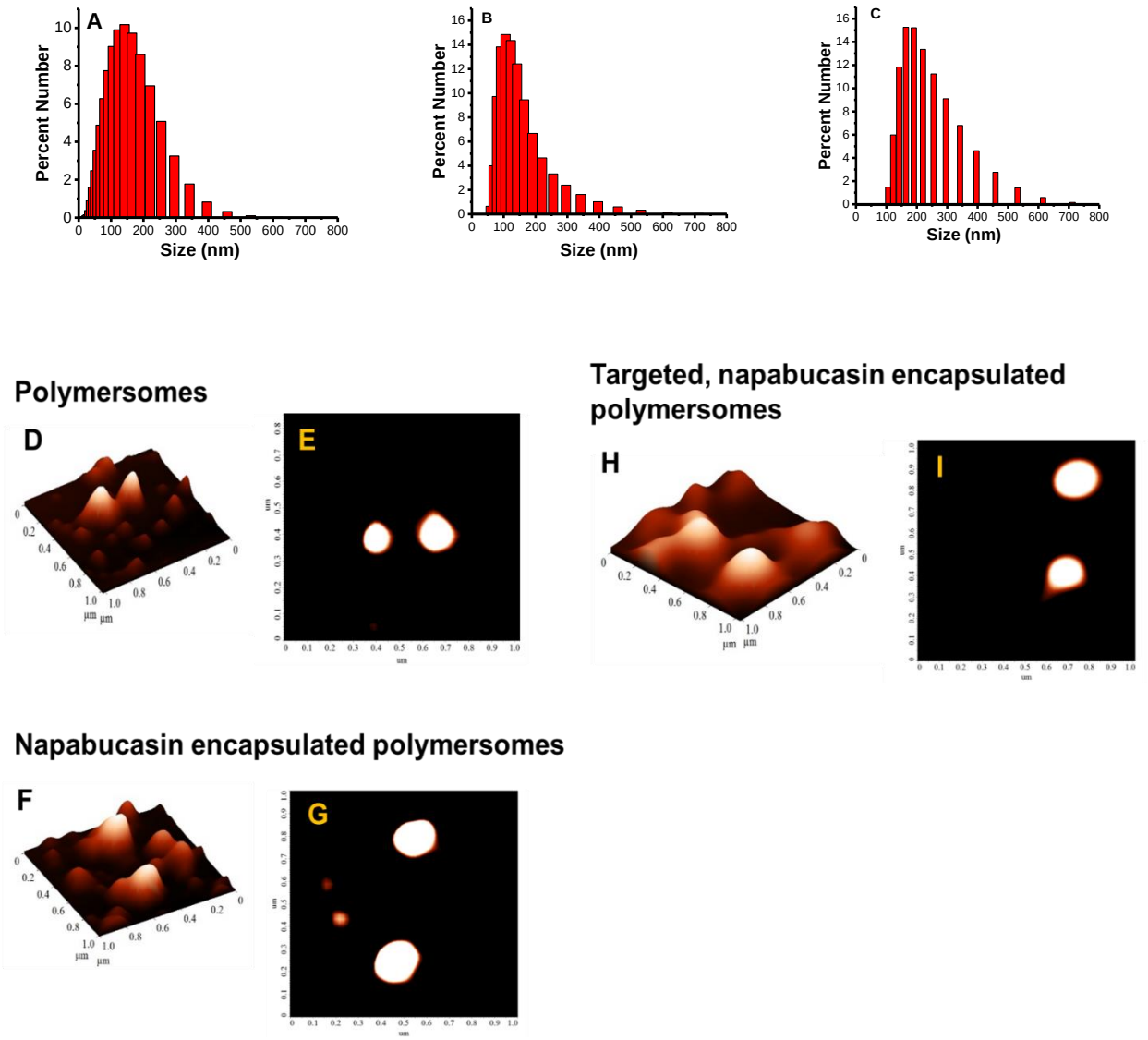

Figure 3.2. The hydrodynamic diameters of the polymersomes by DLS (A–C) and AFM (D–I). (**A**) Polymersomes, (**B**) polymersomes encapsulating napabucasin, and (**C**) peptide-targeted polymersomes encapsulating the stemness inhibitor napabucasin, as determined by dynamic light scattering. Atomic force microscopy (AFM) images of a different formulation of polymersomes (Panels **D** – **I**).

3.4.3. Release of napabucasin from the polymersomes and structural characterization

The reduction triggered release of napabucasin from the polymersomes was investigated with various concentrations of glutathione (GSH) as a function of time (Figure 3A). GSH is the most abundant tripeptide (γ-glutamyl-cysteinyl-glycine) in the cells. It has a major role in

protecting cells from reactive oxygen species (ROS), oxidant-induced toxicity, toxins, mutagens, and drugs.[127] The polymersomes released 57% of the encapsulated napabucasin in the presence of 1-5 mM GSH (mimicking the cytosol[74]) within 2 hours (Figure 3.3A, red and blue traces). However, less than 2% release of napabucasin was observed with 50 µM GSH (mimicking the extracellular environment of cancer cells[74], Figure 3.3A, purple trace). The release of napabucasin from polymersomes was not observed in the presence of 2 µM GSH (mimicking the reducing agent concentration in the blood[74], green trace, Figure 3.3A). Atomic force microscopy after the release of napabucasin revealed that the morphology and structure of polymersomes were distorted (Figure 3.3B, 3.3C).

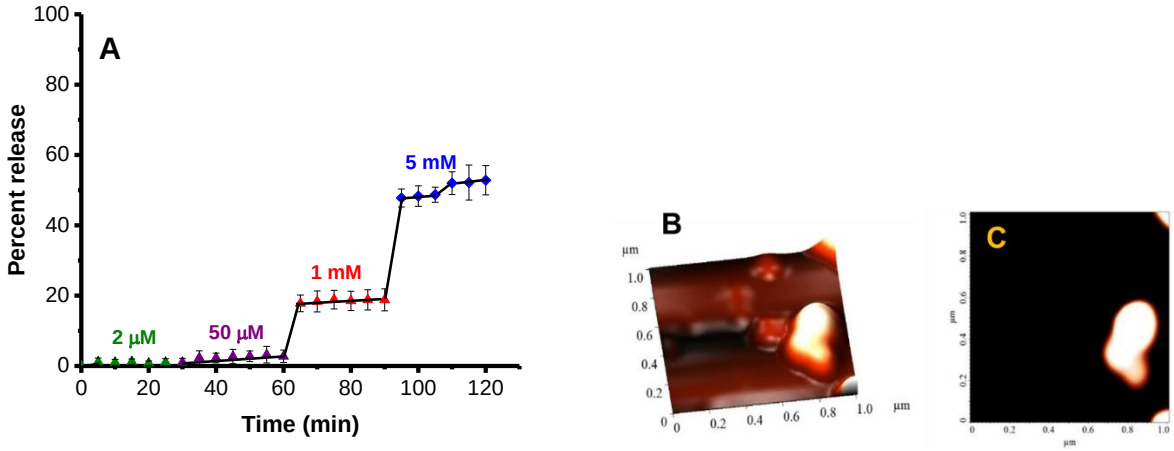

Figure 3.3. Reduction - mediated release profile of encapsulated napabucasin from the polymersomes. (**A**)The drug-encapsulated vesicles were treated with 2 µM (green), 50 µM (purple), 1 mM (red), and 5 mM (blue) concentrations of GSH. The lines connecting the data points are also shown. (**B**, **C**) Structural characterization of the polymersomes after release study employing atomic force microscopy.

3.4.4. Cellular internalization of polymersomes

To investigate whether the iRGD peptide has any advantage for internalization in the cancer stem cells, iRGD targeted and non-targeted control polymersomes were prepared, incorporating 5% of the DPPE–lissamine rhodamine lipid (structure shown in Figure 3.1). Prostate

and pancreatic cancer stem cells (monolayer cultures) were incubated with iRGD targeted and control polymersomes for 3 hours, the cell nuclei were stained with the HOESCHT 33342 dye and imaged employing a fluorescence microscope. Red fluorescence (from the lissamine rhodamine dye) was observed inside both prostate (Figure 3.4D-F) and pancreatic cancer stem cells (Figure 3.4J-L), indicating cellular internalization of the iRGD-decorated polymersomes. However, the control polymersomes without the iRGD peptide did not internalize in the cells (Figure 3.4A-C, and 3.4G-I).

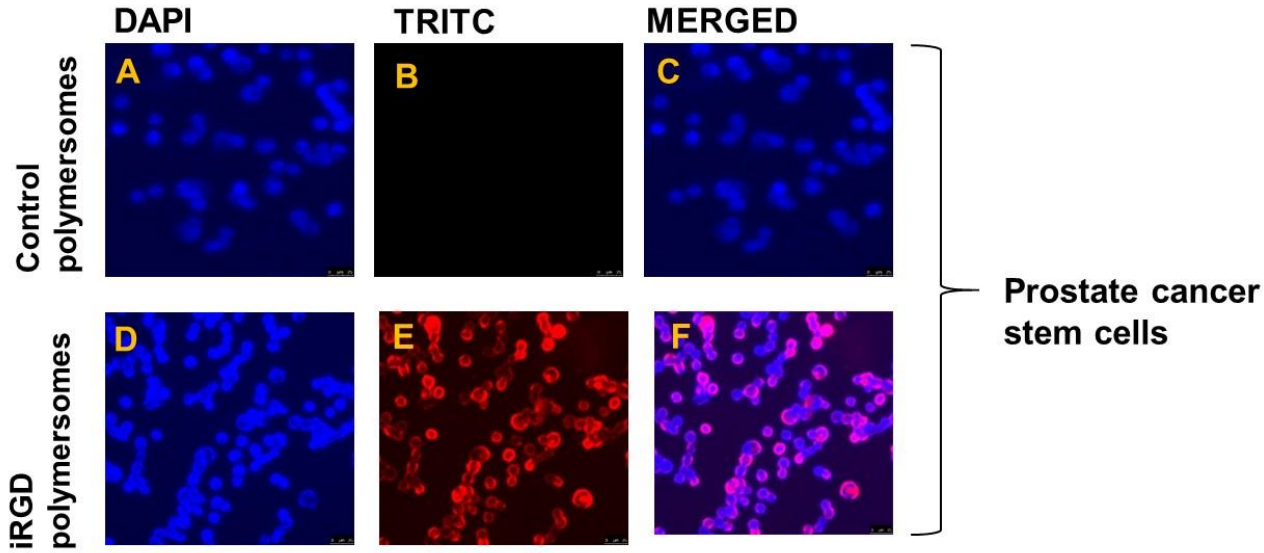

Figure 3.4. Cellular uptake studies in monolayer and microtumor cultures of prostate and pancreatic cancer stem cells**.** Panels (**A**-**F**): prostate cancer stem cells (scale bar: 25 µm), and Panels (**G**-**L**): pancreatic cancer stem cells (scale bar: 25µm). (**M**, **N**) Cellular uptake studies in a microtumor slice 200 µm from the surface of prostate cancer stem cells (**M**) and pancreatic cancer stem cell spheroids (**N**). The co-localization of the red fluorescence from the lissamine rhodamine dye and the blue from HOECHST 33342 indicated that peptide-targeted polymersomes were internalized in the cells. The blue fluorescence from the HOECHST 33342 dye indicates the cell nuclei.

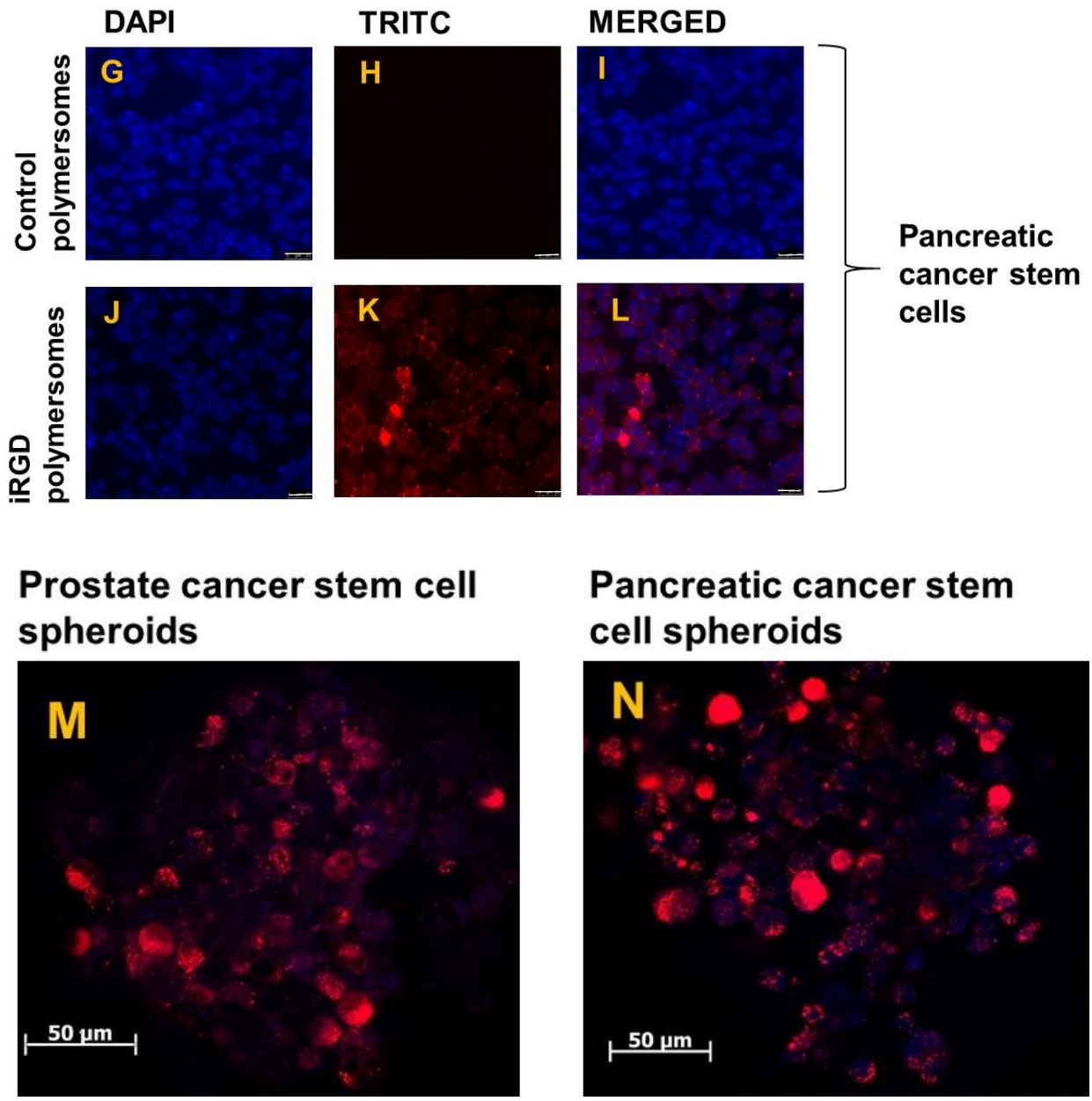

Figure 3.4. Cellular uptake studies in monolayer and microtumor cultures of prostate and pancreatic cancer stem cells**.** (continued)
Panels (**A**-**F**): prostate cancer stem cells (scale bar: 25 µm), and Panels (**G**-**L**): pancreatic cancer stem cells (scale bar: 25µm). (**M**, **N**) Cellular uptake studies in a microtumor slice 200 µm from the surface of prostate cancer stem cells (**M**) and pancreatic cancer stem cell spheroids (**N**). The co-localization of the red fluorescence from the lissamine rhodamine dye and the blue from HOECHST 33342 indicated that peptide-targeted polymersomes were internalized in the cells. The blue fluorescence from the HOECHST 33342 dye indicates the cell nuclei.

To investigate the depth of the penetration of iRGD targeted polymersomes, we prepared three-dimensional spheroids of prostate and pancreatic cancer stem cells were prepared using the 35-well 3D petri dishes (Microtissues). The microtumors fully formed after 3-4 days. The microtumors were incubated with the iRGD targeted polymersomes for 8 hours. Subsequently, the microtumors were washed with sterile PBS, and the nuclei were stained with HOESCHT 33342. Finally, microtumors were frozen and sliced with a microtome into 15 μm sections. We observed the red fluorescence from the polymersome-incorporated LR dye was observed in both prostate and pancreatic cancer stem cells colocalized with the blue nuclear stain in a slice 200 μm from the surface. These images show iRGD targeted polymersomes penetrating at least 200 μm into microtumors of prostate and pancreatic cancer stem cells (Figure 3.4 **M**, **N**).

3.4.5. Neuropilin -1 expression on the cancer stem cells

Neuropilin-1 (NR-1) is a 130-140 kDa type I transmembrane protein [145] that interacts with an isoform of vascular endothelial growth factor (VEGF). It is an endothelial cell-specific mitogen and acts as a coreceptor for class 3 semaphorins. The neuropilin receptor has roles in cell survival, migration, and invasion [146] Expression of NR-1 in the epithelial cells of uterus, endometrium, lung, and kidney have been reported.[145] Glinka at el showed that NR-1 is expressed in breast cancer stem-like cells, activates the NF-KB, and aids in the tumor spheroids formation.[147] Since there was no prior report, the expression of the neuropilin-1 receptor on prostate and pancreatic cancer stem cells was investigated by employing western blotting. Prostate and pancreatic cancer stem cells were shown to express the neuropilin-1 receptor (Figure 3.5). Hence, it is likely that that the cellular internalization of the iRGD-targeted polymersomes (Figure 3.4) is mediated by the neuropilin-1 receptor on the surface of the cancer stem cells.

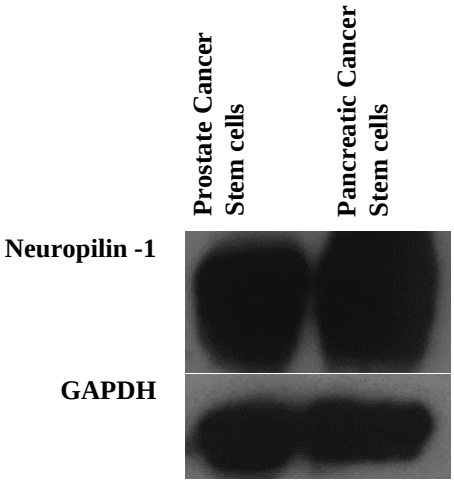

Figure 3.5. Expression of neuropilin-1 in prostate and pancreatic cancer stem cells as determined by Western Blotting.

3.4.6. Viability of prostate and pancreatic cancer stem cells in monolayer cultures

After validating the expression of neuropilin-1 on the cancer stem cells, the effectiveness of the peptide-targeted, drug-encapsulated polymersomes was determined in both prostate and pancreatic cancer stem cells. The monolayer cultures of both prostate and pancreatic cancer stem cells were treated with the polymersomes, polymersomes encapsulating napabucasin, peptide-targeted napabucasin-encapsulating polymersomes, and the free drug (napabucasin) for 48 hours. The cell viability was determined by the Alamar Blue assay (Figure 3.6A, B). The result shows that the targeted polymersomes encapsulating napabucasin significantly ($p<0.5$) reduced cell viability in both prostate and pancreatic cancer stem cells (30% and 19%, respectively) compared to the control polymersomes and vesicles encapsulating napabucasin. We also observed that increasing the concentration of encapsulated napabucasin from 1 μM to 4 μM led to a pronounced decrease in the cell viability (Figures 3.6A and B).

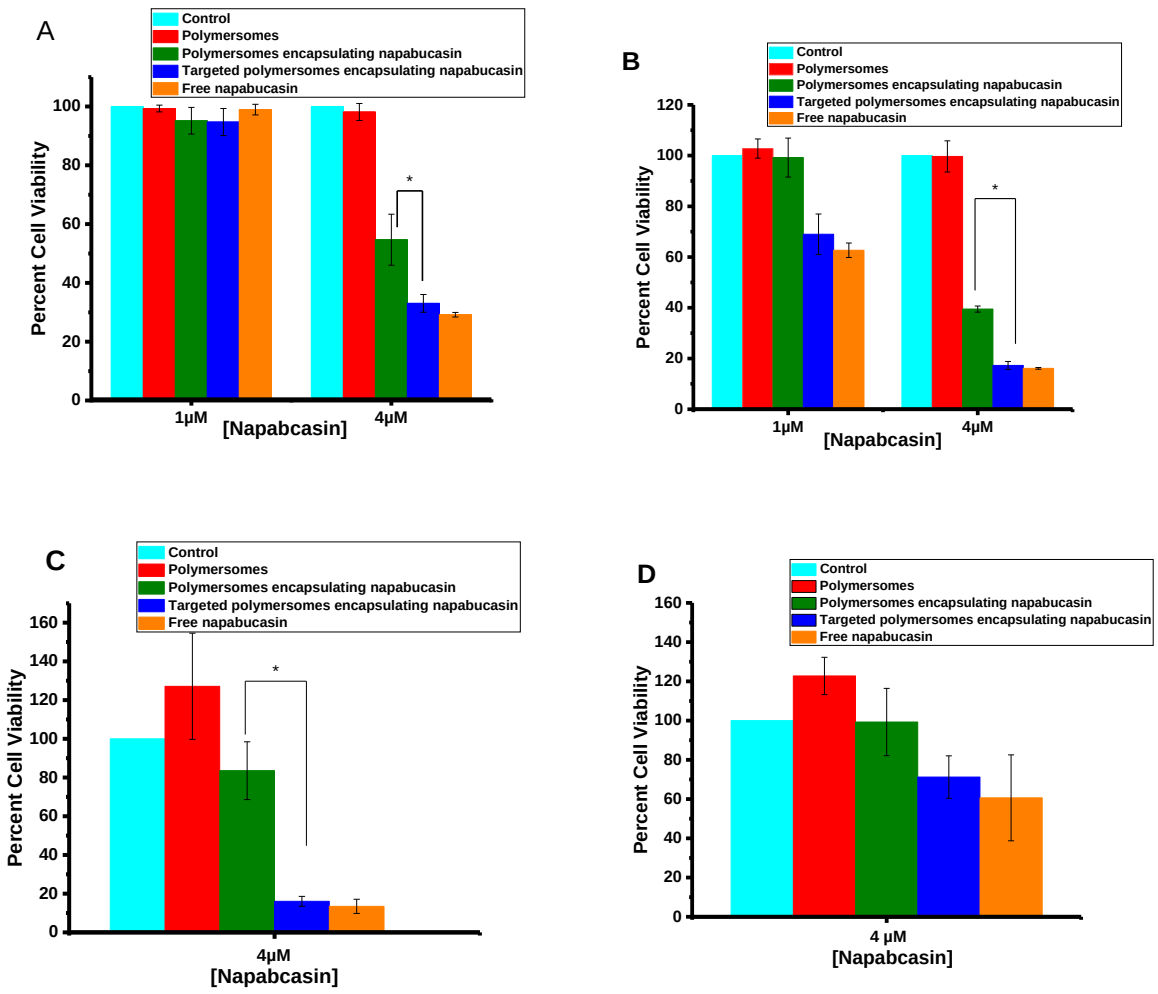

Figure 3.6. The viability of prostate and pancreatic cancer stem cells in monolayer and spheroid cultures. (A) Monolayer cultures of prostate cancer stem cells, (B) monolayer cultures of pancreatic cancer stem cells, (C) microtumors of prostate cancer stem cells, and (D) microtumors of pancreatic cancer stem cells in cultures. Cell viability with media only (control, media treated, cyan bar), polymersomes (red bar), non-targeted polymersomes encapsulating napabucasin (green bar), peptide-targeted polymersomes encapsulating napabucasin (blue bar), and free napabucasin (orange bar, N = 4).

3.4.7. Viability of prostate and pancreatic cancer stem cells in microtumors

Microtumors of prostate and pancreatic cancer stem cells were prepared in 35-well 3D petri dishes. The formed microtumors were randomly assigned to five groups: control, polymersomes, non-targeted polymersomes encapsulating napabucasin, peptide-targeted polymersomes encapsulating napabucasin, and free napabucasin. The cultured microtumors were

treated for 48 hours, and subsequently, Alamar Blue assay was performed to determine the cell viability. Targeted-polymersomes encapsulating napabucasin were observed toreduce the viability of prostate cancer stem cells to 19% and pancreatic cancer stem cell to 65% (Figure 3.6C and 3.6D). The significantly reduced cell viability compared to the control groups indicated that the peptide-targeted polymersomes could penetrate the spheroids through the neuropilin-1 receptor and internalize in the cells. The interaction between CendR motif and NR-1 contributed to the cellular internalization of the targeted polymersomes.[45] Furthermore, the cytotoxicity increased when the vesicles were targeted with the cyclic iRGD peptide, which facilitates the internalization of polymersomes into the cells. However, increased effectiveness of the targeted polymersomes for the prostate cancer stem cells compared to the pancreatic cancer stem cells remains unexplained.

3.4.8. Cancer stemness protein expression

The stemness protein expression of prostate cancer stem cells was investigated by western blot. Proteins were extracted from the prostate cancer stem cells after treatment with a different formulation of polymersomes. The expression of cancer stemness markers such as Notch-1 and Nanog were significantly decreased after treatment with polymersomes encapsulating napabucasin, targeted polymersomes encapsulating napabucasin, and free napabucasin compared to the control groups (Figure 3.7 and Supplementary Data). Zhang and Li at el also reported the decreased expression of Nanog after treatment with napabucasin.[7, 120]

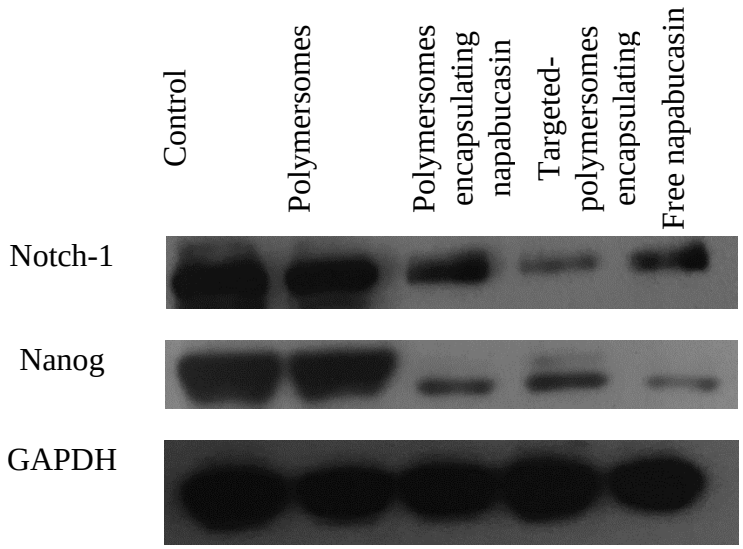

Figure 3.7. Effect of cancer stemness inhibitor (napabucasin) on the expression of two stemness marker proteins, Notch and Nanog.

3.4.9. Cell apoptosis assay by flow cytometry

The apoptotic effects of the polymersomes on the prostate and pancreatic cancer stem cells were examined by staining of the cells with Annexin V-FITC and propidium iodide (PI) followed by flow cytometry analysis. Annexin V is a Ca^{2+} dependent phospholipid binding protein[148] that has a high affinity for phosphatidylserine. Phosphatidylserine is present in the inner leaflet of healthy cell membranes but is rapidly translocated to the outer leaflet during the early stages of apoptosis[149] and therefore serves as a marker for those cells that have committed to apoptotic cell death. In contrast, PI crosses the membranes of dead or dying cells, intercalates with DNA, emits red fluorescence[148, 149], and serves as a non-specific marker of cell death regardless of mechanism. After treatment with the targeted-polymersomes encapsulating napabucasin, 76% of the prostate cancer stem cells showed early apoptosis, whereas the polymersomes themselves were not toxic (Figure 3.8A). Treatment of pancreatic cancer stem cells with targeted polymersomes encapsulating napabucasin led to 83% of cells staining positive for PI, and 13% exhibiting signs of early apoptosis (Figure 3.8B). iRGD-targeted polymersomes

encapsulating napabucasin leads to significant stem cell death with signs of apoptosis in both prostate and pancreatic cancer stem cells.

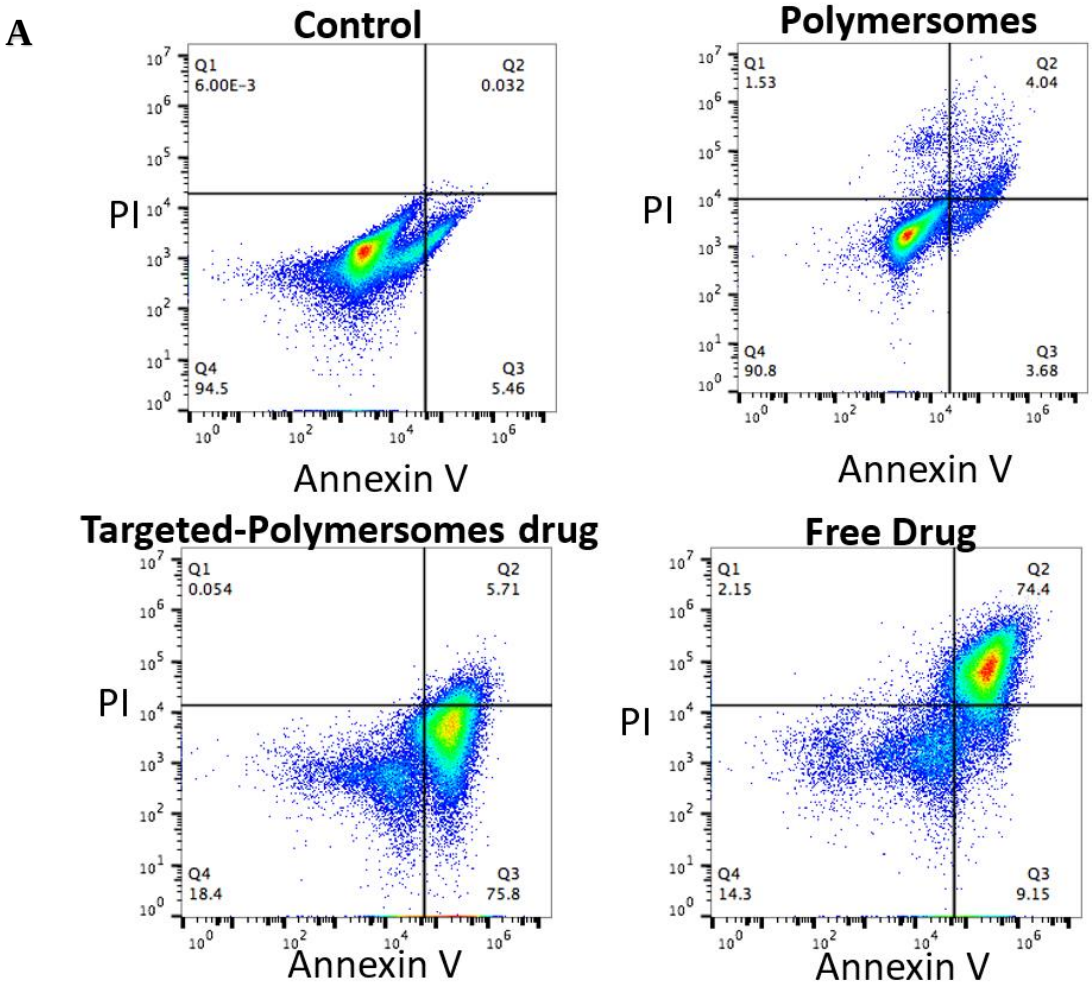

Figure 3.8. Flow cytometry analysis of the effect of napabucasin. Prostate cancer stem cells (A) and pancreatic cancer stem cells (B) with Annexin V and PI staining.

B

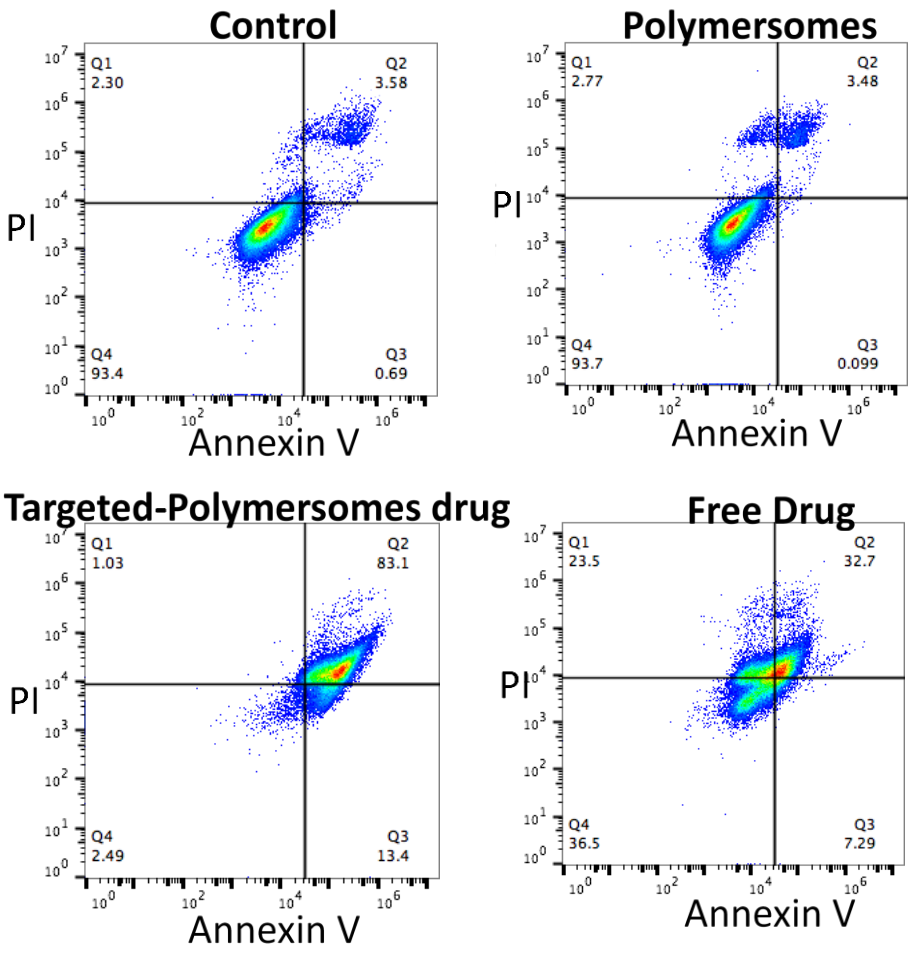

Figure 3.8. Flow cytometry analysis of the effect of napabucasin. (continued) Prostate cancer stem cells (A) and pancreatic cancer stem cells (B) with Annexin V and PI staining.

3.5. Conclusion

We have demonstrated that neuropilin-1 is a target receptor overexpressed in both pancreatic and prostate cancer stem cells. The iRGD peptide-decorated polymersomes encapsulating the cancer stemness inhibitor napabucasin were developed to provide effective targeting to the neuropilin-1 receptors. Significant growth inhibition and decreased cancer stemness protein expression in cancer stem cells in the presence of napabucasin-encapsulating, targeted polymersomes. The iRGD targeted polymersomes penetrated the microtumors of prostate and pancreatic cancer stem cells to at least 200 μm. The result of this study will provide new directions in targeting cancer stem cells for overcoming recurrence in prostate and pancreatic cancers. Further pharmacokinetic and immunogenicity studies of the targeted polymersomes encapsulating napabucasin would overcome the chemotherapeutic side effects of cancer treatment.

OVERAL CONCLUSION AND FUTURE DIRECTIONS

Heterogeneity is the inherent trait of cancer. Accumulation of genetic alterations in the same tumor may cause a mixed response, resistance, metastasis, and recurrence of disease after initial treatment. Tumor microenvironment, epithelial to mesenchymal transition, hypoxia, and cancer stem cells contribute to tumor remodeling and progression.[7] Advanced scientific approaches to further investigate the heterogeneity and effect of the tumor microenvironment is essential to find the specific target to develop an effective therapeutic treatment. Nanocarriers can surpass the limitations of conventional treatments, such as poor water solubility, bioavailability and biodistribution.[150] Multifunctional nanoparticles, such as stimuli-responsive nanoparticles which are long-circulating, target the cancer cells, and release their encapsulated drugs in response to a microenvironment trigger to enhance the antitumor efficacy.[150] We successfully prepared redox-sensitive polymeric nanoparticles. These polymersomes can target different overexpressed receptors, such as prostate-specific membrane antigen, neuropilin-1, folate receptor, etc. We developed and characterized targeted, redox-responsive echogenic polymersomes that encapsulate hydrophobic chemotherapeutic drugs. Echogenic characteristic of polymersomes enables them to be tracked by diagnostic ultrasound. We demonstrated drug release from the polymersomes in vitro using monolayer cultures of cancer cells and microtumors. We also found that prostate and pancreatic cancer stem cell express the neuropilin-1 receptor.

In Chapter 1, we exploited the PSMA expression and designed targeted, redox-sensitive polymersomes that encapsulate docetaxel and mocetinostat. These polymersomes released the encapsulated drugs in response to the reducing agent concentration in the cytosol of prostate cancer cells. We observed that co-administration of mocetinostat and docetaxel has a synergetic

effect and significantly reduced the viability of the LNCaP cells. We have used a redox-sensitive polymer in preparation of nanoparticles. Since most of the solid tumor is hypoxic it would be an interesting idea to test these formulations with solid tumors.

In chapter 2, we prepared nucleus-targeted, echogenic, redox-sensitive polymersomes to deliver the cancer stemness inhibitor BBI608 to pancreatic cancer cells. We used dexamethasone as a targeting moiety to dilate the nuclear pore complexes. We encapsulated the cancer stemness inhibitor napabucasin in the polymersomes. The release of the cancer stemness inhibitor in the pancreatic cancer cell lead to decreased viability after treatment. The echogenic character of polymersomes was determined. We observed that echogenic polymersomes were trackable by diagnostic frequency ultrasound. Ultrasound imaging of the polymersomes in a mouse model would give us better understanding of the accumulation of the targeted polymersomes in the tumor. It would be interesting to investigate if iRGD peptide-targeted echogenic polymersomes could be used as a diagnostic tool for cancer detection.

In chapter 3, we demonstrated the expression of neuropilin-1 receptor on prostate and pancreatic cancer stem cells. We synthesized the iRGD peptide to target the neuropilin-1 receptor on both prostate and pancreatic cancer stem cells. Reduction-sensitive, iRGD incorporated polymersomes encapsulating BBI608 significantly decreased the viability of both prostate and pancreatic cancer stem cells. We observed that the expression of cancer stemness proteins, such as Notch-1 and Nanog decreased substantially after the treatment compared to the control.

We also established the preliminary data on the penetration of iRGD peptide-decorated polymersomes in microtumors. Further investigation of iRGD peptide targeting of stimuli-

responsive polymersomes in a mouse model can help to evaluate the effectiveness of the targeted, tumor-penetrating delivery system.

REFERENCES

[1] Siegel, R. L., Miller, K. D., and Jemal, A. (2016) Cancer statistics, 2016, *CA: a cancer journal for clinicians 66*, 7-30.

[2] Kleppe, M., and Levine, R. L. (2014) Tumor heterogeneity confounds and illuminates: assessing the implications, *Nat Med 20*, 342-344.

[3] Agliano, A., Calvo, A., and Box, C. (2017) The challenge of targeting cancer stem cells to halt metastasis, In *Seminars in Cancer Biology*, Elsevier.

[4] Clarke, M. F., Dick, J. E., Dirks, P. B., Eaves, C. J., Jamieson, C. H. M., Jones, D. L., Visvader, J., Weissman, I. L., and Wahl, G. M. (2006) Cancer Stem Cells—Perspectives on Current Status and Future Directions: AACR Workshop on Cancer Stem Cells, *Cancer Research 66*, 9339-9344.

[5] Shackleton, M. (2010) Normal stem cells and cancer stem cells: similar and different, In *Seminars in cancer biology*, pp 85-92, Elsevier.

[6] Lee, H. E., Kim, J. H., Kim, Y. J., Choi, S., Kim, S., Kang, E., Chung, I., Kim, I., Kim, E., and Choi, Y. (2011) An increase in cancer stem cell population after primary systemic therapy is a poor prognostic factor in breast cancer, *British journal of cancer 104*, 1730.

[7] Li, Y., Rogoff, H. A., Keates, S., Gao, Y., Murikipudi, S., Mikule, K., Leggett, D., Li, W., Pardee, A. B., and Li, C. J. (2015) Suppression of cancer relapse and metastasis by inhibiting cancer stemness, *Proceedings of the National Academy of Sciences 112*, 1839-1844.

[8] Verga Falzacappa, M. V., Ronchini, C., Reavie, L. B., and Pelicci, P. G. (2012) Regulation of self-renewal in normal and cancer stem cells, *Febs j 279*, 3559-3572.

[9] Hermann, P. C., Bhaskar, S., Cioffi, M., and Heeschen, C. (2010) Cancer stem cells in solid tumors, In *Seminars in cancer biology*, pp 77-84, Elsevier.

[10] Gu, G., Yuan, J., Wills, M., and Kasper, S. (2007) Prostate cancer cells with stem cell characteristics reconstitute the original human tumor in vivo, *Cancer research 67*, 4807-4815.

[11] Reya, T., Morrison, S. J., Clarke, M. F., and Weissman, I. L. (2001) Stem cells, cancer, and cancer stem cells, *Nature 414*, 105-111.

[12] Lai, E. C. (2004) Notch signaling: control of cell communication and cell fate, *Development 131*, 965-973.

[13] Polakis, P. (2007) The many ways of Wnt in cancer, *Current opinion in genetics & development 17*, 45-51.

[14] Dessaud, E., McMahon, A. P., and Briscoe, J. (2008) Pattern formation in the vertebrate neural tube: a sonic hedgehog morphogen-regulated transcriptional network, *Development 135*, 2489-2503.

[15] Hernandez-Vargas, H., Ouzounova, M., Le Calvez-Kelm, F., Lambert, M. P., McKay-Chopin, S., Tavtigian, S. V., Puisieux, A., Matar, C., and Herceg, Z. (2011) Methylome analysis reveals Jak-STAT pathway deregulation in putative breast cancer stem cells, *Epigenetics 6*, 428-439.

[16] Hubbard, J. M., and Grothey, A. (2017) Napabucasin: An Update on the First-in-Class Cancer Stemness Inhibitor, *Drugs 77*, 1091-1103.

[17] Li, C., Heidt, D. G., Dalerba, P., Burant, C. F., Zhang, L., Adsay, V., Wicha, M., Clarke, M. F., and Simeone, D. M. (2007) Identification of pancreatic cancer stem cells, *Cancer research 67*, 1030-1037.

[18] Hermann, P. C., Huber, S. L., Herrler, T., Aicher, A., Ellwart, J. W., Guba, M., Bruns, C. J., and Heeschen, C. (2007) Distinct populations of cancer stem cells determine tumor growth and metastatic activity in human pancreatic cancer, *Cell stem cell 1*, 313-323.
[19] Peer, D., Karp, J. M., Hong, S., Farokhzad, O. C., Margalit, R., and Langer, R. (2007) Nanocarriers as an emerging platform for cancer therapy, *Nat Nano 2*, 751-760.
[20] Rancea, M., von Tresckow, B., Monsef, I., Engert, A., and Skoetz, N. (2014) High-dose chemotherapy followed by autologous stem cell transplantation for patients with relapsed or refractory Hodgkin lymphoma: A systematic review with meta-analysis, *Critical Reviews in Oncology/Hematology 92*, 1-10.
[21] Neoptolemos, J. P., Dunn, J. A., Stocken, D. D., Almond, J., Link, K., Beger, H., Bassi, C., Falconi, M., Pederzoli, P., Dervenis, C., Fernandez-Cruz, L., Lacaine, F., Pap, A., Spooner, D., Kerr, D. J., Friess, H., and Büchler, M. W. (2001) Adjuvant chemoradiotherapy and chemotherapy in resectable pancreatic cancer: a randomised controlled trial, *The Lancet 358*, 1576-1585.
[22] Li, C. Q., and Zhang, G. X. (2008) Nanosize delivery as an emerging platform for cancer therapy, *Cancer biology & therapy 7*, 1860-1862.
[23] Brigger, I., Dubernet, C., and Couvreur, P. (2012) Nanoparticles in cancer therapy and diagnosis, *Advanced Drug Delivery Reviews 64*, 24-36.
[24] Peer, D., Karp, J. M., Hong, S., Farokhzad, O. C., Margalit, R., and Langer, R. (2007) Nanocarriers as an emerging platform for cancer therapy, *Nature nanotechnology 2*, 751-760.
[25] Gao, Y., Li, Y., Li, Y., Yuan, L., Zhou, Y., Li, J., Zhao, L., Zhang, C., Li, X., and Liu, Y. (2015) PSMA-mediated endosome escape-accelerating polymeric micelles for targeted therapy of prostate cancer and the real time tracing of their intracellular trafficking, *Nanoscale 7*, 597-612.
[26] Farokhzad, O. C., Jon, S., Khademhosseini, A., Tran, T.-N. T., LaVan, D. A., and Langer, R. (2004) Nanoparticle-aptamer bioconjugates a new approach for targeting prostate cancer cells, *Cancer research 64*, 7668-7672.
[27] Kroon, J., Buijs, J. T., van der Horst, G., Cheung, H., van der Mark, M., van Bloois, L., Rizzo, L. Y., Lammers, T., Pelger, R. C., and Storm, G. (2015) Liposomal delivery of dexamethasone attenuates prostate cancer bone metastatic tumor growth in vivo, *The Prostate 75*, 815-824.
[28] Katti, K. S., Molla, M., Karandish, F., Haldar, M. K., Mallik, S., and Katti, D. R. (2016) Sequential culture on biomimetic nanoclay scaffolds forms three-dimensional tumoroids, *Journal of Biomedical Materials Research Part A*.
[29] Cheng, C. J., and Saltzman, W. M. (2012) Polymer Nanoparticle-Mediated Delivery of MicroRNA Inhibition and Alternative Splicing, *Molecular Pharmaceutics 9*, 1481-1488.
[30] Lewin, M., Carlesso, N., Tung, C.-H., Tang, X.-W., Cory, D., Scadden, D. T., and Weissleder, R. (2000) Tat peptide-derivatized magnetic nanoparticles allow in vivo tracking and recovery of progenitor cells, *Nature biotechnology 18*, 410-414.
[31] Liu, X., Liu, C., Laurini, E., Posocco, P., Pricl, S., Qu, F., Rocchi, P., and Peng, L. (2012) Efficient delivery of sticky siRNA and potent gene silencing in a prostate cancer model using a generation 5 triethanolamine-core PAMAM dendrimer, *Mol Pharm 9*, 470-481.
[32] Katti, K. S., Molla, M., Karandish, F., Haldar, M. K., Mallik, S., and Katti, D. R. (2016) Sequential culture on biomimetic nanoclay scaffolds forms three-dimensional tumoroids, *Journal of Biomedical Materials Research Part A 104*, 1591-1602.

[33] Liu, G.-Y., Chen, C.-J., and Ji, J. (2012) Biocompatible and biodegradable polymersomes as delivery vehicles in biomedical applications, *Soft Matter 8*, 8811-8821.
[34] Lee, J. S., and Feijen, J. (2012) Polymersomes for drug delivery: Design, formation and characterization, *Journal of Controlled Release 161*, 473-483.
[35] Wang, A. Z., Langer, R., and Farokhzad, O. C. (2012) Nanoparticle delivery of cancer drugs, *Annual review of medicine 63*, 185-198.
[36] Gabizon, A., Catane, R., Uziely, B., Kaufman, B., Safra, T., Cohen, R., Martin, F., Huang, A., and Barenholz, Y. (1994) Prolonged circulation time and enhanced accumulation in malignant exudates of doxorubicin encapsulated in polyethylene-glycol coated liposomes, *Cancer research 54*, 987-992.
[37] Nahire, R., Haldar, M. K., Paul, S., Ambre, A. H., Meghnani, V., Layek, B., Katti, K. S., Gange, K. N., Singh, J., and Sarkar, K. (2014) Multifunctional polymersomes for cytosolic delivery of gemcitabine and doxorubicin to cancer cells, *Biomaterials 35*, 6482-6497.
[38] Matsumura, Y., and Maeda, H. (1986) A new concept for macromolecular therapeutics in cancer chemotherapy: mechanism of tumoritropic accumulation of proteins and the antitumor agent smancs, *Cancer research 46*, 6387-6392.
[39] Bae, Y. H., and Park, K. (2011) Targeted drug delivery to tumors: myths, reality and possibility, *Journal of Controlled Release 153*, 198.
[40] Byrne, J. D., Betancourt, T., and Brannon-Peppas, L. (2008) Active targeting schemes for nanoparticle systems in cancer therapeutics, *Advanced Drug Delivery Reviews 60*, 1615-1626.
[41] Musumeci, F., Radi, M., Brullo, C., and Schenone, S. (2012) Vascular endothelial growth factor (VEGF) receptors: drugs and new inhibitors, *Journal of medicinal chemistry 55*, 10797-10822.
[42] Backer, M. V., Gaynutdinov, T. I., Patel, V., Bandyopadhyaya, A. K., Thirumamagal, B., Tjarks, W., Barth, R. F., Claffey, K., and Backer, J. M. (2005) Vascular endothelial growth factor selectively targets boronated dendrimers to tumor vasculature, *Molecular cancer therapeutics 4*, 1423-1429.
[43] Chen, J., Wu, H., Han, D., and Xie, C. (2006) Using anti-VEGF McAb and magnetic nanoparticles as double-targeting vector for the radioimmunotherapy of liver cancer, *Cancer letters 231*, 169-175.
[44] Horton, M. A. (1997) The αvβ3 integrin "vitronectin receptor", *The International Journal of Biochemistry & Cell Biology 29*, 721-725.
[45] Sugahara, K. N., Teesalu, T., Karmali, P. P., Kotamraju, V. R., Agemy, L., Girard, O. M., Hanahan, D., Mattrey, R. F., and Ruoslahti, E. (2009) Tissue-penetrating delivery of compounds and nanoparticles into tumors, *Cancer cell 16*, 510-520.
[46] KC, L. (1998) Detection of tumor angiogenesis in vivo by alphaVbeta3-targeted magnetic resonance imaging, *Nat Med 4*, 623-626.
[47] Arap, W., Pasqualini, R., and Ruoslahti, E. (1998) Cancer treatment by targeted drug delivery to tumor vasculature in a mouse model, *Science 279*, 377-380.
[48] Murphy, E. A., Majeti, B. K., Barnes, L. A., Makale, M., Weis, S. M., Lutu-Fuga, K., Wrasidlo, W., and Cheresh, D. A. (2008) Nanoparticle-mediated drug delivery to tumor vasculature suppresses metastasis, *Proceedings of the National Academy of Sciences 105*, 9343-9348.
[49] Pasqualini, R., Koivunen, E., and Ruoslahti, E. (1997) [alpha]v Integrins as receptors for tumor targeting by circulating ligands, *Nat Biotech 15*, 542-546.

[50] Ruoslahti, E. (2017) Tumor penetrating peptides for improved drug delivery, *Advanced Drug Delivery Reviews 110*, 3-12.
[51] Gialeli, C., Theocharis, A. D., and Karamanos, N. K. (2011) Roles of matrix metalloproteinases in cancer progression and their pharmacological targeting, *The FEBS journal 278*, 16-27.
[52] Shay, G., Lynch, C. C., and Fingleton, B. (2015) Moving targets: Emerging roles for MMPs in cancer progression and metastasis, *Matrix biology : journal of the International Society for Matrix Biology 44-46*, 200-206.
[53] Karandish, F., and Mallik, S. (2016) Biomarkers and Targeted Therapy in Pancreatic Cancer, *Biomarkers in Cancer 8*, 27-35.
[54] Shankar, S., Ganapathy, S., Hingorani, S. R., and Srivastava, R. K. (2008) EGCG inhibits growth, invasion, angiogenesis and metastasis of pancreatic cancer, *Frontiers in bioscience : a journal and virtual library 13*, 440-452.
[55] Kulkarni, P. S., Haldar, M. K., Nahire, R. R., Katti, P., Ambre, A. H., Muhonen, W. W., Shabb, J. B., Padi, S. K. R., Singh, R. K., Borowicz, P. P., Shrivastava, D. K., Katti, K. S., Reindl, K., Guo, B., and Mallik, S. (2014) MMP-9 Responsive PEG Cleavable Nanovesicles for Efficient Delivery of Chemotherapeutics to Pancreatic Cancer, *Molecular Pharmaceutics 11*, 2390-2399.
[56] Bromberg, J., and Darnell, J. E., Jr. (2000) The role of STATs in transcriptional control and their impact on cellular function, *Oncogene 19*, 2468-2473.
[57] Rogoff, H. A., Li, J., and Li, C. (2017) Cancer stemness and resistance: Napabucasin (BBI-608) sensitizes stemness-high cancer cells to Paclitaxel by inhibiting the STAT3-MUC1 pathway, AACR.
[58] Langleben, A., Supko, J. G., Hotte, S. J., Batist, G., Hirte, H. W., Rogoff, H., Li, Y., Li, W., Kerstein, D., and Leggett, D. (2013) A dose-escalation phase I study of a first-in-class cancer stemness inhibitor in patients with advanced malignancies, American Society of Clinical Oncology.
[59] Jonker, D. J., Stephenson, J., Edenfield, W. J., Supko, J. G., Li, Y., Li, W., Hitron, M., Leggett, D., Kerstein, D., and Li, C. (2014) A phase I extension study of BBI608, a first-in-class cancer stem cell (CSC) inhibitor, in patients with advanced solid tumors, American Society of Clinical Oncology.
[60] Hitron, M., Stephenson, J., Chi, K. N., Edenfield, W. J., Leggett, D., Li, Y., Li, W., Gada, K., and Li, C. (2014) A phase 1b study of the cancer stem cell inhibitor BBI608 administered with paclitaxel in patients with advanced malignancies, American Society of Clinical Oncology.
[61] Garcia, A. A., Hays, J. L., Cote, G. M., Becerra, C., Langleben, A., Lau, S. K., Roman, L. D., McCormick, C. C., Richards, D. A., and Braiteh, F. S. (2016) A phase Ib/II study of cancer stemness inhibitor napabucasin (BB608) combined with weekly paclitaxel in platinum-resistant ovarian cancer, American Society of Clinical Oncology.
[62] Becerra, C., Stephenson, J., Jonker, D. J., Cohn, A. L., Asmis, T. R., Bekaii-Saab, T. S., Conkling, P. R., Garbo, L. E., Lenz, H.-J., and Richards, D. A. (2015) Phase Ib/II study of cancer stem cell (CSC) inhibitor BBI608 combined with paclitaxel in advanced gastric and gastroesophageal junction (GEJ) adenocarcinoma, American Society of Clinical Oncology.
[63] Bekaii-Saab, T. S., Mikhail, S., Langleben, A., Becerra, C., Jonker, D. J., Asmis, T. R., Cote, G. M., Wu, C. S.-Y., Kwak, E. L., Spira, A. I., Braiteh, F. S., Richey, S. L., Hume,

S., Hitron, M., and Li, C. (2016) A phase Ib/II study of BBI608 combined with weekly paclitaxel in advanced pancreatic cancer, *Journal of Clinical Oncology 34*, 196-196.
[64] Larson, T., Ortuzar, W. F., Bekaii-Saab, T. S., Becerra, C., Ciombor, K. K., Hubbard, J. M., Edenfield, W. J., Shao, S. H., Grothey, A., and Borodyansky, L. (2017) BBI608-224: A phase Ib/II study of cancer stemness inhibitor napabucasin (BBI-608) administered with panitumumab in KRAS wild-type patients with metastatic colorectal cancer, American Society of Clinical Oncology.
[65] Frankel, C. (2000) Development and clinical overview of trastuzumab (herceptin), *Seminars in Oncology Nursing 16*, 13-17.
[66] Hynes, N. E., and Stern, D. F. (1994) The biology of erbB-2/nue/HER-2 and its role in cancer, *Biochimica et Biophysica Acta (BBA) - Reviews on Cancer 1198*, 165-184.
[67] Zurrida, S., and Veronesi, U. (2015) Milestones in breast cancer treatment, *The breast journal 21*, 3-12.
[68] Qian, Z. M., Li, H., Sun, H., and Ho, K. (2002) Targeted Drug Delivery via the Transferrin Receptor-Mediated Endocytosis Pathway, *Pharmacological Reviews 54*, 561-587.
[69] Högemann-Savellano, D., Bos, E., Blondet, C., Sato, F., Abe, T., Josephson, L., Weissleder, R., Gaudet, J., Sgroi, D., Peters, P. J., and Basilion, J. P. (2003) The Transferrin Receptor: A Potential Molecular Imaging Marker for Human Cancer, *Neoplasia 5*, 495-506.
[70] Daniels, T. R., Bernabeu, E., Rodríguez, J. A., Patel, S., Kozman, M., Chiappetta, D. A., Holler, E., Ljubimova, J. Y., Helguera, G., and Penichet, M. L. (2012) The transferrin receptor and the targeted delivery of therapeutic agents against cancer, *Biochimica et Biophysica Acta (BBA) - General Subjects 1820*, 291-317.
[71] Low, P. S., and Antony, A. C. (2004) Folate receptor-targeted drugs for cancer and inflammatory diseases, *Advanced Drug Delivery Reviews 56*, 1055-1058.
[72] Zhao, X., Li, H., and Lee, R. J. (2008) Targeted drug delivery via folate receptors, *Expert opinion on drug delivery 5*, 309-319.
[73] Graybill, W. S., and Coleman, R. L. (2014) Vintafolide: a novel targeted agent for epithelial ovarian cancer, *Future oncology 10*, 541-548.
[74] Karandish, F., Haldar, M. K., You, S., Brooks, A. E., Brooks, B. D., Guo, B., Choi, Y., and Mallik, S. (2016) Prostate-Specific Membrane Antigen Targeted Polymersomes for Delivering Mocetinostat and Docetaxel to Prostate Cancer Cell Spheroids, *ACS omega 1*, 952-962.
[75] Ciccarese, C., Massari, F., Iacovelli, R., Fiorentino, M., Montironi, R., Di Nunno, V., Giunchi, F., Brunelli, M., and Tortora, G. (2017) Prostate cancer heterogeneity: Discovering novel molecular targets for therapy, *Cancer Treatment Reviews*.
[76] Kamerkar, S., LeBleu, V. S., Sugimoto, H., Yang, S., Ruivo, C. F., Melo, S. A., Lee, J. J., and Kalluri, R. (2017) Exosomes facilitate therapeutic targeting of oncogenic KRAS in pancreatic cancer, *Nature advance online publication*.
[77] Witz, I. P. (2009) The tumor microenvironment: the making of a paradigm, *Cancer Microenvironment 2*, 9-17.
[78] Hirata, E., and Sahai, E. (2017) Tumor microenvironment and differential responses to therapy, *Cold Spring Harbor Perspectives in Medicine*, a026781.
[79] Whiteside, T. (2008) The tumor microenvironment and its role in promoting tumor growth, *Oncogene 27*, 5904.

[80] Mazure, N. M., Chen, E. Y., Yeh, P., Laderoute, K. R., and Giaccia, A. J. (1996) Oncogenic transformation and hypoxia synergistically act to modulate vascular endothelial growth factor expression, *Cancer Research 56*, 3436-3440.
[81] Ganta, S., Devalapally, H., Shahiwala, A., and Amiji, M. (2008) A review of stimuli-responsive nanocarriers for drug and gene delivery, *Journal of controlled release 126*, 187-204.
[82] Kamat, N. P., Robbins, G. P., Rawson, J., Therien, M. J., Dmochowski, I. J., and Hammer, D. A. (2010) A generalized system for photoresponsive membrane rupture in polymersomes, *Advanced functional materials 20*, 2588-2596.
[83] Amstad, E., Kim, S. H., and Weitz, D. A. (2012) Photo-and thermoresponsive polymersomes for triggered release, *Angewandte Chemie 124*, 12667-12671.
[84] Chen, W., and Du, J. (2013) Ultrasound and pH dually responsive polymer vesicles for anticancer drug delivery, *Scientific reports 3*.
[85] Harris, A. L. (2002) Hypoxia—a key regulatory factor in tumour growth, *Nature Reviews Cancer 2*, 38-47.
[86] Danhier, F., Feron, O., and Préat, V. (2010) To exploit the tumor microenvironment: Passive and active tumor targeting of nanocarriers for anti-cancer drug delivery, *Journal of Controlled Release 148*, 135-146.
[87] West, K. R., and Otto, S. (2005) Reversible covalent chemistry in drug delivery, *Current drug discovery technologies 2*, 123-160.
[88] Vaupel, P., Kallinowski, F., and Okunieff, P. (1989) Blood flow, oxygen and nutrient supply, and metabolic microenvironment of human tumors: a review, *Cancer research 49*, 6449-6465.
[89] Kanamala, M., Wilson, W. R., Yang, M., Palmer, B. D., and Wu, Z. (2016) Mechanisms and biomaterials in pH-responsive tumour targeted drug delivery: A review, *Biomaterials 85*, 152-167.
[90] Wilson, W. R., and Hay, M. P. (2011) Targeting hypoxia in cancer therapy, *Nature Reviews Cancer 11*, 393-410.
[91] Perche, F., Biswas, S., Wang, T., Zhu, L., and Torchilin, V. (2014) Hypoxia-Targeted siRNA Delivery, *Angewandte Chemie International Edition 53*, 3362-3366.
[92] Semenza, G. L. (2003) Targeting HIF-1 for cancer therapy, *Nature reviews. Cancer 3*, 721.
[93] Brülisauer, L., Gauthier, M. A., and Leroux, J.-C. (2014) Disulfide-containing parenteral delivery systems and their redox-biological fate, *Journal of Controlled Release 195*, 147-154.
[94] Larson, R. A., Sievers, E. L., Stadtmauer, E. A., Löwenberg, B., Estey, E. H., Dombret, H., Theobald, M., Voliotis, D., Bennett, J. M., and Richie, M. (2005) Final report of the efficacy and safety of gemtuzumab ozogamicin (Mylotarg) in patients with CD33-positive acute myeloid leukemia in first recurrence, *Cancer 104*, 1442-1452.
[95] Mitragotri, S. (2005) Healing sound: the use of ultrasound in drug delivery and other therapeutic applications, *Nature reviews. Drug discovery 4*, 255.
[96] Morishita, R., Tomita, N., Kaneda, Y., and Ogihara, T. (2004) Molecular therapy to inhibit NFκB activation by transcription factor decoy oligonucleotides, *Current opinion in pharmacology 4*, 139-146.
[97] Karandish, F., and Mallik, S. (2016) Biomarkers and targeted therapy in pancreatic cancer, *Biomarkers in cancer 8*, 27.

[98] Siegel, R. L., Miller, K. D., and Jemal, A. (2015) Cancer statistics, 2015, *CA: a cancer journal for clinicians 65*, 5-29.
[99] (2016) American Cancer Society 2016, www.cancer.org.
[100] Wright Jr, G. L., Haley, C., Beckett, M. L., and Schellhammer, P. F. (1995) Expression of prostate-specific membrane antigen in normal, benign, and malignant prostate tissues, *Urologic Oncology: Seminars and Original Investigations 1*, 18-28.
[101] Yao, V., Berkman, C. E., Choi, J. K., O'Keefe, D. S., and Bacich, D. J. (2010) Expression of prostate-specific membrane antigen (PSMA), increases cell folate uptake and proliferation and suggests a novel role for PSMA in the uptake of the non-polyglutamated folate, folic acid, *The Prostate 70*, 305-316.
[102] Laidler, P., Dulińska, J., Lekka, M., and Lekki, J. (2005) Expression of prostate specific membrane antigen in androgen-independent prostate cancer cell line PC-3, *Archives of Biochemistry and Biophysics 435*, 1-14.
[103] Yao, V., Berkman, C. E., and Choi, J. K. (2010) Expression of prostate-specific membrane antigen (PSMA), increases cell folate uptake and proliferation and suggests a novel role for PSMA in the uptake of the non-polyglutamated folate, folic acidDenise S. O'Keefe and Dean J. Bacich contributed equally to this work, *The Prostate 70*, 305.
[104] Ghosh, A., and Heston, W. D. (2004) Tumor target prostate specific membrane antigen (PSMA) and its regulation in prostate cancer, *Journal of cellular biochemistry 91*, 528-539.
[105] Fournel, M., Bonfils, C., Hou, Y., Yan, P. T., Trachy-Bourget, M.-C., Kalita, A., Liu, J., Lu, A.-H., Zhou, N. Z., and Robert, M.-F. (2008) MGCD0103, a novel isotype-selective histone deacetylase inhibitor, has broad spectrum antitumor activity in vitro and in vivo, *Molecular cancer therapeutics 7*, 759-768.
[106] Whittle, J. R., and Desai, J. (2015) Histone deacetylase inhibitors in cancer: What have we learned?, *Cancer 121*, 1164-1167.
[107] Varshosaz, J., Taymouri, S., Hassanzadeh, F., Haghjooy Javanmard, S., and Rostami, M. (2015) Folated synperonic-cholesteryl hemisuccinate polymeric micelles for the targeted delivery of docetaxel in melanoma, *BioMed research international 2015*.
[108] Zeng, S., Zu Chen, Y., Fu, L., Johnson, K. R., and Fan, W. (2000) In vitro evaluation of schedule-dependent interactions between docetaxel and doxorubicin against human breast and ovarian cancer cells, *Clinical cancer research 6*, 3766-3773.
[109] (2016) NIH, National Cancer Institue, http://www.cancer.gov/about-cancer/treatment/drugs/fda-docetaxel.
[110] Zhang, Q., Sun, M., Zhou, S., and Guo, B. (2016) Class I HDAC inhibitor mocetinostat induces apoptosis by activation of miR-31 expression and suppression of E2F6, *Cell Death Discovery 2*.
[111] Nahire, R., Haldar, M. K., Paul, S., Ambre, A. H., Meghnani, V., Layek, B., Katti, K. S., Gange, K. N., Singh, J., Sarkar, K., and Mallik, S. (2014) Multifunctional polymersomes for cytosolic delivery of gemcitabine and doxorubicin to cancer cells, *Biomaterials 35*, 6482-6497.
[112] Marsden, H. R., Gabrielli, L., and Kros, A. (2010) Rapid preparation of polymersomes by a water addition/solvent evaporation method, *Polymer Chemistry 1*, 1512-1518.
[113] Michelet, F., Gueguen, R., Leroy, P., Wellman, M., Nicolas, A., and Siest, G. (1995) Blood and plasma glutathione measured in healthy subjects by HPLC: relation to sex, aging, biological variables, and life habits, *Clinical chemistry 41*, 1509-1517.

[114] Traverso, N., Ricciarelli, R., Nitti, M., Marengo, B., Furfaro, A. L., Pronzato, M. A., Marinari, U. M., and Domenicotti, C. (2013) Role of glutathione in cancer progression and chemoresistance, *Oxidative medicine and cellular longevity 2013*.

[115] Jin, J., Sui, B., Gou, J., Liu, J., Tang, X., Xu, H., Zhang, Y., and Jin, X. (2014) PSMA ligand conjugated PCL-PEG polymeric micelles targeted to prostate cancer cells, *PloS one 9*, e112200.

[116] Kong, B., Seog, J. H., Graham, L. M., and Lee, S. B. (2011) Experimental considerations on the cytotoxicity of nanoparticles, *Nanomedicine 6*, 929-941.

[117] Xu, X., Farach-Carson, M. C., and Jia, X. (2014) Three-dimensional in vitro tumor models for cancer research and drug evaluation, *Biotechnology advances 32*, 1256-1268.

[118] Desoize, B., Gimonet, D., and Jardiller, J. (1997) Cell culture as spheroids: an approach to multicellular resistance, *Anticancer research 18*, 4147-4158.

[119] Tauskela, J. S., Hewitt, K., Kang, L. P., Comas, T., Gendron, T., Hakim, A., Hogan, M., Durkin, J., and Morley, P. (2000) Evaluation of glutathione-sensitive fluorescent dyes in cortical culture, *Glia 30*, 329-341.

[120] Zhang, Y., Jin, Z., Zhou, H., Ou, X., Xu, Y., Li, H., Liu, C., and Li, B. (2016) Suppression of prostate cancer progression by cancer cell stemness inhibitor napabucasin, *Cancer medicine 5*, 1251-1258.

[121] Chen, W., Meng, F., Cheng, R., and Zhong, Z. (2010) pH-Sensitive degradable polymersomes for triggered release of anticancer drugs: a comparative study with micelles, *Journal of Controlled Release 142*, 40-46.

[122] Kulkarni, P., Haldar, M. K., You, S., Choi, Y., and Mallik, S. (2016) Hypoxia-Responsive Polymersomes for Drug Delivery to Hypoxic Pancreatic Cancer Cells, *Biomacromolecules 17*, 2507-2513.

[123] Xu, P., Van Kirk, E. A., Zhan, Y., Murdoch, W. J., Radosz, M., and Shen, Y. (2007) Targeted Charge-Reversal Nanoparticles for Nuclear Drug Delivery, *Angewandte Chemie International Edition 46*, 4999-5002.

[124] Alber, F., Dokudovskaya, S., Veenhoff, L. M., Zhang, W., Kipper, J., Devos, D., Suprapto, A., Karni-Schmidt, O., Williams, R., and Chait, B. T. (2007) The molecular architecture of the nuclear pore complex, *Nature 450*, 695.

[125] Conrad, M., Moreno, S., Sinowatz, F., Ursini, F., Kölle, S., Roveri, A., Brielmeier, M., Wurst, W., Maiorino, M., and Bornkamm, G. (2005) The nuclear form of phospholipid hydroperoxide glutathione peroxidase is a protein thiol peroxidase contributing to sperm chromatin stability, *Molecular and cellular biology 25*, 7637-7644.

[126] Go, Y.-M., and Jones, D. P. (2010) Redox Control Systems in the Nucleus: Mechanisms and Functions, *Antioxidants & Redox Signaling 13*, 489-509.

[127] Schnelldorfer, T., Gansauge, S., Gansauge, F., Schlosser, S., Beger, H. G., and Nussler, A. K. (2000) Glutathione depletion causes cell growth inhibition and enhanced apoptosis in pancreatic cancer cells, *Cancer 89*, 1440-1447.

[128] Huang, S.-L. (2008) Liposomes in ultrasonic drug and gene delivery, *Advanced drug delivery reviews 60*, 1167-1176.

[129] Nahire, R., Haldar, M. K., Paul, S., Mergoum, A., Ambre, A. H., Katti, K. S., Gange, K. N., Srivastava, D., Sarkar, K., and Mallik, S. (2013) Polymer-coated echogenic lipid nanoparticles with dual release triggers, *Biomacromolecules 14*, 841-853.

[130] Paul, S., Russakow, D., Nahire, R., Nandy, T., Ambre, A. H., Katti, K., Mallik, S., and Sarkar, K. (2012) In vitro measurement of attenuation and nonlinear scattering from echogenic liposomes, *Ultrasonics 52*, 962-969.
[131] Huang, S.-L. (2010) Ultrasound-responsive liposomes, *Liposomes: Methods and Protocols, Volume 1: Pharmaceutical Nanocarriers*, 113-128.
[132] Nahire, R., Hossain, R., Patel, R., Paul, S., Meghnani, V., Ambre, A. H., Gange, K. N., Katti, K. S., Leclerc, E., and Srivastava, D. (2014) pH-triggered echogenicity and contents release from liposomes, *Molecular pharmaceutics 11*, 4059-4068.
[133] Paul, S., Nahire, R., Mallik, S., and Sarkar, K. (2014) Encapsulated microbubbles and echogenic liposomes for contrast ultrasound imaging and targeted drug delivery, *Computational mechanics 53*, 413-435.
[134] Zhang, S., and Zhao, Y. (2011) Controlled Release from Cleavable Polymerized Liposomes upon Redox and pH Stimulation, *Bioconjugate chemistry 22*, 523-528.
[135] Discher, B. M., Won, Y. Y., Ege, D. S., Lee, J. C., Bates, F. S., Discher, D. E., and Hammer, D. A. (1999) Polymersomes: tough vesicles made from diblock copolymers, *Science 284*, 1143-1146.
[136] Kopechek, J. A., Abruzzo, T. M., Wang, B., Chrzanowski, S. M., Smith, D. A., Kee, P. H., Huang, S., Collier, J. H., McPherson, D. D., and Holland, C. K. (2008) Ultrasound-Mediated Release of Hydrophilic and Lipophilic Agents From Echogenic Liposomes, *Journal of Ultrasound in Medicine 27*, 1597-1606.
[137] Redmond, S. M., Joncourt, F., Buser, K., Ziemiecki, A., Altermatt, H.-J., Fey, M., Margison, G., and Cerny, T. (1991) Assessment of P-glycoprotein, glutathione-based detoxifying enzymes and O6-alkylguanine-DNA alkyltransferase as potential indicators of constitutive drug resistance in human colorectal tumors, *Cancer research 51*, 2092-2097.
[138] Forsberg, F., Shi, W. T., and Goldberg, B. (2000) Subharmonic imaging of contrast agents, *Ultrasonics 38*, 93-98.
[139] Sarkar, K., Shi, W. T., Chatterjee, D., and Forsberg, F. (2005) Characterization of ultrasound contrast microbubbles using in vitro experiments and viscous and viscoelastic interface models for encapsulation, *The Journal of the Acoustical Society of America 118*, 539-550.
[140] Shi, W. T., and Forsberg, F. (2000) Ultrasonic characterization of the nonlinear properties of contrast microbubbles, *Ultrasound in medicine & biology 26*, 93-104.
[141] Kastrup, L., Oberleithner, H., Ludwig, Y., Schafer, C., and Shahin, V. (2006) Nuclear envelope barrier leak induced by dexamethasone, *Journal of cellular physiology 206*, 428-434.
[142] Vermeulen, L., e Melo, F. d. S., Richel, D. J., and Medema, J. P. (2012) The developing cancer stem-cell model: clinical challenges and opportunities, *The lancet oncology 13*, e83-e89.
[143] Kadonosono, T., Yamano, A., Goto, T., Tsubaki, T., Niibori, M., Kuchimaru, T., and Kizaka-Kondoh, S. (2015) Cell penetrating peptides improve tumor delivery of cargos through neuropilin-1-dependent extravasation, *Journal of Controlled Release 201*, 14-21.
[144] Miao, H.-Q., Lee, P., Lin, H., Soker, S., and Klagsbrun, M. (2000) Neuropilin-1 expression by tumor cells promotes tumor angiogenesis and progression, *The FASEB journal 14*, 2532-2539.

[145] Bielenberg, D. R., Pettaway, C. A., Takashima, S., and Klagsbrun, M. (2006) Neuropilins in neoplasms: Expression, regulation, and function, *Experimental Cell Research 312*, 584-593.
[146] Fuh, G., Garcia, K. C., and de Vos, A. M. (2000) The interaction of neuropilin-1 with vascular endothelial growth factor and its receptor flt-1, *Journal of Biological Chemistry 275*, 26690-26695.
[147] Glinka, Y., Mohammed, N., Subramaniam, V., Jothy, S., and Prud'homme, G. J. (2012) Neuropilin-1 is expressed by breast cancer stem-like cells and is linked to NF-κB activation and tumor sphere formation, *Biochemical and Biophysical Research Communications 425*, 775-780.
[148] Vermes, I., Haanen, C., and Reutelingsperger, C. (2000) Flow cytometry of apoptotic cell death, *Journal of immunological methods 243*, 167-190.
[149] Vermes, I., Haanen, C., Steffens-Nakken, H., and Reutelingsperger, C. (1995) A novel assay for apoptosis. Flow cytometric detection of phosphatidylserine expression on early apoptotic cells using fluorescein labelled Annexin V, *J Immunol Methods 184*, 39-51.
[150] Sawant, R. R., and Torchilin, V. P. (2012) Multifunctional nanocarriers and intracellular drug delivery, *Current Opinion in Solid State and Materials Science 16*, 269-275.

APPENDIX A. SUPPORTING INFORMATION FOR 2

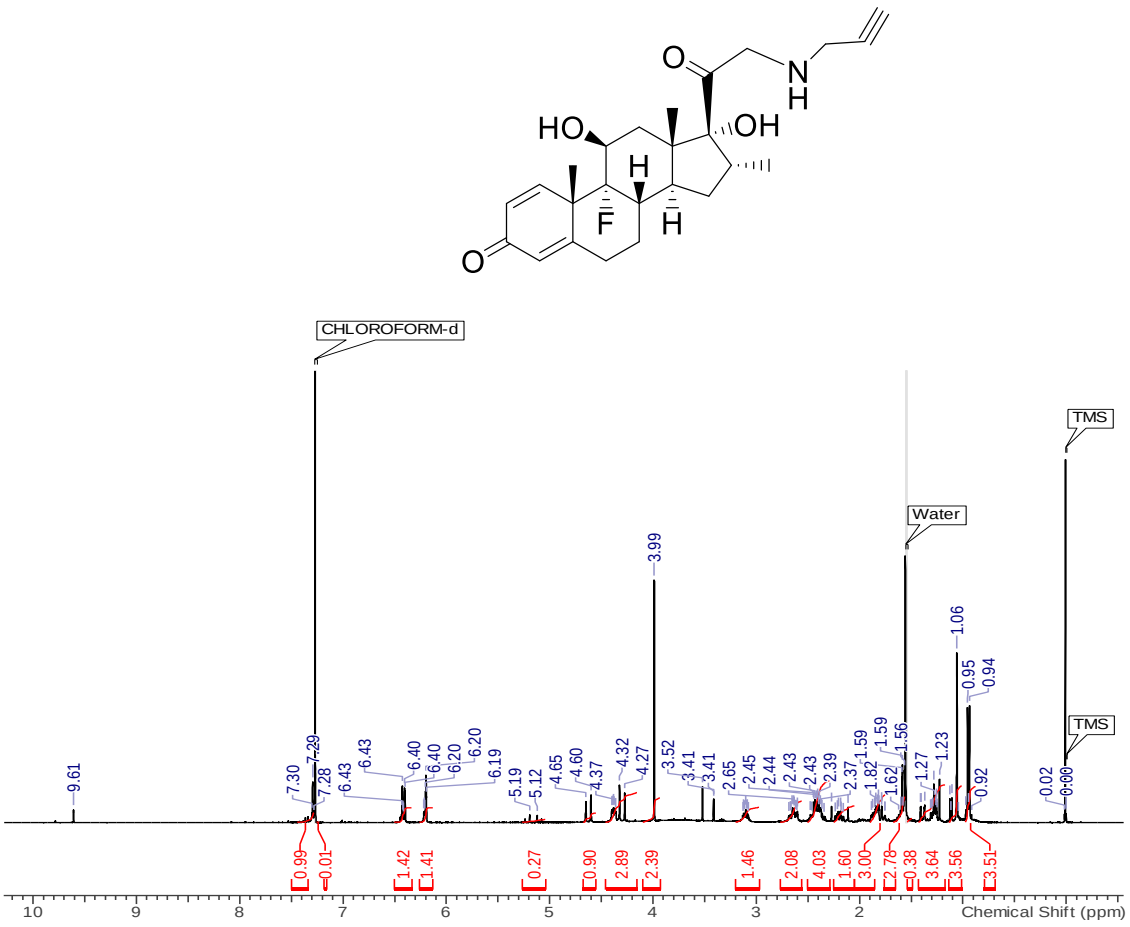

Figure A1.[1]H NMR spectrum of alkyne-dexamethasone (400 MHz, CDCl3)

[1]H NMR (400 MHz, CHLOROFORM-d) δ = 7.37 - 7.28 (m, 1H), 6.46 - 6.37 (m, 3H), 6.23 - 6.17 (m, 3H), 4.63 (d, *J* = 19.8 Hz, 2H), 4.43 - 4.30 (m, 5H), 4.27 (s, 2H), 3.99 (s, 4H), 3.52 (s, 4H), 3.41 (d, *J* = 1.5 Hz, 2H), 3.10 (td, *J* = 3.6, 7.3 Hz, 4H), 2.73 - 2.53 (m, 5H), 2.51 - 2.33 (m, 9H), 2.27 (s, 1H), 2.24 - 2.15 (m, 3H), 2.11 (s, 1H), 1.99 - 1.72 (m, 8H), 1.65 - 1.56 (m, 6H), 1.54 - 1.35 (m, 4H), 1.34 - 1.20 (m, 6H), 1.13 - 1.02 (m, 8H), 1.02 - 0.87 (m, 8H).

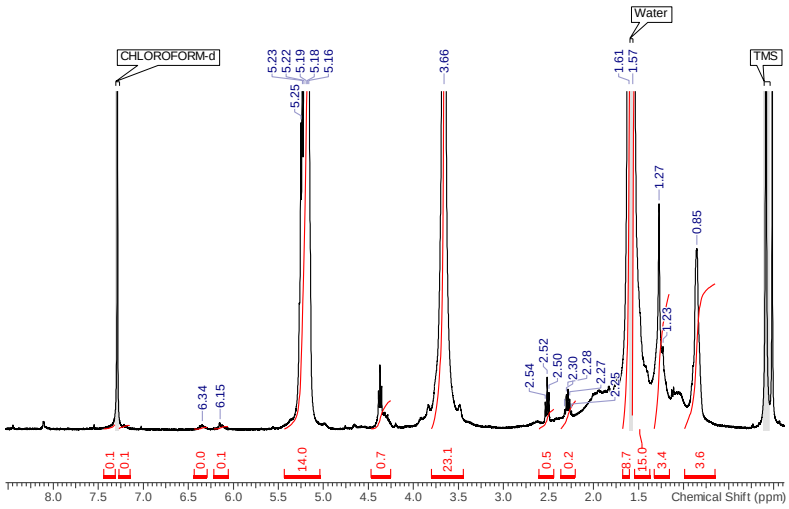

Figure A2.[1]H NMR spectrum of dexamethasone–PEG1900–PLA6000 (400 MHz, CDCl3) [1]H NMR (400 MHz, CHLOROFORM-d) δ = 8.01 - 8.01 (m, 1H), 6.34 (br s, 1H), 6.15 (br s, 1H), 5.43 - 5.04 (m, 22H), 4.47 - 4.25 (m, 1H), 3.66 (s, 38H), 2.61 - 2.44 (m, 1H), 2.28 (td, *J* = 7.5, 15.3 Hz, 1H), 1.33 - 1.16 (m, 5H), 0.85 (br s, 5H).

A.1. Synthesis and characterization of N3-PEG1900-PLA6000

The Hydroxyl-PEG (2000)-Azide (20mg, 0.01mmol) was taken into toluene (5 mL). Stirring the mixture by a magnetic agitator under nitrogen. A Dean-Stark trap was connected to the condenser tube to remove residual moisture, and the temperature of the oil bath was controlled at 125° C to reflux the toluene for 5 h. After the solution was cooled to room temperature under nitrogen, D, L-lactide (80 mg, 0.56mmol) and tin(II) ethoxyhexanoate (8ul, 0.025mmol) were added, and the solution was heated at 125° C to reflux under nitrogen overnight. After cooling to room temperature, the reaction mixture was added dropwise to the cold ether. Vortex, centrifuge, the top clear supernatant was decanted, and the precipitate was washed again with ether, dried under vacuum. analyzed by CDCl3 1H NMR spectroscopy and gel permeation chromatography for purity and molecular weight.

APPENDIX B. SUPPORTING INFORMATION FOR 3

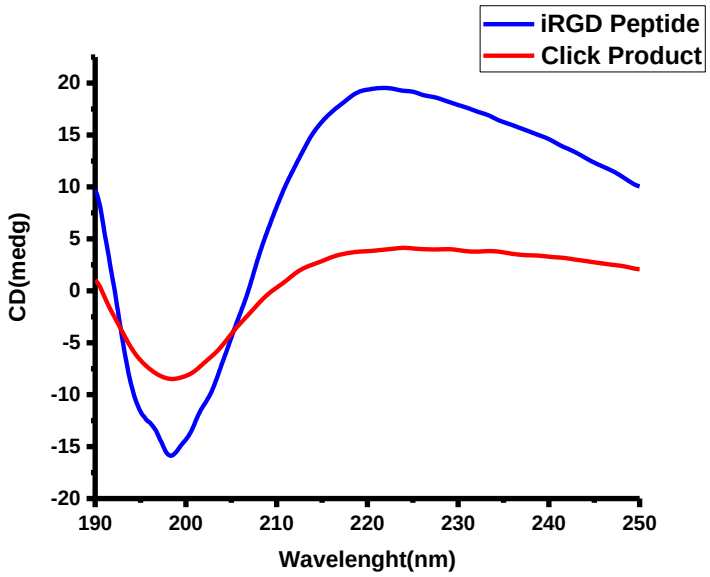

.

Figure B1.CD spectra of hexynoic acid conjugated iRGD peptide before(blue) and after reaction [2+3]-cycloaddition with N3-PEG-PLA(red)

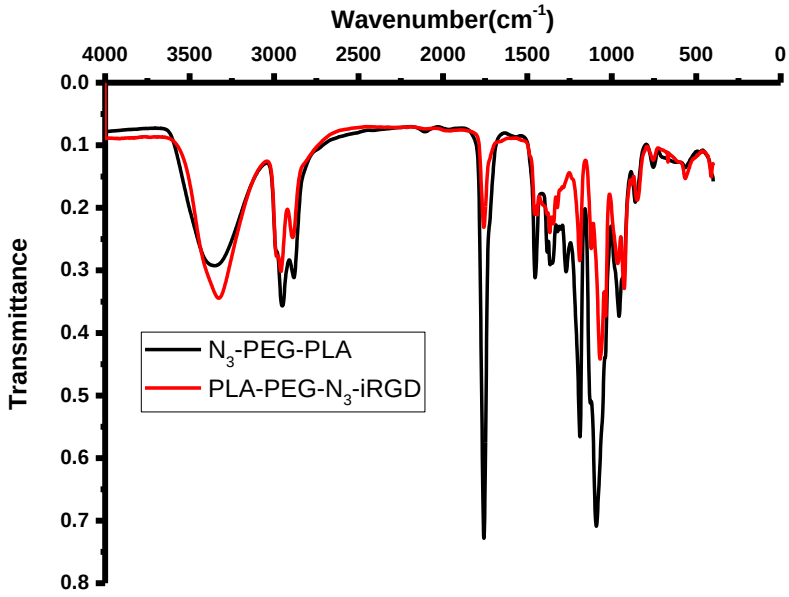

Figure B2. FT-IR characterization of iRGD peptide after and after reaction with N_3-PEG_{1900}-PLA_{6000}

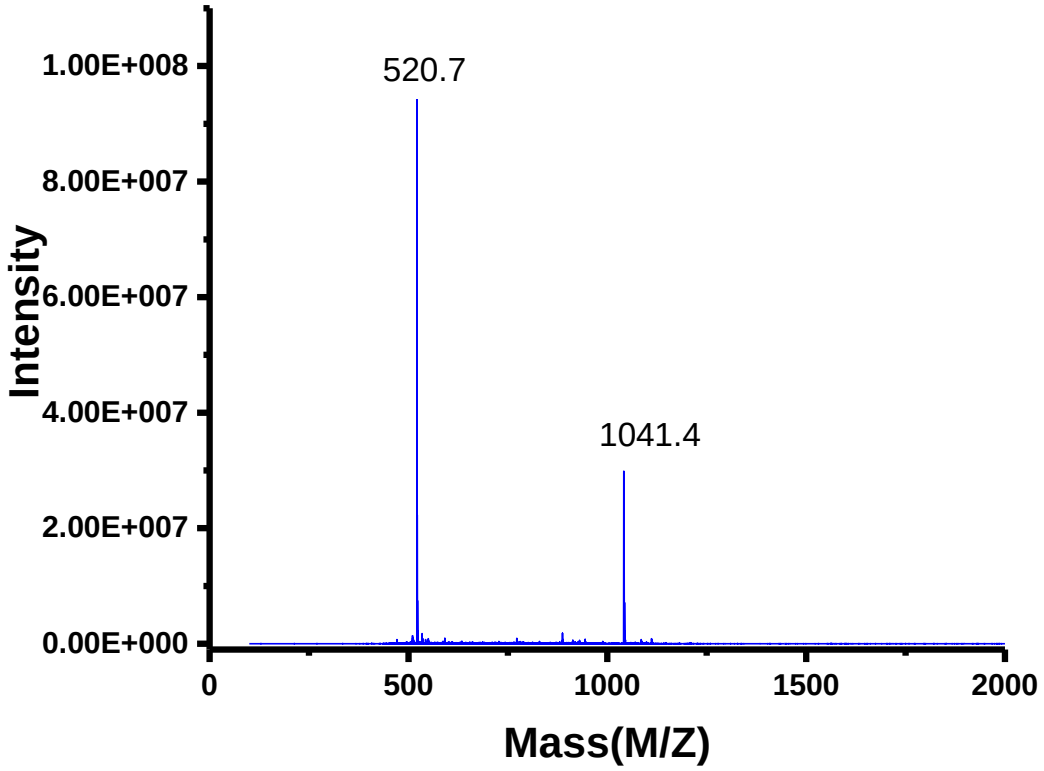

Figure B3. MALDI mass spectrum for hexynoic acid conjugated iRGD peptide

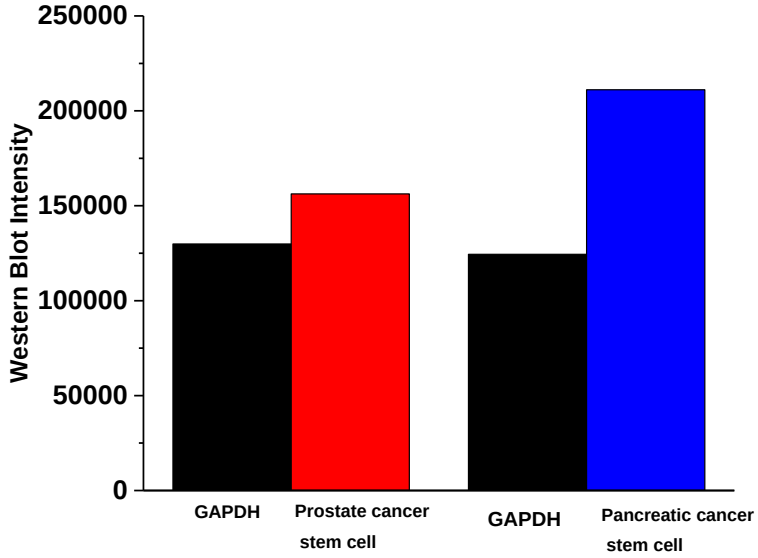

Figure B4. Band Intensity of neuropilin-1 receptor in prostate and pancreatic cancer stem cells. The errors are less than 10% for the intensity measurements.

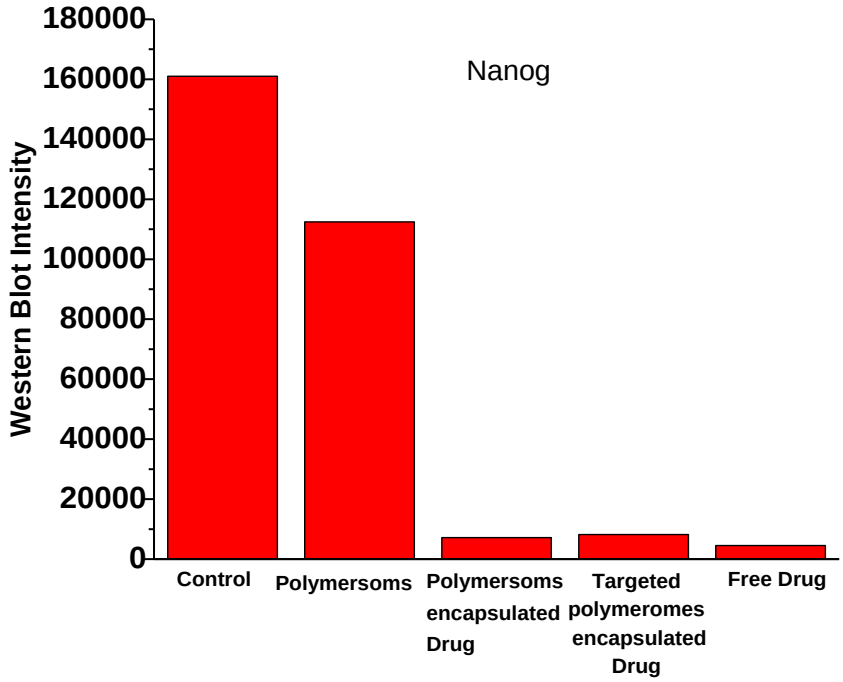

Figure B5. Band intensity of Nanog expression in prostate cancer stem cells after treatment.

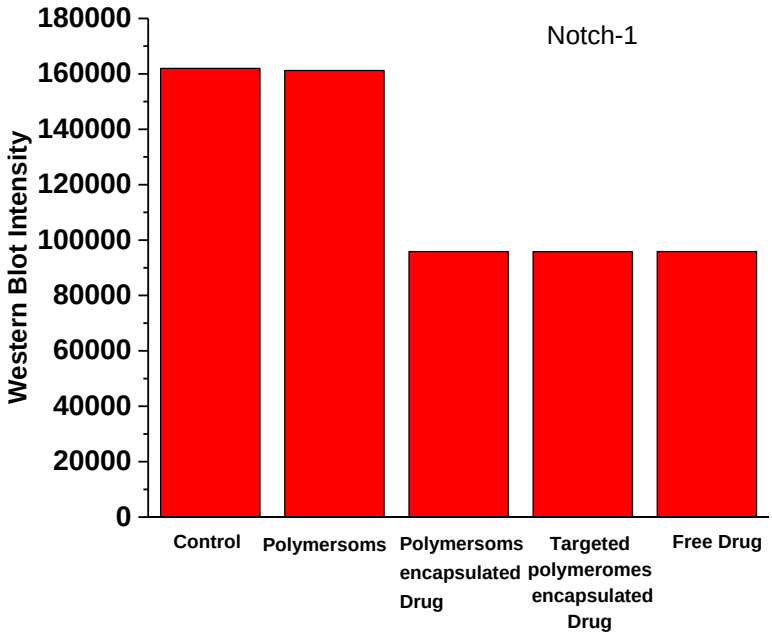

Figure B6. Band intensity of Notch-1 expression in prostate cancer stem cell after treatment. The errors are less than 10% for the intensity measurements.